

**Human Brain Dynamics Investigation based on Functional Magnetic
Resonance Imaging**

By

Ashraf Mahroos Said Saba

The Department of System and biomedical Engineering

Faculty of Engineering

Cairo University

A thesis submitted to the

Faculty of Engineering, Cairo University

In Partial Fulfillment of the

Requirements for the degree of

DOCTORATE OF PHILOSOPHY

In

SYSTEMS AND BIOMEDICAL ENGINEERING

FACULTY OF ENGINEERING, CAIRO UNIVERSITY

GIZA, EGYPT

SEPTEMBER, 2011

**Human Brain Dynamics Investigation based on Functional Magnetic
Resonance Imaging**

By

Ashraf Mahroos Said Saba

The Department of System and biomedical Engineering

Faculty of Engineering

Cairo University

A thesis submitted to the

Faculty of Engineering, Cairo University

In Partial Fulfillment of the

Requirements for the degree of

DOCTORATE OF PHILOSOPHY

In

SYSTEM AND BIOMEDICAL ENGINEERING

Under the supervision of

Prof. Dr. Yasser Mostafa Kadah

The Department of System and biomedical Engineering

Faculty of Engineering, Cairo University

FACULTY OF ENGINEERING, CAIRO UNIVERSITY

GIZA, EGYPT

SEPTEMBER, 2011

**Human Brain Dynamics Investigation based on Functional Magnetic
Resonance Imaging**

By

Ashraf Mahroos Said Saba

The Department of System and biomedical Engineering

Faculty of Engineering, Cairo University

A thesis submitted to the

Faculty of Engineering, Cairo University

In Partial Fulfillment of the

Requirements for the degree of

DOCTORATE OF PHILOSOPHY

In

SYSTEM AND BIOMEDICAL ENGINEERING

Approved by the Examining Committee

Prof. Dr. Yasser Mostafa Kadah ,(THE THESIS MAIN ADVISOR)

Prof. Dr. Abdalla Said Ahmed Mohamed (MEMBER)

Prof. Dr. Mohamed Ibrahim El Adawy (MEMBER)

FACULTY OF ENGINEERING,

CAIRO UNIVERSITY

GIZA, EGYPT

SEPTEMBER, 2011

Abstract

We propose a model that describes the interactions of several Brain Regions based on Functional Magnetic Resonance Imaging (fMRI) time series to make inferences about functional integration and segregation within the human brain. This method is demonstrated using dynamic causal modeling (DCM) augmented by Granger Causality (GC) using real data to show how such models are able to characterize interregional dependence. We extend estimating and reviewing designed model to characterize the interactions between regions and show the direction of the signal over regions. A further benefit is to estimate the effective connectivity between these regions. All designs, estimates, reviews are implemented using Statistical Parametric Mapping CCA toolbox, one of the free best software packages and published toolbox used to design the models and analysis for inferring about fMRI functional magnetic resonance imaging time series.

Extracted time series of studied regions have been analyzed in two ways: First, is to infer easily the causality and the path of signal through connections between regions. Second, is to identify the group regions of target that exhibit similar response patterns over several events and group the conditions from output profiles across set of regions based on Bi-Clustering technique.

Keyword (Dynamic System, Brain Causality, fMRI, Brain connectivity, Effective Connectivity, DCM, Bi-Clustering and Granger Causality)

ACKNOWLEDGMENTS

All my Thanks to ALLAH (GLORY BE TO HIM)

I'd like to thank my thesis advisor, Dr. Yaser Mostafa Kadah, for all his remarkable patience, and my kind and humble friends. I 'd like to mention how much I appreciate all the professors at Cairo and Menia university where I have a great pleasure to know. No acknowledgement will be complete without mention the support ,the encouragement , and love of all my family; my Father, my mother, my brothers, sisters , my wife and my Children.

TABLE OF CONTENTS

	Page
Acknowledgments.....	v
List of Tables	xii
List of figures	x
List of abbreviations	xii
1. Chapter 1. Introduction	1
1.1. Thesis Overview, Problem definition	1
1.1.1. Human Brain Structure	1
1.1.2. Human Brain Construction	4
1.1.3. CSF system – water on the brain	8
1.2. Thesis objective	12
1.2.1. Brain Regions of Visual system.....	14
1.2.2. Brain Dynamics Representation	14
1.3. Thesis organization	16
1.4. Summary.....	17
2. Chapter 2, Background and Literature Review.....	18
2.1. Human Brain Dynamic Representation Layout.	18
2.2. FMRI as a brain investigator.....	22
2.3Types of human brain connectivity.	31
2.3.1. Anatomical connectivity.....	33

2.3.2. Functional connectivity.....	35
2.3.2.1. Model Based Methods.....	37
2.3.2.1.1. Cross Correlation Analysis, CCA.....	38
2.3.2.1.2. Coherent Analysis, CA.....	39
2.3.2.1.3. Statistical Parametric Mapping, SPM.....	40
2.3.2.2. Data Driven Methods.....	41
2.3.2.2.1. Decomposition based Methods.....	41
2.3.2.2.1.1. PCA/SVD.....	42
2.3.2.2.1.2. Independent component analysis.....	43
2.3.2.2.2. Clustering Analysis.....	47
2.3.2.2.2.1. Fuzzy clustering analysis.....	48
2.3.2.2.2.2. Hierarchical clustering analysis.....	49
2.3.2.3. Current Toolboxes.....	51
2.3.3. Effective connectivity.....	52
3.3.3.1. Dynamic System Definition.....	52
3.3.3.2. Effective connectivity Literature Review.....	53
3.3.3.2.1. Psycho Physiological Interaction.....	55
3.3.3.2.2. Structural Equation Modeling.....	56
2.4. Summary.....	57
3. Complementary Dynamic Causal Modeling augmented by PPI.....	59
3.1. Introduction.....	59

3.2. Principle of Dynamic Causal Modeling.....	63
3.3 DCM Construction based on fMRI images time series.	64
3.3.1. Hemodynamic State Equation.....	68
3.3.2. Stimulus Propagation in DCM system.....	70
3.3.3. Parameters Estimations.	71
3.4 Results and Discussions.....	73
3.4.1. Data sets Experimental verification.	74
3.4.2. Interpretations from parameters estimations for all effects.	77
3.4.3. DCM as MIMO system.....	78
3.4.4. Intrinsic connectivity discrimination for all effects.....	79
3.4.5. Induced or changed connectivity.	82
3.4.6. Direct inputs effect and first order kernel with localization.	84
3.5 HRF and PPI Augmentation.	85
3.6 Conclusions.	87
3.7 Summary.	89
4. Extracted Time series analysis using Granger Causality and Bi-clustering ..	90
4.1. Introduction.....	91
4.2. Granger Causality for extracted time series.....	92
4.2.1. GC Mathematical derivation.....	96
4.2.2. GC Results and conclusion.	98
4.3. Biclustering for extracted time series.....	100

4.3.1. Introduction.....	101
4.3.2. Data preparation.....	102
4.3.3. Biclusters types and results.....	103
4.3.3.1. Cheng and church Bicluster.....	103
4.3.3.2. CCC Bicluster with exact pattern.....	105
4.3.3.3. Bicluster inclusion maximal (Bimax).....	109
4.3.3.4. Order Preserving submatrix (OPSM).....	109
4.4 Summary.....	111
5. Discussion, Conclusions and Future work.....	113
5.1 Summary.....	113
5.2 Limitations.....	116
5.3 Challenges and recommendations.....	116
References.....	117
Appendix A. Software Packages Survey.....	114
Appendix B. Expectation Maximization EM.....	115
Appendix C. HRF Parameters Estimation.....	117

LIST OF TABLES

1. Table 3.1 Intrinsic connectivity matrices.....	80
2. Table 3.2 Induced or change on effective connectivity.....	83
3. Table 3.3 Direct effect of the external effects or events.....	84
3. Table A1 Summary of fMRI software analysis packages.....	131

3. Table A2 Priors of HRF Parameters after Estimation.	134
---	-----

LIST OF FIGURES

1. Figures 1.1 A nerve cell or neuron construction.	7
2. Figures 1.2 Perception Action Cycle	11
3. Figures 1.3 Sensing predicting diagram	11
4. Figures 1.4 Schematic of the fMRI data structure and its acquisition process.	13
5. Figures 1.5 a schematic illustrating the concepts of DCM augmented by PPI and Granger Causality.	15
6. Figures 2.1 brain activation for two areas in the brain under specific event.	24
7. Figures 2.2 The relation between attention and consciousness.	29
8. Figures 2.3 Methods used for functional Connectivity, modified	37
9. Figures 2.4 Illustration for decomposition of a FMRI dataset	42
10. Figures 2.5 illustrates the decomposition of a FMRI dataset with certain ICA.	43
11. Figures 2.6 Independent component (IC) maps	45
12. Figures 2.7 Two illustrative signals that are highly correlated	47
13. Figures 3.1 the bilinear state equation of DCM for FMRI	65
14. Figures 3.2 a schematic illustrating the concepts of DCM augmented by PPI . .	67
15. Figures 3.3 Summary of the hemodynamic model used by DCM Based on FMRI images time series.	69
16. Figures 3.4 Simulated BOLD responses of two areas, y_1 and y_2	70
17. Figures 3.5 Estimation Using EM	78

18. Figures 3.6 a Left Three inputs U_i , visual (photic), motion and attention represented by event. Right is outputs of four visual system studying regions.	79
19. Figures 3.7 Intrinsic connectivity and their probabilities for Attention effect (left) and Attention-Motion-Photic effect (right)	81
20. Figures 3.8 Effect of change in effective connectivity between regions after applying external effects or inputs, left is for attention model, right is for attention when combined with Photic and Motion.....	82
21. Figures 3.9 a Left is the localization of anatomical structure for four regions. Right is the first order kernel for all four responses top-down line graphs V5,PPC,PFC and V1 after applying three effects.....	85
22. Figures 3.10 The upper part is the Pyscho Physiologic interaction PPI for V1 against V1 and V5, The lower part is hemodynamic and neural response.....	86
23. Figures 4.1 Schematic illustrating the concepts of DCM augmented Granger Causality and Bi-Clustering Technique	90
24. Figures 4.2 The bar charts show un weighted causal density/flow, and the lines show density/flow weighted by magnitude of causal interaction.	99
25. Figures 4.3 Demonstrations of causal connectivity toolbox	99
26. Figures 4.4 Regions expression matrix visualized as a heatmap	102
27. Figures 4.5 first bicluster for CC and expression profile of this bicluster	104
28. Figures 4.6 Matrix of bicluster for CCC and expression profile of this bicluster7	106
29. Figures 4.7 Matrix of bicluster for CCC and expression profile of this bicluster1283 ..	107
30. Figures 4.8 graphic representations for matrices of seven bicluster and expression	108

31. Figures 4.9 Bicluster of Bimax matrix view and expression profile for 4 regions	110
32. Figures 4.10 Bicluster of OPSM, matrix view and expression profile for 4 regions	111

LIST OF ABBREVIATIONS

MRI	Magnetic Resonance Imaging
BOLD	Blood-Oxygenation-Level-Dependent
fMRI	Functional Magnetic Resonance Imaging
HRF	Hemodynamic Response Function
CBF	Cerebral Blood Flow
CBV	Cerebral Blood Volume
EPI	Echo-Planar Images
FIR	Finite Impulse Response
ICA	Independent Component Analysis
PCA	Principal Component Analysis
ROI	Region of Interest
SPM	Statistical Parametric Mapping
DCM	dynamic causal modelling
GC	Granger Causality
EEG	Electroencephalography
RF	Radio Frequency
TR	Time of Repetition
V1	visual cortex
V5,MT	Brodmann area or middle temporal
PPC	4-Phenyl-4-(1-piperidinyl)-cyclohexanol

PET	positron emission tomography
SNR	signal to noise ratio
CCA	Cross-Correlation Analysis,
CA	Coherent Analysis
SVD	singular value decomposition
fcMRI	Functional connectivity of Magnetic Resonance Imaging
FPR	false-positive rate
FCA	Fuzzy clustering analysis
HCA	Hierarchical clustering analysis
PPI	Psycho-Physiological Interactions
SEM	Structural equation modeling
MIMO	Multiple Inputs Multiple Outputs
VAR	vector autoregressive
GCA	Granger causality analysis
AIC	Akaike information criterion
BIC	Bayesian information criterion
Bimax	Biclusters Inclusion Maximal
OPSM	Order Preserving Submatrix
EM	Expectation Maximization

Chapter 1

Introduction

We will introduce in this chapter the layout of our study, and define in details what is the problem in section one. in section two, we will describe Thesis objective according to what we contribute in solving brain causality or dynamic recognition problem. In the last section, we will give overview of thesis organization.

1.1 Thesis Overview, Problem definition

The problem is how to infer the dynamic of signal through our brain nerves or from region to region, not only how? but also when and where?. Signal goes through area or conducts area by another to do specific function at specific event. I mean that we may have the wire to conduct, but conducting processes is according to trigger comes from different ways. At this point many apparatus designed to characterize this black box like electrophysiological method (EEG). There is still one term in our problem definition which is where? That means location or signal origin and destination, this will be done by using Functional Magnetic Resonance Imaging (fMRI) time series analysis. In this section, we will introduce the basic construction and signal transfer, Human Brain System, and visual studied system [1].

1.1.1. Human Brain Structure

The brain has no moving parts: unlike the heart, lungs or intestines. it does not pulsate, inflate or squeeze. It does not make anything: unlike the kidneys, liver

or spleen, no urine, bile or lymph comes out of it. Unlike the skin or bones, the human brain serves no obvious purpose and yet we just believe it is responsible for thought, emotion and free will. How do we come to such a conclusion and what did people think before? To answer these questions, we must go back to the past and step from conclusion to conclusion to the present day. We begin this tour with three things. First, our knowledge of these early believes is based on archaeological evidence. Second, the history of medicine is hugely biased towards Western historical documentation and so we will inevitably mainly describe this view of things. Finally, attitudes of animal and human experiments were quite different in the past and many of the experiments we will describe are quite unpleasant and would be highly unlikely to be allowed today [1, 2].

An ant is capable of quite complex behavior and yet its “brain” is barely the size of a pinhead. A mosquito can fly, in home on a target and extract blood, with just a dot of a ganglion. A rat is quite intelligent, but has a brain of only about two grams in weight – similar to that of a small part of the human brain, called the hypothalamus. In general, the larger the brain is, the greater intelligence it has. This is not a strict relationship, however, and in fact it may be a surface area which is more important, or brain weight as a proportion of body size. The convolutions on the surface of the brain are called gyri and the dips between them sulci. In humans, the brain is not only very large compared with body size but is also highly wrinkled, giving it its “walnut” appearance. This means we not only have a relatively over-large brain, but also a surface area that is very large. In the cerebral cortex alone, an adult human has ten to twenty billion neurons and sixty

trillion synapses. So where does all this brain extra power go? Is our behavior really that much more complex than, say, a dog's or a pig's? The answer is, probably, yes. First, our interpersonal relationships are very complex. Second, we have a highly developed language ability. Third, we have a developed sense of time, both future and past. Fourth, we are capable of abstract thought. Fifth, we can place ourselves in the position of another person. Finally, we are capable of creating artistic works and solutions to problems. The combination of these is uniquely human, although it seems likely that some other primates and social mammals may be capable, to a lesser extent, of some of them [3,4].

It seems that the critical components needed for brain power are numbers of neurons, numbers of interconnections and numbers of specialized circuits. In general, a bigger brain will provide these in bigger quantities, but this is only a general rule and, as always, there is an evolutionary trade-off between abilities and power on one hand, and maintenance and cost of upkeep on the other one. Our brain uses up twenty per cent of the calories we take in, needs a long gestation (which is still not long enough, so we are helpless after birth for a long time) and needs a large head, making childbirth difficult and dangerous. This is a huge evolutionary burden, so it must be worth it. A brain is a vast collection of nerves, all interconnected in such a way that we can see and experience the world, think about it and act on what we conclude, but what are nerves and how does the brain work?

It comes as a surprise to many people to learn that we run on electricity. A human being is largely water with a few salts thrown in. We conduct electricity

superbly, but not along wires. Nerves and muscles pervade every part of us and are the main routes along which current flows. In fact every cell, not just nerve and muscle cells, is electric [1,4].

1.1.2 Human Brain Construction

All living things are built of cells. These are not just passive building blocks; they are busy active places. To understand the complexity of a cell, imagine an enormous underwater factory floating in the sea, vaguely round in shape. The factory walls are a gigantic soap bubble, perforated by doors and pumps. Although some water and small sea dwellers can leak in and out through the bubble wall, anything important or large has to come in through a pump or a door. The outer layer of the bubble is bristling with antennae and communications panels, sending and receiving signals. Inside, the factory is full of water, but, unlike the salt is pumped out as fast as it can leak in [5].

One of the most important elements in our brain is nerve, which is a part of the body that can lead to numbness or weakness if it is damaged. For a scientist, a nerve is a nerve cell or neuron; a single cell. To a surgeon or pathologist, a nerve is a yellow-white string-like bundle, made of many nerve cells. We will use “nerve cell” or “neuron” when we refer to the single cell and “nerve” when we refer to the much larger bundle of nerve cells.

In nature, there is a strong relationship between the structure of any thing and its function. Nerve cells are a particularly striking example. Because of the need for an extensive communication network, the usual round shape of the cell is deformed into a structure more like a sea urchin; its spines extended into long,

delicate filaments. As the nerve cell grows, its filaments (called dendrites) seek out other nerve cells to contact and communicate with them. Most nerve cells also have at least one extremely long, major, tube-like extension, known as an axon, the construction of the neuron is shown in figure 1.1, and these form the tracks for molecular motors to transport their cargo up and down the axon. The more swollen, rounded, part of the nerve cell is the cell body. The cell bodies of nerve cells tend to combine together and these groups form the grey matter of the brain and spinal cord. From the cell bodies, the axons shoot off to their own destinations, but they too are bundled together, to form a nerve [1].

The commonest transformation is from chemical to electrical, but nerve cells can also change light, sound, temperature, pressure, stretch and even the earth's magnetic field into an electrical signal. The signal starts in the cell body and travels down the axon to be sent on to the next neuron in the chain, or it goes the other way, from axon to the body of the nerve cell. In some sensory nerves, there are two axons. In these neurons, the signal travels up the first axon, into the cell body and down the second axon until it reaches the far end, where it can be transmitted to other cells. You might think the easiest way for nerve cells to communicate would be by passing the electrical signal directly from one to the other, rather like an electrical circuit, but this is not what happens. When the signal reaches the far end, the nerve cell converts it into a chemical that diffuses out into the gap between it and its neighbor. Because it is a transmission of information from a neuron, this chemical is called a neurotransmitter. This region, where the neurotransmitter is released, where one cell ends and the next starts, is

known as a synapse. When the chemical signal is detected by a nerve cell on the other side of the synapse, it is converted back into an electrical signal and the whole thing starts again.

This mixture of electrical and chemical signals is called an electrochemical system; it combined with the physical arrangement of neurons and their connections. Nerves do not conduct electricity like a wire. Instead, they maintain a difference between salt concentrations inside and outside the cell membrane. To understand why this might make electricity, we need to understand what a salt is. Elements can be grouped into two types: those that tend to lose electrons when combining with others thus becoming positively charged and those that tend to gain them thus becoming negatively charged. A salt is made of a pair of such opposite elements, in which the excess electrons of one have been borrowed by the other, forming a bond between them. In water, the elements dissociate, becoming positively and negatively charged ions. In organisms, the most common positive ions are sodium (Na^+) and potassium (K^+). Sodium tends to attract electrons more strongly than potassium and, because the cell pumps sodium out but potassium in, a charge builds up across the cell membrane, with a difference of about 70 mV between the inside and the outside of the cell. When a neurotransmitter signal is received from a neighboring cell, the cell membrane becomes leaky to sodium, so a current of sodium ions begin to leak in faster than they can be pumped out. This makes the inside more positively charged [5].

It is important to realize that there are three stages being described here. The first stage is the normal resting situation. The second is the initial leakiness of

the cell membrane to sodium ions. The third is the catastrophic, massive leakiness to sodium ions that is the action potential, which only occurs when a critical threshold is reached. The action potential method has two immediate advantages. First, a simple form of addition is possible. If a small signal is received, it might not be enough on its own to depolarize the cell membrane sufficiently to trigger an action potential, but many small signals together might. Second, because the signal never degrades, it can travel long distances without the need for repeater stations to boost the power. Comparing with the National Grid, in which large transformers are needed to maintain the electrical voltage because of the drop in power that happens in wires. The main problem with the action potential method is that the speed of conduction of the electrical signal depends on the diameter of the nerve cell. Bigger is faster, but it is still painfully slow. This is why it can take a tenth of a second for you to feel it when you stub your toe [5, 6].

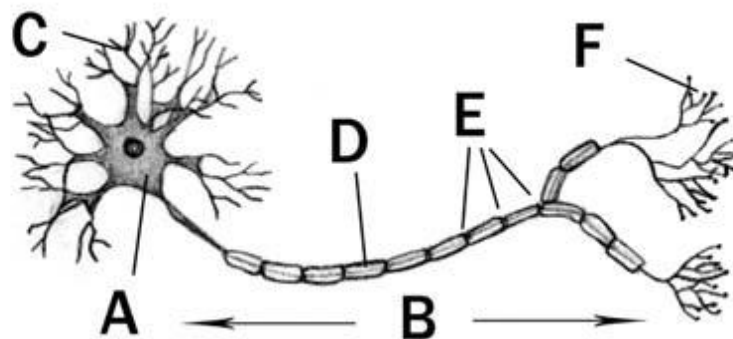


Figure 1.1 A nerve cell or neuron. A: cell body, B: axon, C: dendrites and dendritic branchlets, D: myelin, E: node of Ranvier, F: terminal boutons –these form synapses with other nerves or with muscles [1].

When the signal reaches the far end of an axon, rather than the gates letting in sodium, they let in calcium, which activates the release of the chemical

neurotransmitters into the synapse, ready to begin another action potential in the next cell [1].

The human brain is the most public organ on the face of the earth, open to everything, sending out messages to everything. To be sure, it is hidden away in bone and conducts internal. The brain is undoubtedly quite delicate, but has no pain receptors itself, so can be pressed, squashed or cut without pain. The apparent insensitivity of the cerebral cortex to direct mechanical and chemical stimulation was, until the nineteenth century, used as an argument against it having any important functions. There are certainly large reserves as in other organs, such as the kidney and liver. This is just as well, give many circumstances in which a significant number of brain cells can be damaged, for example, each time a footballer heads the ball. These reserves are not endless, as we can see clearly in some retired professional boxers who have developed dementia or a Parkinson's disease like condition, caused by loss of too many neurons. Apart from the risk of these diffuse brain injuries, there is also the risk of direct damage to a particular region of the brain and subsequent loss of function, be it paralysis, loss of speech or blindness. This means we need a rigid casing for trauma protection, which is what the skull provides [1,6].

1.1.3 CSF system – water on the brain

Just as one would not send a valuable fragile item in a cardboard box without protecting it with bubble wrap, the brain is cushioned in a liquid, cerebrospinal fluid (CSF). This provides an effective shock-absorption system for all but the heaviest of blows to the head. Interestingly, it is far less effective at

dealing with acceleration injuries, such as those experienced in car crashes, where the majority of the damage of the brain tends to occur on the opposite side to the force – the so-called contracoup injury. Recently, it has been suggested that the relatively reduced density of the brain, compared with the surrounding CSF, is responsible for this phenomenon. Perhaps humans are evolutionarily well adapted to deal with everyday knocks or even aggressive blows to the head from the blunt weapons of our enemies, but not, as yet, prepared for the dangers of high speed travel.

The main role of CSF is to provide a stable and optimal environment for brain cells, allowing efficient transport of chemicals across their membranes. A highly specialized barrier exists between the blood supply to the brain and the CSF. This is the blood–brain barrier, which regulates the flow of natural chemicals. This maintains equilibrium and also prevents the brain being exposed to toxic substances (which includes drugs) that might have managed to enter the bloodstream – which means the treatment of brain diseases using medicines can be challenging. Healthy CSF is clear and colorless, like water, even though it has a role similar to blood. CSF can provide information on the chemical status of the central nervous system, as it can be extracted easily using a needle inserted into the spine below the level of the spinal cord; a procedure known as a spinal tap or lumbar puncture. Laboratory analysis of the fluid can be an important first clue to infections, certain types of brain hemorrhage and inflammatory diseases of the central nervous system [1,6].

In the 1970s, Basar and coworkers tried to determine the dynamics of brain responses in an abstract way and named their approach a Program for Biological System Analysis. They tried to show, based on existing neurophysiological data, what particular neural responses could give rise to general transfer functions. The program was extended and modified in 1998 and designated the Brain Dynamics Research Program (Basar, 1976, 1980, and 1998). In the meantime, a number of other research groups applied some of the steps or the global concept of the program. In addition to the classical analysis tools of general systems theory, some supplementary experimental methods and methods based on the special natures of living systems are parts of this program.

We developed certain research principles or strategies that allowed us to add to our knowledge about brain functioning. In fact, every neuroscientist has his own surroundings and develops his own definitions and classifications of signals studied. This approach has helped to expand our knowledge of global brain dynamics and global brain functions as reflected by EEG and oscillatory brain responses. The main idea of how we can interact with the outside environment is to observe and then our brain percept what we observe according to the event and to hidden memorized information. After that we directly make a feedback and do an action in this environment. Figure 1.2 shows the cycle [7,8].

This cycle allows us to discover fundamental quantitative limits of the interaction of organisms with their environments. When the environment is approximately stationary, the efficiency of the perception action cycle is determined by the ability of the organism to extract and represent information

from the past that is biologically valuable for its future, in multiple time scales. This observation suggests an intriguing analogy between the combined perception and action, according to the observation and the recognizing of the past, our brains infer and predict unknowns figure 1.3 shows sensing predicting diagram [7].

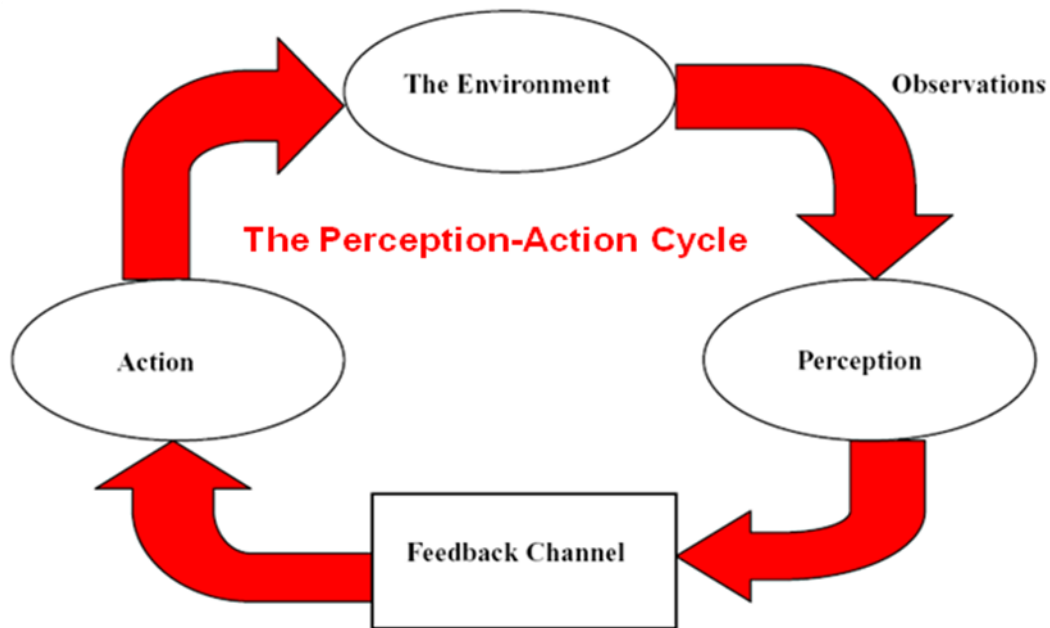


Figure 1.2 Perception Action Cycle

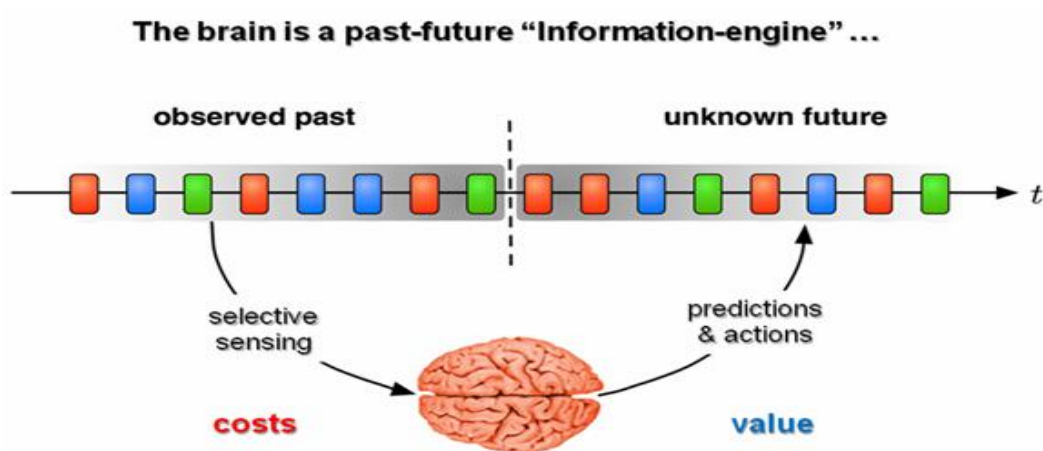


Figure 1.3 sensing predicting diagram

1.2 Thesis Objective

Neural activity can be broadly or particularly defined. It could be set to include all of the electrical, magnetically, chemical and biological events associated with it, which is, at the current scientific state-of-the-art, impossible to measure in a unified way. In the case of fMRI, it is very particularly defined, because the BOLD signal does not measure brain function directly. Rather, BOLD fMRI brain activation studies use brain perfusion as a proxy for brain function. Without making direct measurements of brain function means without measuring computations performed in neuronal cell bodies, action potentials traveling along axons, or neurotransmitter trafficking at synaptic junctions, these approaches take advantage of neuro-vascular physiological events like perfusion and oxygen metabolism that locally change the diamagnetic oxygen presence near neural activity. Specifically, BOLD fMRI sensitizes MRI acquisitions to the local decreases in deoxy haemoglobin due to reactive hyperemia [9,10] accompanying neuronal activation[11].

Schematic of the fMRI data structure and its acquisition process is shown in figure 1.4. Structured brain stimulus is applied to the participant and on each time-point a volume (cubes) of n images are taken and a 3D movie of the brain with sample time of TR is obtained. The obtained intensity 1D movie of each voxel and the applied paradigm are then used for function or dynamic representation algorithms. We will describe in detail which of those are related to functionality and other to dynamics or causalities.

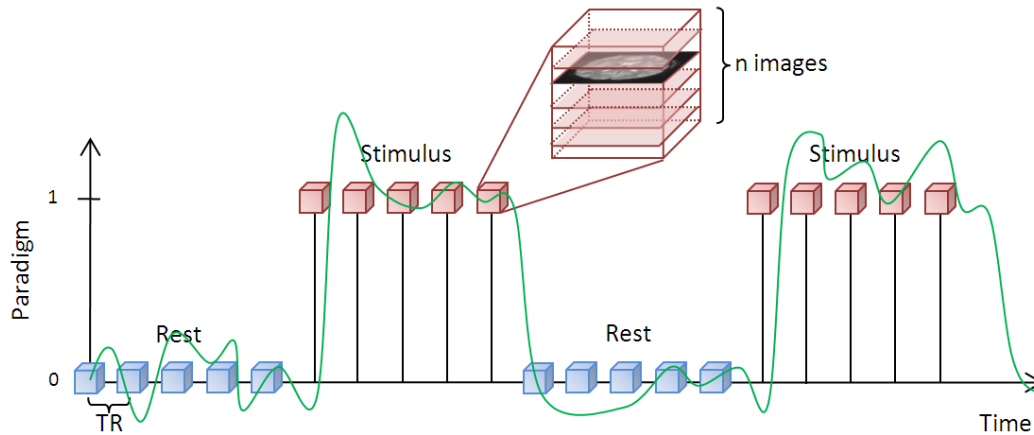


Figure 1.4: Schematic of the fMRI data structure and its acquisition process.

For BOLD FMRI, image data are typically acquired slice wise using single-shot echo planar imaging (EPI). A frequency-selective RF (Radio Frequency) pulse is applied in the presence of a static magnetic field gradient to selectively excite nuclear spins in a virtual slice; the slice-select gradient is then turned off, and the signals from these spins are encoded along the dimensions of the slice using rapidly switched magnetic field gradients. Within approximately 50 ms, a dataset is acquired, which, when Fourier transformed, will yield an image of the slice in question. This is rapidly repeated for all the slices as in figure 1.4, typically around 30 to 40 in the brain, such that a complete multi slice volume is built up within a Time of Repetition (TR), after which the process is repeated. For a typical TR of 3 s, if 200 volumes are acquired, then we have a volume movie consisting of 200 volumes of the brain, each consisting of 30 to 40 slices, we acquired over 600 s. During these 600 s, a neurobehavioral paradigm is played out in which the research participant is exposed to sensory stimuli or asked to perform some set of mental and motor tasks or some combination of them. So we have a situation where 600 s of temporally structured brain activity. These

activities like watching flashing lights every other 30 s, tapping one's fingers every other 20 s, or reading words. We are accompanied by the acquisition of a brain volume movie with 3 s temporal resolution, which core unit is the brain movie of each Volume Element (voxel) [12-15].

1.2.1 Brain Regions of Visual system

We applied all algorithms and methods to solve our problem to 4 regions of visual system. These regions [16-17] which we used to specify the interaction and connectivity between them are primary visual cortex. V1 is an atomically equivalent to Brodmann area. Visual area V5, also known as visual area MT (middle temporal), is a region of extra striate visual cortex that is thought to play a major role in the perception of motion, the integration of local motion signals into global percepts and the guidance of some eye movements. 4-Phenyl-4-(1-piperidinyl)-cyclohexanol, PPC, is an organic chemical which is often found as a metabolite of phencyclidine, the dorsolateral prefrontal cortex, DL-PFC or DLPFC, consists of the lateral portions of Brodmann areas and is connected to the orbitofrontal cortex. Its function is responsible for motor planning, organization, and regulation.

1.2.2 Brain Dynamics Representation

We propose a model that describes the interactions of several Brain Regions based on Functional Magnetic Resonance Imaging (fMRI) time series to make inferences about functional integration and segregation within the human brain. The method is demonstrated using dynamic causal modeling (DCM) augmented by Granger Causality (GC) using real data to show how such models

are able to characterize interregional dependence. We extend estimating and reviewing designed model to characterize the interactions between regions and showing the direction of the signal over regions. A further benefit is to estimate the effective connectivity between these regions. All designs, estimates, reviews are implemented using Statistical Parametric Mapping (SPM) and GCCA toolbox, one of the free best software packages and published toolbox used to design the models and analysis for inferring about FMRI functional magnetic resonance imaging time series.

Extracted time series planned to cover all possibilities of events applied to visual system, figure 1.5 shows block diagram and flow work our study. We will go through DCM in details in chapter three, we will use extracted time series for studied brain regions to infer causal relations easily. This can be done by applying Granger Causality, GC and Biclustering techniques to group time series with similar function of regions under applied condition; it will be described in chapter four.

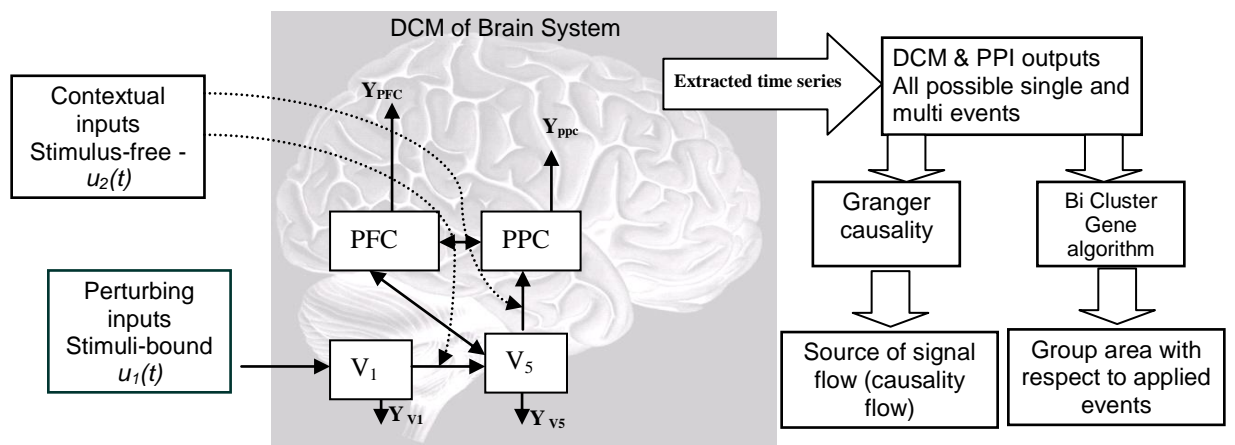


Figure 1.5, a schematic illustrating the concepts of DCM augmented by PPI and Granger Causality

What we introduced in our thesis is to assist in many perspectives. First is to solve problems relating to specific center in our brain. Second is to assist surgeon in his decision if the issue related to tumor or disease in specific region in the brain, also to make brain map for our brain behaviors under multiple conditions.

Finally, it can be used to read our minds and change bad believes and behaviors to the best, we used non invasive technique which may be expensive but will change to make our life happy when we change our culture beside save our health.

1.3 Thesis Organization

The organization of thesis chapters from chapter one to five based on describing and defining the problem and specifying the layout of thesis chapters in chapter one. Introducing background and the literature review of our idea based on fMRI images time series, all types of brain connectivity will be described in details starting from anatomical as a selector of a region of interest to be studied. Then we go through functional connectivity as a verifier for connection between regions if it is function or not, finally effective connectivity as a dynamic tester of connectivity between regions that tests if the target connection is effective or not under any condition, chapter three undertake the line from previous chapter in effective connectivity representing brain dynamic. Dynamic Causal modeling technique is one of the best models used in representing brain dynamics, using visual system in this model in different events to study and infer signal dynamic from region to another. DCM will be augmented by Psycho Physiological

Interaction, PPI, and will be added to each region during studying visual system by DCM. Chapter 4 will start from the extracted data of four regions of interest to of DCM to infer easily and directly the causality and signal path using Granger Causality GC and then will apply biclustering techniques.

1.4. Summary

We introduced and define the main idea of our work in this thesis, define the problem by introducing full description of the mechanism and structure of how neurons and brain regions interacts, we introduced thesis objective and in which fields of medical we can used and apply, and then put the plan and organization of thesis chapters.

Chapter 2

Background and Literature Review

In this chapter, we introduced the background and literature review of brain dynamic representation. We described general layout of brain dynamic history of different apparatus and methods in first section, in the next section we concentrated specifying and clarifying why we use FMRI as one of the best tools used since few years to infer brain dynamic locally and causally.

In the next following sections we introduced the role of attention and all types of brain connectivity, anatomical is the base for existing region and its connection to another, functional connectivity is the verifier for this existing of connection between region and another, finally effective connectivity is the best formalization of the human brain dynamic representation, we introduced the literature review. Starting from limitation of previous methods to complement with Dynamic Causal Modeling, DCM, we will specify and design DCM in the next chapter.

2.1. Human Brain Dynamic Representation Layout.

In the contrast, the phrenology school of the Viennese physician Thomas Gall argued that specific types of brain function were associated with particular regions of brain should be localized by palpating the overlying bumps on the skull surface. The notion that particular regions of the brain acted as specific functional modules formed the foundation for the concept of discreet cortical localization. The notion of cortical functional localization remains supported by current

science, although we now think more in terms of specific types of computational processes being performed by individual brain regions [book and two references [18-19].

Phrenology introduced the way to a different localized approach to mapping the mind based on lesion experiments and studies. Many scientists investigate from the observation that damage to different areas of the brain produced relatively specific deficits in patients by comparing it to normal one. One particularly well known 19th century example was a patient made famous by the eminent French neurologist Charcot and known to us as “Tan” because this was the only sound that he could utter. Charcot was impressed that Tan’s inability to speak was not associated with either mental deficiency, problems of movement, or impairment of language comprehension. When his patient finally died, Charcot found a single large tumor pushing on and damaging the lower left side of the front of the brain. He therefore hypothesized this area of the brain had a specific function for spoken language [20].

Although human lesion studies such as these provide valuable information concerning the brain regions necessary to perform a task, they are limited in several respects. Most lesions affect adjacent regions, making it difficult to interpret the results unequivocally. In addition, the presence of focal abnormal brain tissue may lead to changes in the functioning of adjacent normal looking tissue by indirect effects. For example, an expanding tumor could cause bruising of the adjacent brain tissue necessary for a specific task with subsequent

deterioration in brain function, the region occupied by the lesion itself not actually being necessary for task performance [19-21].

A completely new appreciation of the ways in which the brain becomes structurally specialized for sensation, cognition and direction of action is developing with use of the extraordinary ability of magnetic resonance imaging to resolve small changes in the healthy living brain that end up to change behavior. Surprisingly reminiscent of aspects of the recent theories, there are now intriguing examples of situations in which small local variations in brain shape were correlated directly change in brain function. For example, it has been reported that there is a relationship between the size of the brain region which controls hand function and the number of years of practice of a musical skill, suggesting that the structural variability in this brain region occurs as a consequence of experience or use rather than reflecting individual differences within the population [21]. Similarly, a recent study reported that London taxi drivers have an increased size of the part of the brain involved in the type of memory used for map reading [22]. The limitations of these cross-sectional studies however are that they do not allow us yet to conclude confidently that structural variation interact and affect behavior.

The firing of a neuron subsequent of an increase in synaptic input is a crucial neuronal event in dynamic system perspective. Whilst statistical techniques are crucial to the detection of synchrony and change in neuroscience data, the study of dynamics uniquely permits an understanding of their causes. Indeed, over recent decades, dynamical formulations of brain activity have

become sufficiently advanced to give rough outline to a unified theory of brain dynamics. Such a theory will also inform studies of brain connectivity. What is the origin of the brain's dynamic character? During the 20th century, extraordinary progresses add basic neurophysiological processes and their role in neural phenomena such as neuronal firing and action potential propagation. Incorporating these processes into a set of evolution equations yielded quantitatively accurate spikes and thresholds, leading to the Nobel Prize for Hodgkin and Huxley. These equations are based upon the physical properties of cell membranes and the ion currents passing through Transmembrane proteins [23].

Extending this theory from a patch of cell membrane to whole neurons and thence to populations of neurons in order to predict macroscopic signals such as the electroencephalogram (EEG) is a dominant focus in this field today. Linking neuronal dynamics to theories of cognition also remains a major goal. Dynamics has a spatial as well as a temporal character. All forms of information processing in neuronal systems understood as particular types of spatiotemporal dynamics and their trends. There was established a link between statistics and dynamics and proposals that provide putative network-based cognitive mechanisms with a biophysical underpinning. Attempts to employ dynamics to unify neurophysiological phenomena [24].

The advent of FMRI and other imaging technology has opened new perspectives of research examining how the brain functions at the macroscopic level. In recent studies, researchers treat each voxel as the basic unit of analysis,

within each voxel there lie perhaps tens of thousands of neurons that are connected into local networks, performing elementary computations that are fundamental to the brain's higher functions. Despite the existence of a large literature on neural network theory and models, it is focused on the relationship between network connectivity and dynamics at this level, with the hope that the principles uncovered here will be generally applicable to networks at larger scales as well [25].

2.2. fMRI as a Brain Investigator

Functional magnetic resonance imaging, fMRI, is a relatively recent imaging technique that is able to avoid some of the problems in the interpretation of lesion or purely structural imaging studies. It aims to determine the neurobiological correlate of behavior by identifying the brain regions or functioning modules that become active during the performance of specific tasks in vivo. In addition, the non-invasive and relative safety of the technique allow repeated studies to be carried out within a given subject so that important questions, such as the relationship between experience-dependent use and changes in brain structure or function can be addressed [14].

The Oxford physiologist Charles Sherrington made the observation that when a small area of exposed cat brain was stimulated electrically making the changes that occur when the region becomes active in thought, his increases the blood supply to the brain locally, ensuring an adequate supply of oxygen to regions working harder in thinking[15].

This effect can be used to precisely map areas of the brain involved in brain function. The local increase in energy requirements arising as a consequence of neuronal firing is largely met through an increase in oxygen-based metabolism with the increased demand for oxygen being delivered seconds later by an increase in the local blood flow, the hemodynamic response [26-28].

If the MRI experiment is done while a mental task is given to a subject, a so-called functional magnetic resonance image (fMRI) image is generated, from this changes from image to another we can see how different tasks activate different parts of the brain relatively specifically. When we listen to music, for example, a specialized area in the so-called auditory cortex along the sides of the brain shows increased signal [23]. Vision activates a region in the back of the brain the occipital cortex, localized precisely to regions of the visual field [23] as shown in figure 2.1. Touch brings increased signal along the side of the brain, particularly in the side of the brain opposite to the part of the body that is touched and movements activate regions in the front and the top of the brain in cortex specialized for motor control [23].

On the basis of the differences in timing activation in the brain, the areas responsible for hearing (in the middle of the brain in grey) and vision (in the back of the brain in white) could be localized by functional magnetic resonance imaging (fMRI) (Image courtesy of Dr. S. Smith from www.fmrib.ox.ac.uk).

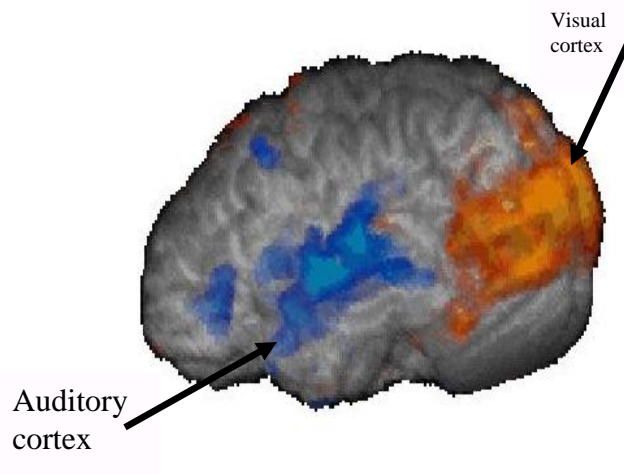


Figure 2.1 brain activation for two areas in the brain under specific event related to these regions [53].

FMRI therefore is able to identify the brain regions that become more active during specific task performance. However, there are several caveats to interpretation of the increase in FMRI signal. It is likely that the magnitude and extent of the hemodynamic response is a measure of more than a single energy-requiring process. It may reflect not only the frequency of local excitatory synaptic input, but also the extent of the post-synaptic depolarization neuronal firing [24-28].

FMRI is one of the most advanced functional neuro imaging techniques for mapping brain activation. The technique is commonly used for research purposes in healthy subjects as well as for medical diagnosis of diseases and provides high-resolution images of neural activity out of the detected blood oxygen level dependent BOLD signal [29-32]. Combining several such 3 dimensional images produces a time series for each voxel volume element which reflects the hemodynamic response of this voxel. This response is associated with

neural activity as higher levels of oxygen is supplied to active regions in order to constitute energy source for the firing neurons in those regions. The spatial resolution of fMRI images is around $\sim 1\text{mm}^3$ while the temporal resolution is in the order of seconds, which is about three orders of magnitude larger than the time scale of neuronal events. The result is brain functionality map, which goes beyond the capabilities of traditional anatomical based techniques and helps to understand the brain organization [15].

The fMRI technique is based on the phenomenon that neural activity in the brain leads to increasing blood flow in the vasculature of the active regions. The immediate result is a local reduction in deoxyhaemoglobin since oxygen extraction remains stable at that time [33]. This reduction affects the T2* weighted magnetic resonance image signal because the deoxyhaemoglobin, which is considered the source of the fMRI signal, is a paramagnetic protein [34-35]. This enables to observe brain functions in noninvasive manner and without the use of any exogenous contrast enhancing agent on a clinical strength (1.5 T) scanner [36-39] using the appropriate imaging sequence. The ability to observe human brain functional activity using the fMRI signal was certified as this technique approved some known anatomically distinct processing areas in the motor cortex [40-41] visual cortex [42], and Broca's area of speech [43]. Other studies show significant correlation between fMRI and conventional EEG in locating some specific functionality regions in the human brain [44-45]. This leads to growing number of research center that adopt fMRI techniques following increasing number of studies in that area.

However, while the fact that changes in BOLD signal are well correlated with changes in blood flow is commonly accepted the precise relationship between neural signals and BOLD is still under active research [45].

Comparing to other brain activity imaging techniques, fMRI has some significant advantages, for example: Noninvasive technique as there is no need for injection of exogenous contrast enhancing agents. For comparison, the earlier positron emission tomography method (PET) does demand the injection of some radioactive isotopes [46].

Various methods of fMRI analysis have been implemented, as individual research centers develop their own unique methods to acquire and process the fMRI data. This leads to the status in which there is no standard method for either research or clinical use. there are few software packages number of toolboxes applied are more, these packages are FSL[47-48], SPM [49], AFNI [50-51], and Brain Voyager which are used by most of the research centers. None of those packages defines single specific method but a collection of few different techniques; in details we introduced survey of these packages in Appendix A.

Common analysis contains three main stages. The first preprocessing step tries to enlarge the SNR (signal to noise ratio) in order to improve the ability to detect the activation events versus false changes in the signal due to some artifacts. The preprocessing may include registration of the images (each image taken on different time) in order to correct head movements, spatial smoothing of the data, and temporal smoothing. Second step is statistical analysis which highlights the voxels that response to the stimulus. Third step is calculating the

probability values, which indicate the statistical confidence, and displaying the activation images [45].

The activation images are usually produced by overlaying anatomy image taken by structural MRI with activation map which colors only the activated regions. The color of each pixel represents the level of confidence that the corresponding voxel is an active one and usually only those that reach some threshold are actually colored the rest keep their original structural color.

The role of attention

Attention, as well as working memory, is often thought to require a workspace of interconnected brain areas. According to the global workspace model, conscious awareness is not possible without attention (Dehaene & Naccache, 2001; Dehaene et al., 2006). When a stimulus is not attended, then this stimulus will be processed subliminally or pre-consciously, but it will never be consciously perceived as shown in figure 2.2. Whether or not the presentation of a stimulus results in conscious awareness therefore depends on two factors: the bottom-up stimulus strength (i.e. the loudness of a sound) and whether or not top-down attention is directed towards the stimulus.

According to Dehaene et al. (2006), there are three levels of processing: subliminal, preconscious and conscious. At what level a stimulus is processed depends on the the bottom-up stimulus strength (on the vertical axis at the left) and the amount of top-down attention on the horizontal axis. Colored circles indicate the amount of activation in local areas. Interactions between local areas are depicted by the small arrows. Top-down attentional control, either towards the

stimulus or away from it, is illustrated with the large arrows. Some states lie on a continuum, as depicted by the dashed curves. The thick lines with separators indicate that there is a sharp transition between the states.

When a stimulus is of sufficient strength and attention is focused towards the stimulus, then this stimulus will be consciously perceived. For this to occur, bottom-up activation in the early visual areas should exceed a dynamical threshold in order for a self-amplifying system to get into action. This means that as soon as the activation exceeds the threshold, feed forward activity is propagated towards higher order areas (figure. 2.2, bottom right). This then triggers large-scale activation in many brain areas within the global network, including the frontal and parietal areas. These higher order areas also send back recurrent activation towards the lower areas, which keeps the information active within the entire network [53].

The coherent activity in all these areas results in a conscious, unitary and reportable experience of the stimulus. This experience can last longer than the presence of the stimulus that triggered the experience, as the information is maintained in the network and thus in working memory[54].

When presented stimuli are not attended and they elicit little bottom-up activation, then the stimuli are processed subliminally. In this case the stimulus is of insufficient strength to exceed the threshold and activate the self-amplifying system (figure. 2.2, top left). Thus activation quickly dies out, does not enter working memory and the stimulus is unnoticed. However, subliminal processing can also occur when stimuli are attended. In this case, despite top-down attention,

bottom-up activation is too low to exceed the threshold that results in widespread activation figure.2.2, top right. Pre-conscious processing occurs when there is potentially enough bottom-up activation for a conscious experience, but there is a lack of top-down attentional activation figure. 2.2, bottom left.

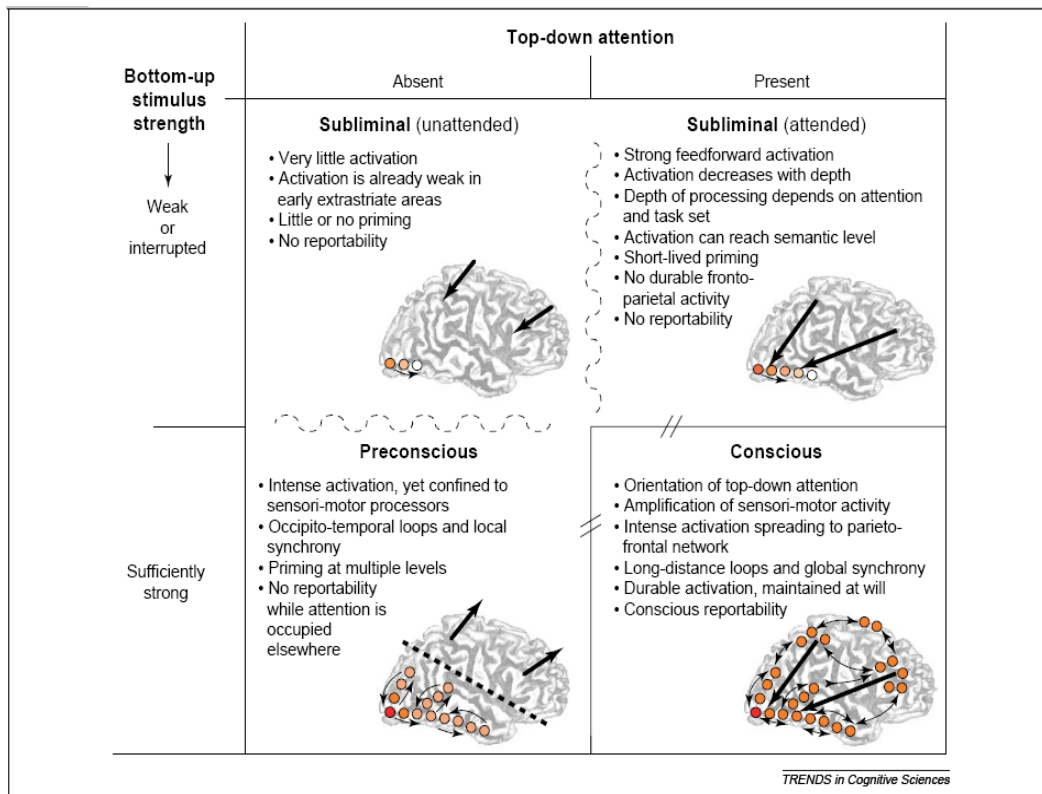


Figure 2.2: The relation between attention and consciousness [61].

Due to this, feed forward and feedback processing only occurs in the lower sensory areas, but does not result in widespread activation to the frontal and parietal areas and long-distance synchrony. The difference between subliminal and pre-conscious processing is that preconscious activation has the potential to result in conscious awareness, once attention is directed towards the stimulus, while subliminal activation cannot. Pre-conscious information is kept active for a few hundred milliseconds in a sensory buffer. If during this brief period attention

is directed towards this information in the sensory buffer, then the activation caused by the stimulus can still be enhanced by attentional activation, thereby exceeding the activation threshold and resulting in conscious perception[54].

The difference between attention and consciousness is a widely discussed topic. From the above description it follows that attention does not automatically result in conscious awareness. On the other hand, an important aspect of the global workspace model is that there cannot be conscious awareness without attention (Dehaene et al., 2006). Attention and consciousness are therefore two intimately linked, but nonetheless distinct processes. Some however, argue that conscious awareness can occur without attention (Lamme, 2004; Koch & Tsuchiya, 2008). Arguments in favour of this are generally in line with arguments in favour of regarding phenomenal experiences as consciousness, as described above (Block, 2005). Such experiences are never reportable and are therefore not considered as conscious. In chapter 4, evidence of recurrent processing and synchronisation will be discussed, that some regard as proof that pre-conscious experiences are conscious. One way to circumvent the discussion of whether attention is required for conscious awareness is to argue that cognitive control, attention, working memory and consciousness are fundamentally the same processes (Maia & Cleeremans, 2005). Information is not processed in separate modules (on a local scale), but instead on a more global scale. Under the influence of prefrontal processes some of this global information is enhanced (biased) and becomes conscious. This information is then sustained in working memory and is attended. Consciousness, working memory, attention and cognitive control are all

mere dynamics of this global competition. This idea is not so different from the global workspace model. In both cases consciousness arises from the dynamic global integration of information. By looking into other theories of information integration, we can investigate if the global workspace model is a suitable model to explain the neural processes that are required for conscious experiences.

2.3 Human brain connectivity's types

Neural connections of the mammalian cerebral cortex exhibit specific patterns ranging in scale from interconnections linking whole brain regions to intra areal patterns of connections between cell populations or individual cortical neurons (Cajal, 1909; Brodmann, 1909; Zeki, 1993; Salin and Bullier, 1995; Swanson, 2003). Detailed anatomical and physiological studies have revealed many of the basic components and interconnections of cortical microcircuitry (Douglas and Martin, 1991), and of their arrangement into columns and minicolumns (Mountcastle, 1978; 1997). Columns and other localized populations of neurons maintain connections within and between brain regions, constituting large-scale patterns of anatomical connectivity. While the large-scale networks of human cortex remain largely unmapped (Sporns et al., 2005), comprehensive descriptions of anatomical patterns of cortical connectivity have been collated for several other mammalian species (e.g. Felleman and Van Essen, 1991; Scannell et al., 1999). Closer analysis has revealed that these patterns are neither completely regular nor completely random, but combine structural aspects of both of these extremes (reviewed in Sporns et al., 2004).

This basic insight has sparked significant interest in characterizing the structure of brain networks, using methods that are also applied in parallel efforts to map and describe other biological networks, e.g. those of cellular metabolism, gene regulation, or ecology. This chapter is intended as an overview of recent quantitative approaches to brain networks (see also Sporns, 2005), with an emphasis on theoretical and computational studies that inform us about the structural features that determine functional brain dynamics [23,55].

Anatomical and functional segregation refers to the existence of specialized neurons and brain areas, organized into distinct neuronal populations grouped together to form segregated cortical areas.

The term connectivity has multiple meanings, a fundamental distinction is that between structural, functional and effective connectivity, anatomical connectivity is the set of physical or structural synaptic connections linking neurons within the network, as well as their associated structural biophysical attributes encapsulated in parameters such as strength or effectiveness. Anatomical connections range in scale from local circuits to large-scale networks of inter-regional pathways.

Functional connectivity describes patterns of deviations from statistical independence between distributed and often spatially remote neuronal units, measuring their correlation/covariance, spectral coherence or phase-locking. It is highly time-dependent on a scale of hundreds of milliseconds and does not make any explicit reference to causal effects or an underlying structural model [56-58].

Effective connectivity describes the network of causal effects of one neural system over another and can be inferred experimentally through perturbations or time series analysis. Unlike functional connectivity, effective connectivity is not model-free, but usually requires the specification of a causal model including structural parameters [23].

The relationship between anatomical, functional and effective connectivity in the cortex currently represents one of the most significant challenges to computational cognitive neuroscience. An emerging view suggests that structural connection patterns are major determinants of the functional dynamics of cortical circuits and systems, as captured by functional or effective connectivity [59].

2.3.1. Anatomical Connectivity

Neural connections of the mammalian cerebral cortex exhibit specific patterns ranging in scale from interconnections linking whole brain regions to intra areal patterns of connections between cell populations or individual cortical neurons (Cajal, 1909; Brodmann, 1909; Zeki, 1993; Salin and Bullier, 1995; Swanson, 2003). Detailed anatomical and physiological studies have revealed many of the basic components and interconnections of cortical micro circuitry (Douglas and Martin, 1991), and of their arrangement into columns and mini columns (Mountcastle, 1978; 1997). Columns and other localized populations of neurons maintain connections within and between brain regions, constituting large-scale patterns of anatomical connectivity. While the large-scale networks of human cortex remain largely unmapped (Sporns et al., 2005), comprehensive descriptions of anatomical patterns of cortical connectivity have been collated for

several other mammalian species (e.g. Felleman and Van Essen, 1991; Scannell et al., 1999) [62].

Anatomical connectivity is the set of physical or structural (synaptic) connections linking neurons within the network, as well as their associated structural biophysical attributes encapsulated in parameters such as strength or effectiveness. Anatomical connections range in scale from local circuits to large-scale networks of inter-regional pathways. Their physical pattern may be thought of as relatively static at shorter time scales (seconds to minutes), but may be plastic or dynamic at longer time scales (hours to days), for example during learning or development [23].

In the brain, the mapping of functional deficits to underlying structural perturbations is experimentally challenging, but essential for a more complete understanding of brain damage and recovery. It is currently unknown which structural measures best capture the potential effects of vertex or edge lesions, although candidate measures of edge vulnerability (Kaiser and Hilgetag Kaiser, 2004) have been defined and have led to the identification of edges whose loss most affects global structural measures. Such edges often correspond to “bridges”, i.e. edges linking segregated clusters of brain regions. The issue of defining measures of robustness or vulnerability in brain networks is conceptually linked to the problem of objectively defining the functional contributions of individual network elements (Keinan et al., 2004)[64].

Finally, we should note that measures of structural, functional and effective connectivity increasingly intersect, as in the analysis of functional or

effective connectivity patterns as graphs (Dodel et al., 2002; Salvador et al., 2005a; Eichler, 2005). Applications of connectivity analyses to EEG, MEG and fMRI data sets have been reviewed in several other chapters in this volume (Ferec and Nunez, 2007; Darvas and Leahy, 2007; Bressler and McIntosh, 2007). Essentially, patterns of cross-correlation or coherence can be conceptualized as undirected graphs with edges that represent the existence and, in some cases, the strength of the statistical relationship between the linked vertices. Studies of patterns of functional connectivity (based on coherence or correlation) among cortical regions have demonstrated that functional brain networks exhibit small-world (Stam, 2004; Salvador et al., 2005b; Achard et al., 2006; Salvador et al., 2007) and scale-free properties (Eguiluz et al., 2005), possibly reflecting the underlying structural organization of anatomical connections. For example, it is an open question if nodes in structural and functional neuronal connectivity matrices maintain similar patterns of connectivity and exhibit similar local properties such as clustering [65].

2.3.2. Functional Connectivity

Functional connectivity is defined as the correlations between spatially remote neurophysiological events [68]. This definition provides a simple characterization of functional interactions and it is a statement solely about the observed correlations and not on how these correlations are mediated.

fMRI analysis techniques focus on revealing regions which are activated under those behavioral conditions, rather than characterizing the networks involved in the generation of those behaviors. Thus, with respect to localization

assumptions, these studies are analogous to lesion analysis studies and incorporate some of the same limitations. Because the information in the brain is kept as dynamic networks (similar to artificial neural networks), describing the brain activity solely by highlighting the activated regions clearly illustrates only part of the significant information. Another disadvantage that those methods have is the need to generate the expected response to the stimulus, which is only an estimation of this response which leads to imprecision in the results[68].

Since the mid of 1990s, functional connectivity study using fMRI has drawn increasing attention of neuroscientists, computer scientists and neurophysiologists, since it opens a new window to explore functional network of human brain with relatively high resolution.

Methods used for functional connectivity analysis via fMRI are generally grouped into two types: model-based methods and data-driven methods. Model-based methods such as cross-correlation analysis (CCA) are based on prior knowledge. Since they are easy to implement and interpret, model-based methods are widely used. Data-driven methods (either based on clustering or decomposition), however, need no prior knowledge. Thus, it is quite useful for resting-state fMRI studies where no prior information about the spatial or temporal pattern. Figure 2.3 clarifies the discrimination for all different types of methods applied in functional connectivity [69].

Although interesting research findings about functional connectivity detection with fMRI viewed in the literature, as far as we know, there are few dedicated reviews on methods for functional connectivity investigation with

FMRI. Therefore, this section aims to provide such a review. We will focus on the methods for detecting functional connectivity with FMRI [70].

2.3.2.1. Model-Based Models

All best and applied methods applied to infer functional connectivity are model-based. That is, these methods select some regions of interest ROIs, as so-called seeds, and determine whether other regions are connecting to these seeds by defining certain metrics, and thereby generate the connectivity map of human brain[71].

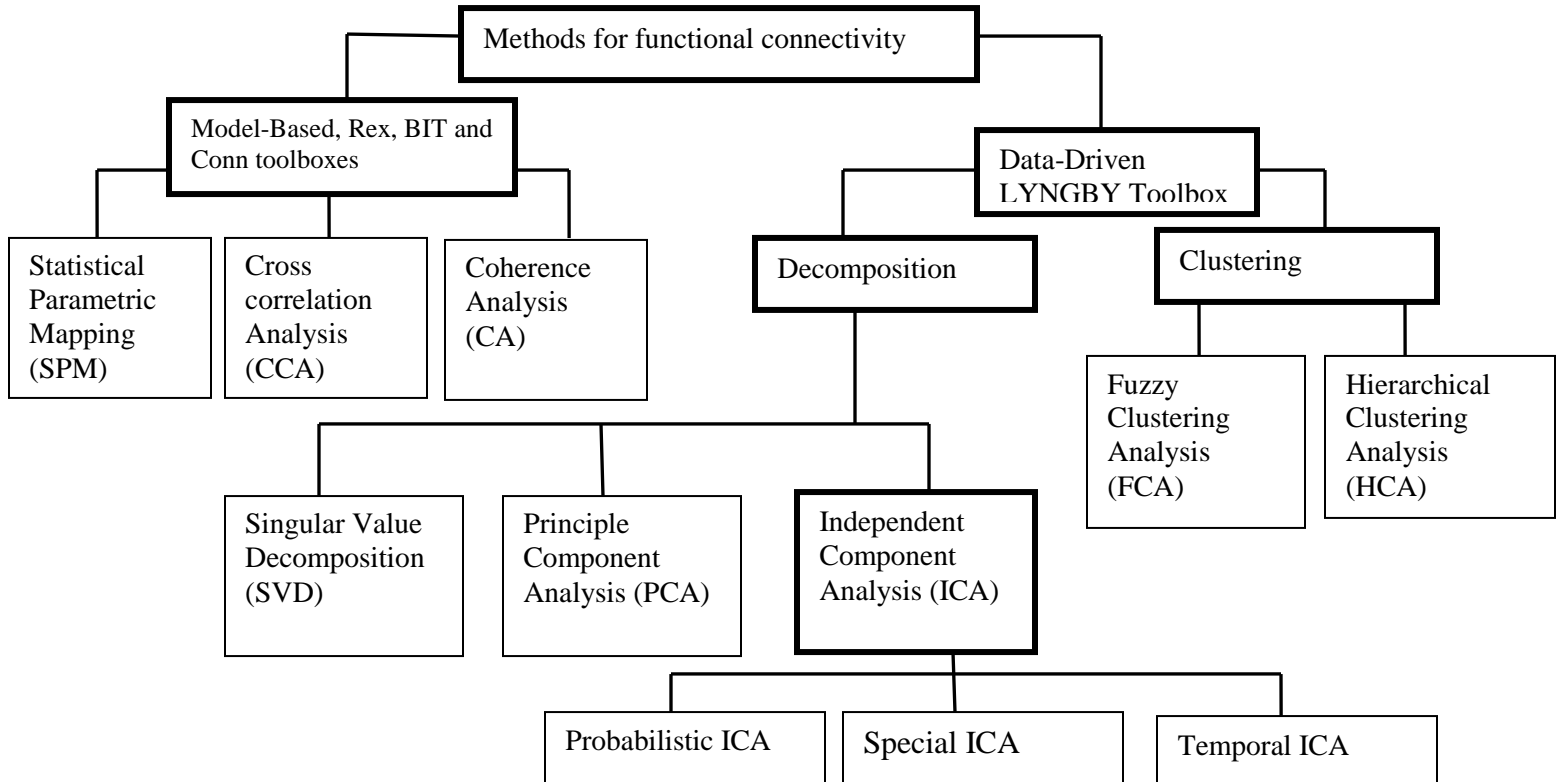


Figure2.3. Methods used for functional Connectivity, modified [71]

These methods are typically depending on strong prior neuroscience knowledge or experience. According to the metrics used as connectivity

measurement, we will review these methods in the following subsections and introduce review for current toolboxes applied based on these methods [71].

2.3.2.1.1. Cross-Correlation Analysis, CCA

Cross-correlation analysis is a mature technique that has been widely used in many fields. Cao and Worsley introduced this technique into fMRI study in Ref. [72]. Intrinsically, if one part of brain is functionally connected to a certain seed, there should be correlation in terms of their BOLD time courses. For a fMRI BOLD time course $F_x(k)$ and a seed $F_y(k)$ (which is also a time course), CCA estimates the correlation at lag μ as:

$$\text{Corr}_{x,y}(\mu) = \frac{\text{Cov}_{x,y}(\mu)}{\sqrt{\text{Var}(x) \times \text{Var}(y)}} \quad (2.1)$$

where $\text{Var}(x)$ and $\text{Var}(y)$ are the variances of $F_x(k)$ and $F_y(k)$, respectively; $\text{Cov}_{x,y}(\mu)$ is the cross variance of $F_x(k)$ and $F_y(k)$ at lag μ :

$$\text{Cov}_{x,y}(\mu) = E\{((F_x(k) - E(F_x)) \times (F_y(k) - E(F_y)))\} \quad (2.2)$$

and E means the expected value, and $E(F_x)$ and $E(F_y)$ are the expectation or the mean of $F_x(k)$ and $F_y(k)$, respectively. If $\text{Cov}_{x,y}(\mu)$ is above a certain threshold, we consider that the two BOLD time courses $F_x(k)$ and $F_y(k)$ are functionally connected. The hemodynamic response of blood makes full-lag-space calculation of cross-correlation unnecessary. Although the hemodynamic response function (HRF) varies across different subjects or even across different brain regions of the same subject, the duration of HRF is limited. That is, it will return to baseline after limited time, which is a few dozen seconds in general [15-16, 73]. Thus, people generally need to compute the correlation with a time window of a dozen time points or so (the exact number depends on the TR of

FMRI scan). In fact, many cross-correlation studies compute only the correlation with zero lag.

2.3.2.1.2. Coherent Analysis, CA

While CCA used for FMRI data analysis on both model-based and resting-state dataset, using correlation at zero lag as the connectivity measurement has been controversial [74]. First, correlation is dependent and sensitive to the shape of HRF, which has been reported to vary cross different subjects and different brain regions. Second, high correlation can be detected between regions that actually have no blood flow fluctuations. Over changes from noises such as cardiac activity and blood vessel activity in the brain would also lead to change correlation [75]. To overcome these problems, a new metric called coherence is proposed by Sun et al. [76]. Coherence is the spectral representation of correlation in frequency domain. For the same time courses $F_x(k)$ and $F_y(k)$ defined in Eq. (1), the coherence is expressed as:

$$\text{Coh}_{x,y}(\lambda) = \frac{\|F_{x,y}(\lambda)\|^2}{F_{x,x}(\lambda)F_{y,y}(\lambda)} \quad (2.3)$$

Where $F_{x,y}(\lambda)$ is the cross spectrum, defined by the Fourier transform of the cross covariance as follows:

$$F_{x,y}(\lambda) = \sum_{iu} \text{Cov}_{x,y}(u) \times e^{-j\lambda u} \quad (2.4)$$

And $F_{x,x}(\lambda)$ is the power spectrum, so is $F_{y,y}(\lambda)$. They are defined as:

$$F_{x,x}(\lambda) = \sum_{iu} \text{Cov}_{x,x}(u) \times e^{-j\lambda u} \quad (2.5)$$

$$F_{y,y}(\lambda) = \sum_{iu} \text{Cov}_{y,y}(u) \times e^{-j\lambda u} \quad (2.6)$$

The expression of correlation in frequency domain enables researchers to study time course relationship in a natural and intrinsic way. For example, blood

flow fluctuations usually have a period of 10 s or so. Thus, the coherence at low frequency below 0.1 Hz is particularly related to functional connectivity; while cardiac activity usually works at a frequency of around 1.25 Hz, thus, coherence at this frequency band may arise from the cardiac activity instead of real frequency of functional connectivity.

2.3.2.1.3. Statistical Parametric Mapping, SPM

Statistical parametric mapping (SPM) is a model-based method based on e activation patterns induced by cognitive tasks in FMRI. Over the years, SPM has come to refer to the conjoint use of the general linear model (GLM) and Gaussian random field (GRF) theory to make classical inferences about spatially extended data through statistical parametric maps. SPM uses GLM to estimate the parameters that could explain the data and uses GRF to resolve the multiple comparison problems in making statistically powerful inferences. SPM will be described in details in the section of toolbox [77].

SPM methodology has been recently used for functional connectivity detection, with resting-state FMRI dataset by Greicius et al. [77]. After scaling and filtering steps across all brain voxels, this method averages the voxels in certain seed, and considers it as a covariate of interest in the first-level SPM analysis. Then contrast images corresponding to this repressor were determined individually for each subject and entered into a second-level random effect analysis, in order to determine the brain areas that show significant functional connectivity across subjects.

The essence of this method is to mimic a stimulus based on the selected seed, and uses it in the same way as the real stimulus in cognitive tasks is, since there is no designed cognitive activity in resting-state FMRI study. The modeling and statistical reference are the same with those in SPM [77].

Seeds-based methodology renders the detected functional connectivity sensitive to seed selection [78-79]. It is common that different seeds would lead to detection of different connectivity. Secondly, the requirement for prior knowledge constrains the exploration of possible functional connectivity. With priors-based method, one may only focus on brain regions related to the prior knowledge, and neglect other parts or functions of brain. Therefore, the full exploration of brain goes beyond the capability of this type of methods, and might need data-driven methods such as decomposition analysis and clustering analysis [paper].

2.3.2.2. Data-driven Methods

To overcome the limitations of model-based methods, analysis methods that are independent of prior information or assumed model have been implemented. There are generally two types of data-driven methods for functional connectivity detection, decomposition-based analysis and clustering analysis.

2.3.2.2.1. Decomposition-based methods

Decomposition-based techniques are principal component analysis (PCA), singular value decomposition (SVD) and independent component analysis (ICA). This type tries to express the original FMRI dataset as a linear combination of basis vectors (PCA/SVD) or statistically independent components (ICA).

2.3.2.2.1.1. PCA/SVD

Principal component analysis, PCA, and singular value decomposition, SVD; The core of PCA/SVD is to represent the observed fMRI time courses X with a combination of orthogonal contributors, it is shown figure 2.4. Each contributor is made of a temporal pattern (a principal component) multiplied with a spacial pattern (an eigen map). Mathematically, the SVD of X (T time points \times N voxels) is:

$$X = USV^T = \sum_{i=1}^p S_i U_i V_i^T \quad (2.7)$$

where the S_i is the singular value of X ; U_i is the i th principal component; and V_i is the corresponding eigen map; p is the number of chosen components.

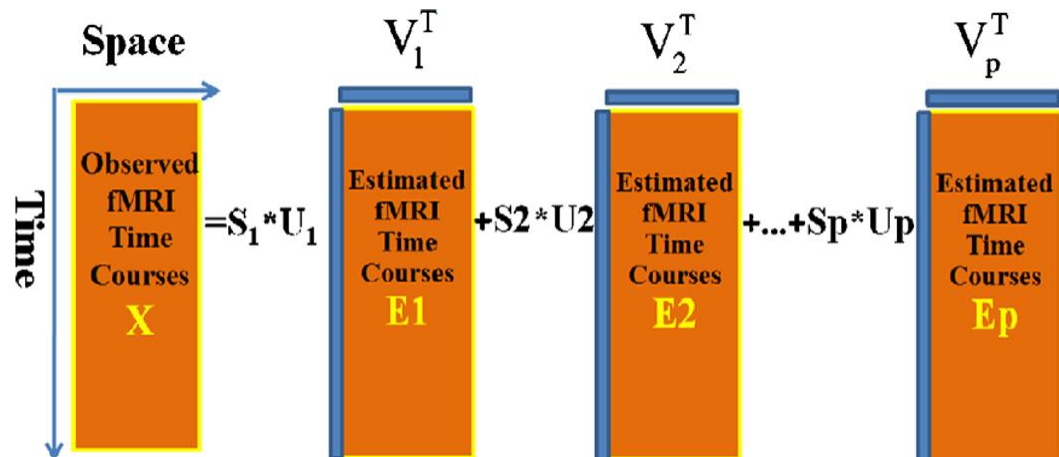


Figure 2.4 Illustration for decomposition of a fMRI dataset X using SVD. S_i is the singular value of X ; U_i is the i th principal component; and V_i is the corresponding eigen map; p is the number of chosen components [71].

2.3.2.2.1.2. Independent component analysis

Independent component analysis is a recently developed popular method for functional connectivity detection. Since it needs no prior information about the spatial or temporal patterns of source signals, ICA is well suited for resting-state fMRI study. Therefore, there is increasing interest in applying ICA algorithm to resting-state fMRI study for functional connectivity detection.

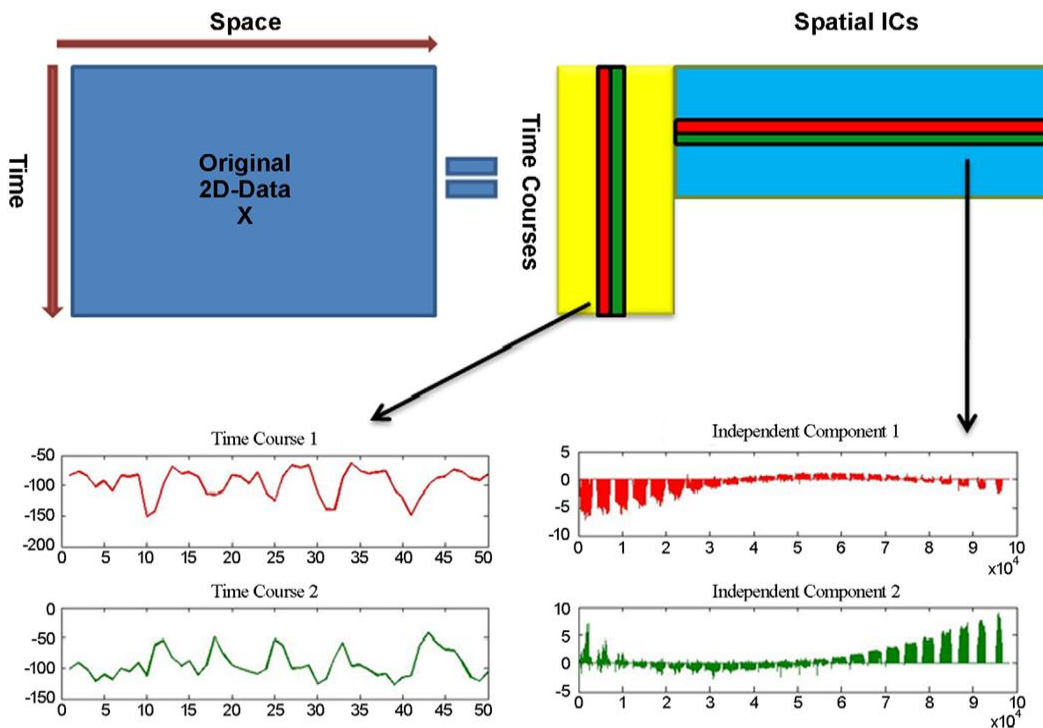


Figure 2.5 illustrates the decomposition of a fMRI dataset using a certain type of ICA

As shown in figure 2.5, Independent Component Analysis specifies the decomposition of a fMRI dataset with spatial ICA to be exact. Like PCA/SVD, ICA seeks to find a linear combination of components. The difference is that ICA would find components that are as statistically independent as possible [80], while PCA/SVD would find orthogonal components. For fMRI data X (T time points \times N voxels), the ICA model can be expressed as:

$$X = AC = \sum_{i=1}^N A_i C_i \quad (2.8)$$

where C_i is the i th underlying signal source (IC component); A is the mixing matrix with a dimension of $T \times N$. Different sources are independent from each other:

$$P(C_1, C_2, \dots, C_N) = \prod_{i=1}^N P(C_i) \quad (2.9)$$

Here, $P(C_i)$ is the probability of the i th underlying signal source. Denoting W as the pseudo reverse of A (W also called un mixing matrix), we can obtain the independent components (ICs) simply by:

$$C = WX \quad (2.10)$$

Very similar to PCA/SVD, ICA decomposes the original time sources into independent component components statically independent and corresponding IC maps that measure the correlation. By thresholding these IC maps, one would obtain the connectivity maps with corresponding underlying sources as specified in figure 2.6.

According to whether to decompose the data into spatially independent components and spatially independent time course (sICA), or temporarily independent components and temporarily independent time course (tICA), ICA could be divided into spatial ICA (sICA) and temporal ICA (tICA). Then the question is which type one should choose for functional connectivity detection.

Since the introduction of ICA into fMRI study [81], both sICA and tICA have been widely used. However, the criterion for which one to use seems to be task dependent.

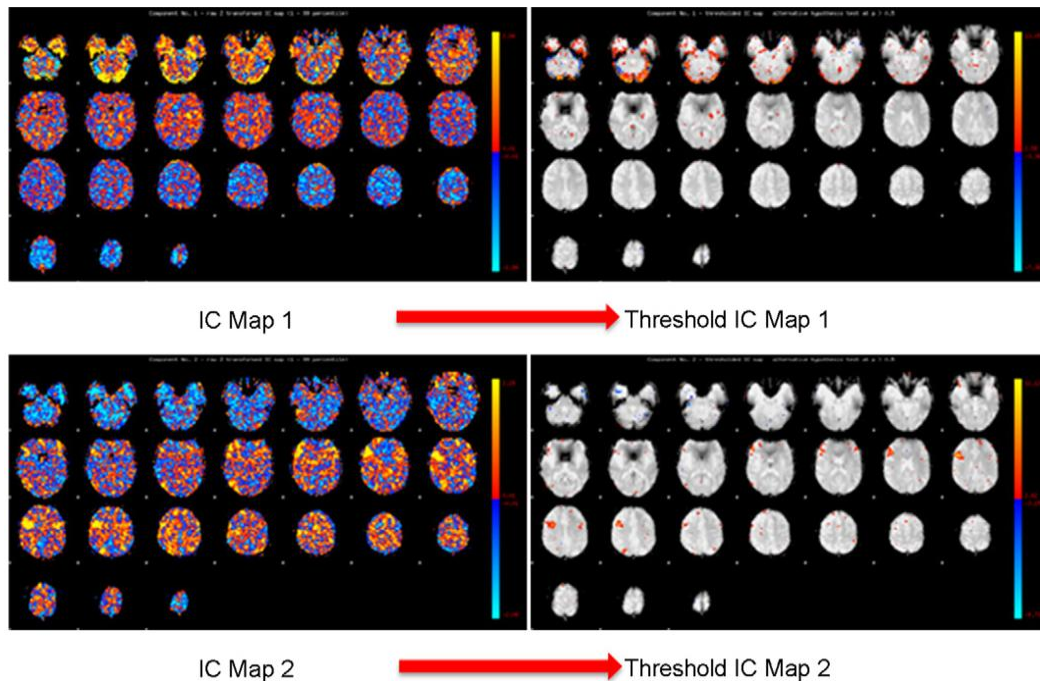


Figure 2.6 Independent component (IC) maps thresholding. IC map1 and IC map2 are 3D representation of IC 1 and IC 2 in

Researchers reported that sICA and tICA can have diverging results, depending upon the characteristics of the underlying signals to be estimated [81]. If the underlying signals are spatial correlated but not temporarily, one may want to choose tICA instead of sICA since sICA would probably not yield the correct activation pattern if the null spatial correlation is strongly violated, and vice versa for tICA.

Despite the increasing popularity of applying ICA algorithm to fcMRI study, especially on resting-state fMRI data, there are some pitfalls that need mentioning.

Firstly, ICA is grounded on the assumption of components (signal sources) independence, whether spatially or temporally. Violation of this assumption would decrease the effectiveness of ICA considerably [81].

Secondly, how to choose the number of independent components and how to threshold the IC maps have become open questions. Ma et al. studied these questions and concluded that when the number of ICs is smaller than that of the source signals, ICA results become highly dependent on the number [79]. Actually, thresholding IC maps directly is difficult. In practice, it is common to convert an independent map with a non-Gaussian distribution into a z-map with a Gaussian distribution [80-81]. Ma et al.'s results show that the z-map conversion tends to overestimate the false-positive rate (FPR)[79]. This overestimation, however, is not very severe and may be acceptable in many cases.

Last but not least, ICA is a noise-free generative model. The observed fMRI datasets are completely explained by the source signals contained in matrix C and the mixing matrix A , and thus precludes the assessment of statistical significance of the source estimates within the framework of null-hypotheses. To solve this problem, Beckmann et al. recently developed a new model called probabilistic ICA or pICA, which assumes that the observed p -dimensional time series are generated from a set of q ($q < p$) statistically independent non-Gaussian sources (spatial maps) via a linear and instantaneous 'mixing' process corrupted by additive Gaussian noise $\eta(t)$:

$$X_i = AS_i + \mu + \eta_i \quad (2.11)$$

Here X_i refers to the p -dimensional column vector of individual measurements at voxel location i ; A is mixing matrix; S_i denotes the q -dimensional column vector of non-Gaussian source signals contained in the data;

μ is constant part; and η_i denotes Gaussian noise $\eta_i \sim N(0, \sigma^2 \Sigma_i)$. For more information about pICA, please refer to [82].

2.3.2.2.2. Clustering Analysis

Clustering analysis methods have been widely used in FMRI study to find the activity patterns. These methods include fuzzy clustering analysis, vector quantization, self-organizing maps, and neural gas network [82-83]. The primary goal of clustering analysis in FMRI study is to partition the data into different clusters based on the intensity proximity of the time course. Time courses that are close enough are considered to be in one cluster.

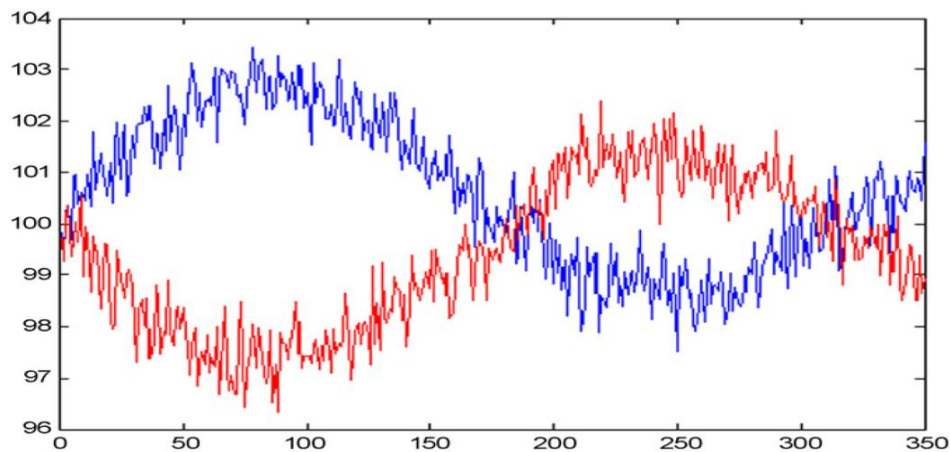


Figure 2.7 Two illustrative signals that are highly correlated (the correlation coefficient is -0.8824). However, the intensity distance is considerable [79].

However, clustering analysis based on intensity proximity is not enough for functional connectivity detection in Functional connectivity, FC, of FMRI study as shown in figure 2.5, Instead of characterizing the distance by intensity proximity, clustering methods in FC of FMRI study often use the similarity between time courses as the distance measurement [83].

2.3.2.2.2.1. Fuzzy clustering analysis

Fuzzy c-means (FCA) is a clustering analysis method which allows fuzzy partition of the dataset. The main idea behind it is the minimization of an objective function, which is usually defined as the total distance between all patterns and their cluster centers:

$$J(M, C) = \sum_{i=1}^{i=N} \sum_{j=1}^{j=N} M_{ij}^{\phi} D_{ij}^2 \quad (2.12)$$

Here, M_{ij} is a metric which measures the probability of voxel i belongs to cluster j ; D_{ij} is the distance between voxel i and the centroid C_j of cluster j ; N is the number of voxels of brain; K is the number of initial clusters; ϕ is a weighting component. The objective function is subject to:

$$\sum_{i=1}^{i=k} M_{ij} = 1, i = 1, 2, \dots, N; \quad \sum_{j=1}^{j=N} M_{ij} = 1, j = 1, 2, \dots, N; \quad M_{ij} \in [0, 1] \quad (2.13)$$

For fcMRI study, Golay et al. [84] proposed two distance metrics D_{cc}^1 and D_{cc}^2 based on Pearson's correlation coefficient $CC_{x,y}$ between two time courses $F_x(k)$ and $F_y(k)$:

$$D_{cc}^1 = \left(\frac{1 - CC_{x,y}}{1 + CC_{x,y}} \right)^{\beta}, D_{cc}^2 = 2(1 - CC_{x,y}) \quad (2.14)$$

where $CC_{x,y}$ is the cross-correlation of $F_x(k)$ and $F_y(k)$ at lag zero. These distances characterize the degree of correlation between two fMRI time courses. Brain regions whose distance is under a certain threshold are considered functionally connected. Golay et al. compared three distance metrics: Euclidean distance, D_{cc}^1 and D_{cc}^2 , and found that fuzzy clustering analysis based on time course similarity generates effective connectivity results, while results using distance metric D_{cc}^1 outperforms the other two.

A potential question for FCA might be how many clusters should be chosen. It has been reported that different number of clusters significantly affects the connectivity results, especially when the number of underlying function networks are more than that of initially selected clusters [79-84]. Golay et al. recommended using a large number of clusters initially, which may help to obtain a clear yet complete description of the clusters without redundancy or acquisition of insignificant cluster centers. However, cluster selection problem is intrinsic for FCA and might not be completely solved within the framework of FCA.

Besides the cluster initialization issue in FCA, the distance metrics proposed by Golay et al. might be contaminated by structured noises such as human heart beat and respiration. These noises contribute to the distance metrics D_{cc}^1 and D_{cc}^2 at a relative high frequency domain (around 1 Hz), while the distance contributors we are interested are low frequency oscillations (<0.1 Hz) that represent synchrony in cerebral blood flow and oxygenation between different brain regions. To simplify solution for the above problems, Cordes et al. [85] introduced a hierarchical clustering analysis method using a new distance measurement based on frequency analysis.

2.3.2.2.2. Hierarchical clustering analysis

Different from FCA which uses an empirically chosen number of initial clusters, hierarchical clustering analysis considers each voxel as one cluster at the beginning, and merges the close clusters based on certain distance measurement. Closeness could be measured by different ways, which distinguishes single-

linkage from complete-linkage and average-linkage clustering. For HCA details please refer to [85].

Cordes et al. adopted a single-linkage HCA algorithm, and defined a new distance by combining correlation analysis and frequency decomposition. The Pearson's correlation coefficient $CC_{x,y}$ between two time courses $F_x(k)$ and $F_y(k)$ can be decomposed as

$$CC(x, y) = \frac{\sum_f N(Re(\omega f)Re(\phi f) + Im(\omega f)Im(\phi f))}{S} = \sum_f CC_f(x, y) \quad (2.15)$$

where ωf and ϕf are complex frequency component of $F_x(k)$ and $F_y(k)$, respectively; $Re(*)$ and $Im(*)$ refer to the real and imaginary component of signal $*$; S is defined as

$$S = \sqrt{\sum_{k=0}^{N-1} F_x^2(k) \sum_{k=0}^{N-1} F_y^2(k)} \quad (2.16)$$

Cordes et al. defined the distance $D(x,y)$ between $F_x(k)$ and $F_y(k)$ as [56]:

$$D(x, y) = 1 - \sum_{\mathcal{F}=0}^{0.1\text{HZ}} CC_{\mathcal{F}}(x, y) \quad (2.17)$$

Intuitively, this distance applies a low-pass filter to Pearson's correlation coefficient and then builds a reverse increase function to map the output into distance. This filtering process extracts from correlation coefficient the information that reflects synchrony in cerebral blood flow and oxygenation between different brain regions. Experiments based on both simulated data and human brain data show that structured contaminations such as respiratory or cardiac noises are generally well-removed [85]. Hierarchical clustering analysis is often computationally expensive, and is thought to be more severe when applied to 3D human brain data. For whole human brain connectivity analysis using this

method, improvements in the theoretical methods and more careful studies are needed [85].

2.3.2.3. Current software and toolboxes

As we specified in the above section of FMRI all software packages and introduce comparisons of these packages in Appendix A. There are many toolboxes and software implemented and introduced to solve and use above methods, one of the best and traditional famous software is Statistic Parametric Mapping, SPM, **SPM** refers to the construction and assessment of spatially extended statistical processes used to test hypotheses about functional imaging data. It is used for data comes from all apparatus can scan Human brain like EEG, PET and FMRI.

In our thesis, we made a survey for varieties of methods and algorithms, which can be applied to infer and represent human brain behaviors. The complete view for studying anything or region in the brain is to infer where this region exist, which we defined anatomical view, then what is the tasks or perturbation happens when external event occur in this region and other regions, which we meant functional connectivity. The last view is to infer when tasks happens under specific events and the causality of these outputs, which it meant effective connectivity, all of these are applied in SPM, other software packages and other toolboxes.

Many toolboxes can be run separately or under SPM-FMRI software like Lyngby, it is a Matlab toolbox for the analysis of functional magnetic resonance imaging FMRI time series. The main purpose of the toolbox is to model four-

dimensional fMRI and to derive parameter sets from them that will allow easy interpretation and identification.

2.3.3. Effective Connectivity

In this section, we will introduce a background of dynamic system and literature review for fMRI effective connectivity as a brain dynamic investigator

2.3.3.1. Dynamic System Definition

Dynamic system representation is the use of observed data to estimate parameters of a model that maps a physical system. This model may be linear or non-linear, formulated in discrete or continuous time and parameterized in the time or frequency domain. The aim is to construct a mathematical description of a system's response to input. Human Brain is functionally integrated and is dynamic and non-linear system. They have to be dynamic, because the brain is a physical system whose state evolves continuously in time. This means that the current state of the brain affects its state in the future. Models have to be non-linear, because biological systems depend on non-linear phenomena for much of their characteristic behavior [86]. The motivation for non-linear dynamic models is that their non-additive characteristics enable them to reproduce sufficiently complex behavior, of the sort observed in biological systems. However, non-linear models are often mathematically intractable, calling for approximation techniques. On the other hand, linear dynamic models can be analyzed in closed form. Consequently, there exists a large body of theory for handling them: linear models adhere to the principle of superposition, which means that the system's response to input is additive. There are no interactions between different inputs or

between inputs and the intrinsic states of the system. This means the response is a linear mixture of inputs [86].

To overcome this complexity of nonlinearity, we made linear approximations to a generic non-linear model. These models have the advantage that they capture some essential non-linear features, while easily remaining mathematically tractable. This policy has engendered bilinear models (Rao, 1992), where non-linear terms are limited to interactions that can be modeled as the product of two variables (inputs and states). Despite constraints on high-order nonlinearities, bilinear models can easily model plasticity in effective connections. It is used a bilinear model to illustrate the concepts of linear and bilinear coupling and how they are used to model effective connectivity.

2.3.3.2. Effective Connectivity Literature Review

Effective connectivity describes the causal influences that neural units exert over another [86]. Another definition is that effective connectivity depends on experiment- and time-dependent, simplest possible circuit diagram that would replicate the observed timing relationships between the recorded neurons [88]. Both definitions emphasize that determining effective connectivity requires a causal model of the interactions between the elements of the neural system of interest.

Such causal models can be defined within the general mathematical framework provided by dynamic systems theory [89-90]. A system is characterized by time-variant properties x_i ($1 \leq i \leq n$) or state variables, which interact with each other, i.e. the evolution of each state variable depends on at

least one other state variable. For example, the postsynaptic membrane potential depends on which and how many ion channels are open; vice versa, the probability of voltage-dependent ion channels opening depends on the membrane potential. Such functional dependencies can be expressed quite naturally by a set of ordinary differential equations in which a set of parameters θ determine the form and strength of the causal influences between the state variables. In neural systems, these parameters usually include time constants or synaptic strengths of the connections between the system elements. Additionally, in the case of non-autonomous systems (i.e. systems that exchange matter, energy or information with their environment) we need to consider the inputs into the system, e.g. sensory information entering the brain. Representing the set of all m known inputs by the m -vector function $u(t)$, one can define a general state equation for non-autonomous deterministic systems [87]:

$$\frac{dx}{dy} = F(x, y, \theta) \quad (2.18)$$

Dynamic or causal system can simply represented by above form of general state equation that provides a causal description of how system dynamics results from system structure, because it describes when and where external inputs enter the system and also how the state changes induced by these inputs evolve in time depending on the system's structure. Given a particular temporal sequence of inputs $u(t)$ and an initial state $x(0)$, one can obtain a complete description of how the dynamics of the system starting by equation 18 and integrate to give the following equation:

$$x(\tau) = x(\mathbf{0}) + \int_0^\tau F(x, y, \theta) dt \quad (2.19)$$

Equation 19 therefore provides a general form for models of effective connectivity in neural systems. It assumes that all processes in the system are deterministic and occur instantaneously [91-92]. The framework outlined here is concerned with dynamic systems in continuous time and thus uses differential equations. The same basic ideas, however, can also be applied to dynamic systems in discrete time using difference equations, dynamic system can be simply represented linearly as described in other modalities like PET or EEG, in the following subsections we will introduce the review of methods or algorithms used to infer effective connectivity [87].

2.3.3.2.1. Psycho-Physiological Interactions

Psycho-Physiological Interactions, PPI, are one of the simplest models available to assess interactions in fMRI Time series data. Given reference time series y_0 obtained from a reference voxel or region, PPI computes connectivity maps of this reference voxel with all other voxels y_i in the brain according to the regression-like equation

$$y_i = ay_0 + b(y_0 \times u) + cu + X\beta + e \quad (2.20)$$

Here, a is the strength of the intrinsic (context-independent) connectivity between y_0 and y_i . The bilinear term $y_0 \times u$ represents the interaction between physiological activity y_0 and a psychological variable u which can be construed as a contextual input into the system, modulating the connectivity between y_0 and y_i . The third term describes the strength c by which the input u determines activity in

y_i directly, independent of y_0 . Finally, β are parameters for effects of no interest X and e is a Gaussian error term [86].

PPI, where the bilinear term represents an interaction between an input or psychological variable and a response or physiological variable y_i measured at the i -th brain region. Any linear model can be augmented to include a PPI as we enhance our designed model –Bilinear model- in the following chapter by PPI.

2.3.3.2.2. Structural Equation Modeling

Structural equation modeling, SEM, or path analysis, is a multivariate method used to test hypotheses regarding the influences among interacting variables. Its roots go back to the 1920s, when path analysis was developed to quantify unidirectional causal flow in genetic data and developed further by social scientists in the 1960s (Maruyama, 1998). It was criticized for the limitations inherent in the least squares method of estimating model parameters, which motivated a general linear modeling approach from the 1970s onwards. It is now available in commercial software packages, including LISREL, EQS and AMOS [86].

SEM shares the same limitations as the linear model approach or PPI which are static model and represent only hemodynamic level not neural beside also temporal information is discounted. These problems are confounded with an inability to capture non-linear features and temporal dependencies. By moving to dynamic models, we acknowledge the effect of an input's history and embed a priori knowledge into models at a more plausible and mechanistic level. We will

describe all elements of the best and new used model, Dynamic Causal Modeling, DCM [86].

2.4. Summary

This chapter is the core of the background and literature review of our thesis, we started from human brain dynamic system history giving the layout of the brain as a dynamic and a complex system and specifying the preliminary efforts for inferring and investigating human brain complexities, we went through the improvement of technologies and focusing on FMRI.

We gave a general background for FMRI as human brain investigator and the concept of activation process and the role of attention; also we differentiate why we use it instead of other modalities. After that, we introduced all brain connectivity's types and discriminated the differences between these connectivity and literature review of each one; we answered the question for defining what is inside our brains? The first which region will interact means anatomical, and then is there any connection and the functionality between this target region and other one? Meant functional connectivity, the last one is at what time this region interacts and affects the surrounding ones? that means considering external inputs or internal changes in regions, this meant effective connectivity or dynamic system representation,

Take from these mentioned above lines to start in the following chapters. We use DCM in the next chapter while we overcome the limitations of the previous methods and give a complementary view for dynamic mapping and causality. This idea is to build a complete DCM, enhance with PPI, and give a

complementary view of different outputs after applying several combinations of effects, and then use extracted time series of this designed model to infer the causality and path of signal using Granger Causality. Chapter 4 clarifies the Granger Causality and its algorithm.

Finally, we will apply Biclustering to identify and group target regions that exhibit similar response patterns over several events and group the conditions from output profiles across set of regions based on Bi-Clustering technique.

Chapter 3

Complementary Dynamic causal modeling Augmented by PPI and first order kernel

In this chapter, we present an approach to the identification of Human brain as nonlinear input-state-output systems. We used a bilinear approximation to the dynamics of interactions among target brain region. We developed this approach for the analysis of effective connectivity using experimentally designed inputs and fMRI responses. In this construction, the coupling parameters represent effective connectivity and the bilinear parameters reflect the changes in connectivity induced by inputs. This allows one to characterize fMRI experiments, conceptually, as an experimental manipulation of integration among brain regions that discovered using evoked responses to perturbations or trial-bound inputs, like Attention, Photic or Motion applied to infer the dynamic of signal propagation in visual system. Studying selected system based on varying the external inputs and seeing the differences to complete the view under all varieties of effects, single effect, double or triple.

3.1 Introduction

One of the best algorithm used to investigate not only the interactions but also the causality is the dynamic causal modeling, (DCM), proposed by Friston et al. [93]. However, DCM approach requires a complete pre-specification of the connectivity structure. That estimated via Bayesian algorithms, it also requires the prior densities of the parameters of interest. Modelling interactions among

neuronal populations, at a cortical level, uses neuroimaging (hemodynamic or electromagnetic) time series. It presents the motivation and procedures for DCM of evoked brain responses.

The aim of this modelling is to estimate, and make inferences about, the coupling among brain areas and how that coupling is influenced by changes in experimental context, applying DCM which represents a fundamental departure from existing approaches to effective connectivity because it measures brain responses and infer their nonlinear and dynamic nature. The basic idea is to construct a reasonably realistic neuronal model of interacting cortical regions. DCM represents neuronal or synaptic activity that transformed into a measured response. This enables the parameters of the neuronal model to be estimated from observed data and then PPI to view and verify the interaction each region over another.

We introduced a complete form for time series of applied inputs to visual system; this idea can be generalized if we will study another target area in the brain by Applying different events.

As with previous mentioned algorithm in previous chapter for analyses of effective connectivity, the focus is on experimentally induced changes in coupling as Psycho Physiologic Interactions, PPI. However, unlike previous methods in neuroimaging, the causal model ascribes responses to designed deterministic inputs, as opposed to treating inputs as unknown and stochastic.

The behind construction which produce these interactions is synaptic activity; it is transformed into a measured response. This enables the parameters

of the neuronal model, effective connectivity, estimates from observed data. These supplementary models may be forward models of electromagnetic measurements or hemodynamic models of fMRI measurements. In this chapter we will focus on fMRI, this idea accomplished by using a dynamic input-state-output model with multiple inputs and outputs. The inputs correspond to conventional stimulus functions that encode experimental manipulations. The state variables cover both the neuronal activities and other neurophysiological or biophysical variables needed to form the outputs. The outputs measured electromagnetic or hemodynamic responses over the brain regions.

DCM assumes the responses that come from designed changes in inputs. An important conceptual aspect of dynamic causal models, for neuroimaging, belongs to how the experimental inputs enter the model and cause neuronal responses. Experimental variables can affect responses in one of two ways. First, they can affect responses through direct influences on specific anatomical nodes. This would be appropriate, for example, in modelling sensory evoked responses in early visual cortices. The second class of input exerts its effect through a modulation of the coupling among nodes. These sorts of experimental variables would normally be more enduring; for example attention to a particular attribute. As described before in previous chapter for representation of dynamic system we extend to assume the following equation for n regions at m events and then we build a complete bilinear system.

$$\frac{dx}{dt} = \begin{bmatrix} f_1(x_1, \dots, x_n) \\ \vdots \\ f_n(x_1, \dots, x_n) \end{bmatrix} = F(x, u, \theta) \quad (3.1)$$

The specific form of the dependencies f_i needs to be specified, i.e. the nature of the causal relations between state variables. This requires a set of parameters θ , which determine the form, and strength of influences between state variables. In neural systems, these parameters usually correspond to time constants or synaptic strengths of the connections between the system elements. The Boolean nature of θ , i.e. the pattern of absent and present connections, and the mathematical form of the dependencies f_i represent the structure of the system. Second, in the case of non-autonomous systems (and these are the ones of interest to biology) we need to consider the input into the system, e.g. sensory information entering the brain [94].

Before we proceed to DCM, it is worth pointing out that we have to introduce assumptions in this section to clarify the priors to the general state equation representing our system. We assumed that all processes in the system are deterministic and occur instantaneously. In addition, we have to model the inputs assume that we know the inputs that enter the system. This is a tenable assumption in neuroimaging because the inputs are experimentally controlled variables, e.g. Attention, Motion or Photo lead changes in stimuli or instructions. It may also be helpful to point out that using time-invariant dependencies f_i and parameters θ is not a restriction. Although the mathematical form of f_i per seconds is static, the use of time-varying inputs u allows for dynamic changes in what components of f_i are activated. For example, input functions that can only take values of one or zero and that are multiplied with the different terms of a polynomial function can be used to induce time-dependent changes from

nonlinear to linear behavior by switching off all higher order terms in the polynomial or vice versa. In addition, there is no principled distinction between states and time-invariant parameters; therefore, estimating time-varying parameters treated as a state estimation problem.

3.2. Principles of Dynamic Causal Modelling (DCM)

An important limitation of previous methods for determining effective connectivity from functional imaging data, as structural equation modelling multivariate autoregressive models MAR –it will be described in chapter 4 and we will mention the disadvantages if we use it only to infer the system dynamic– these algorithms operate at the level of the measured signals.

This is a serious problem because the causal architecture of the system that we would like to identify expressed at the level of neuronal dynamics, these perturbations cannot directly observed using non-invasive techniques. In the case of fMRI data, for example, previous models of Effective Connectivity, EC designed based on measuring time series, which result from a hemodynamic convolution of the underlying neural activity. Since classical models did not include the forward model linking neuronal activity to the measured hemodynamic data, analyses of inter-regional connectivity performed at the level of hemodynamic responses are problematic. A similar situation was seen with EEG data where there is a big difference between signals measured at each electrode and the underlying neuronal activity: changes in neural activity in different brain regions lead to changes in electric potentials that superimpose

linearly. The scalp electrodes therefore record a mixture, with unknown weightings, of potentials generated by a number of different sources.

Therefore, to enable inferences about connectivity between neural units we need models that combine both neural population dynamics and the transformation from neural activity to the measured signal. Such models make it possible to fit jointly the parameters of the neural and of the forward model such that the predicted time series are optimally similar to the observed time series. This combination of a model of neural dynamics with a biophysical forward model is a core feature of DCM. Currently, DCM implementations exist for both fMRI data and event-related potentials (ERPs) as measured by EEG/MEG. These modality-specific implementations are briefly summarized in the next sections.

3.3. DCM Construction based FMRI images time series

DCM for FMRI uses a simple model of neural dynamics in a system of n interacting brain regions. It models the change of a neural state vector x in time, with each region in the system represented by a single state variable, using the following bilinear differential equation [95]:

$$\frac{dx}{dt} = F(x, u, \theta^n) = \left(A + \sum_{j=1}^m u_j B^{(j)} \right) x + Cu \quad (3.2)$$

Note that this neural state equation follows the general form for deterministic system models introduced by Equation 3.2, i.e. the modeled state changes are a function of the system state itself, the inputs u and some parameters $\theta^{(n)}$ that define the functional architecture and interactions among brain regions at a neuronal level. The neural state variables represent a summary index of

neural population dynamics in the respective regions. The neural dynamics are driven by experimentally controlled external inputs that can enter the model through direct influences on specific regions by evoked responses in early sensory cortices, the C matrix represents this formulation, or they can modulate the coupling among regions during learning or attention; the B matrices represents this formulation. Given this bilinear state equation, the neural parameters, $\theta^{(n)} = \{A, B, C\}$, this can be expressed as partial derivatives of F:

$$A = \left. \frac{\partial F}{\partial x} \right|_{u=0}, B^{(j)} = \frac{\partial^2 F}{\partial x \partial u_j}, C = \left. \frac{\partial F}{\partial u} \right|_{x=0} \quad (3.3)$$

As can be seen from these equations, the matrix A represents the effective connectivity among the regions in the absence of input, the matrices $B^{(j)}$ encode the change in effective connectivity induced by the jth input u_j , and C embodies the strength of direct influences of inputs on neuronal activity. Figure 3.1 summarizes this bilinear state equation and shows a specific example model.

state effective modulation system input
changes connectivity of connectivity state parameters

General bilinear state equation

$$\frac{dx}{dt} = \left(A + \sum_{j=1}^m u_j B^{(j)} \right) x + Cu$$

Figure 3.1 the bilinear state equation of DCM for fMRI

DCM applied for FMRI images time series combines neural dynamics with an experimentally validated hemodynamic model that describes the transformation of neuronal activity into a BOLD response. This so-called Balloon

model was initially formulated before [96] Briefly, it consists of a set of differential equations that describe the relations between four hemodynamic state variables, using five parameters $\theta^{(h)}$. More specifically, changes in neural activity produces a vasodilatory signal that leads to increases in blood flow and subsequently to changes in blood volume and deoxyhaemoglobin content. The predicted BOLD signal is a non-linear function of blood volume and deoxyhaemoglobin content. This hemodynamic model is summarized by Figure 3.2.[95-96].

The combined neural and hemodynamic parameter set $\theta = \{\theta^{(n)}, \theta^{(h)}\}$ is estimated from the measured BOLD data, using a fully Bayesian approach with empirical priors for the hemodynamic parameters and conservative shrinkage priors for the coupling parameters. Details of the parameter estimation scheme, which rests on a gradient ascent procedure embedded into an expectation maximization (EM) algorithm [97].

After estimating the parameters of a DCM from measured BOLD data, the posterior distributions of the parameter estimates can be used to test hypotheses about connection strengths. Here, DCM was applied to fMRI data from a single subject, testing the hypothesis that in a hierarchical system of visual areas attention to motion enhanced the backward connections from the inferior frontal gyrus (IFG) or V1 onto superior parietal cortex (SPC) and from SPC onto V5, respectively [98]. For statistical inference at the group level, various options exist. The simplest approach is to enter the conditional estimates of interest into a classical second-level analysis [93].

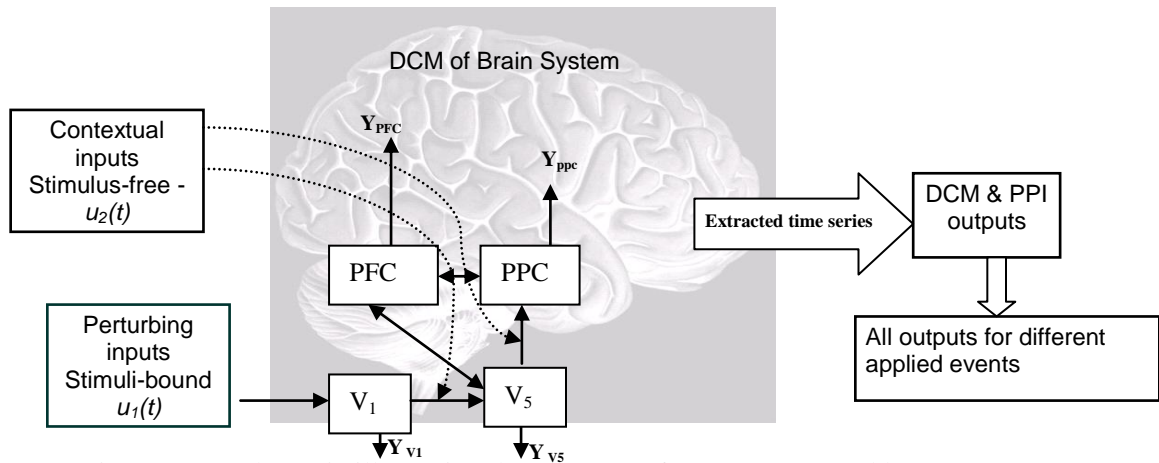


Figure 3.2 a schematic illustrating the concepts of DCM augmented by PPI

We envisage that DCM can be used primarily to answer questions about the modulation of effective connectivity through inferences about the third set of parameters as described above. These will be referred to as bilinear in the sense that an input-dependent change in connectivity can be construed as a second-order interaction between the input and activity in a source region, when causing a response in a target region. The key role of bilinear terms reflects the fact that the more interesting applications of effective connectivity address changes in connectivity induced by cognitive set or time. In short, DCM with a bilinear approximation allows one to claim that an experimental manipulation has "activated a pathway" as opposed to a cortical region. Bilinear terms correspond to psychophysiological interaction terms in classical regression analyses of effective connectivity (Friston et al 1997) and those formed by moderator variables (Kenny & Judd 1984) in structural equation modelling (Büchel & Friston 1997). This bilinear aspect speaks again to the importance of multifactorial designs that allow these interactions to be measured and the central

role of the context in which region-specific responses are formed (see McIntosh 2000).

Additional constraints, on the intrinsic connections and their modulation by contextual inputs, can also be specified but they are not necessary. These additional constraints can be used to finesse a model by making it more parsimonious, allowing one to focus on a particular connection. We will provide examples of this below. Unlike structural equation modelling, there are no limits on the number of connections that can be modeled because the assumptions and estimations scheme used by dynamic causal modelling are completely different, relying upon known inputs.

3.3.1. Hemodynamic State Equations

The remaining state variables of each region are biophysical states engendering the BOLD signal and mediate the translation of neuronal activity into hemodynamic responses. Hemodynamic states are a function of, and only of, the neuronal state of each region [98]. In brief, for the i th region, neuronal activity z_i causes an increase in a vasodilatory signal s_i that is subject to auto-regulatory feedback. Inflow f_i responds in proportion to this signal with concomitant changes in blood volume v_i and deoxyhaemoglobin content q_i

$$\begin{aligned} \dot{s}_i &= z_i - \kappa_i s_i - \gamma_i (f_i - 1), \dot{f}_i = s_i, \tau_i \dot{v}_i = f_i - v_i^{1/\alpha} \tau_i \\ \dot{q}_i &= f_i E(f_i, \rho_i) / \rho_i - v_i^{1/\alpha} q_i / v_i \end{aligned} \quad (3.4)$$

Outflow is related to volume $f_{out}(v) = v^{1/\alpha}$ through Grubb's exponent α the oxygen extraction is a function of flow $E(f, \rho) = 1 - (1 - \rho)^{1/f}$ where ρ is resting oxygen extraction fraction [99]. The BOLD signal is taken to be a static

nonlinear function of volume and deoxyhaemoglobin that comprises a volume-weighted sum of extra- and intra-vascular signals

$$y_i = g(q_i, v_i) = V_0(k_1(1 - q_i) + k_2(1 - q_i / v_i) + k_3(1 - v_i)) \quad (3.5)$$

$$k_1 = 7\rho_i, k_2 = 2, k_3 = 2\rho_i - 0.2$$

$V_0 = 0.02$ is resting blood volume fraction. Again it should be noted that the particular forms of Equations (3.4) and (3.54) are specific to BOLD-fMRI and should, obviously, be replaced by appropriate state and output equations for other modalities. A list of the biophysical parameters $\theta^h = \{\kappa, \gamma, \tau, \alpha, \rho\}$ is provided in the following schematic describing hemodynamic model is shown in Figure 3.3. The estimation of these parameters is clarified in Appendix C.

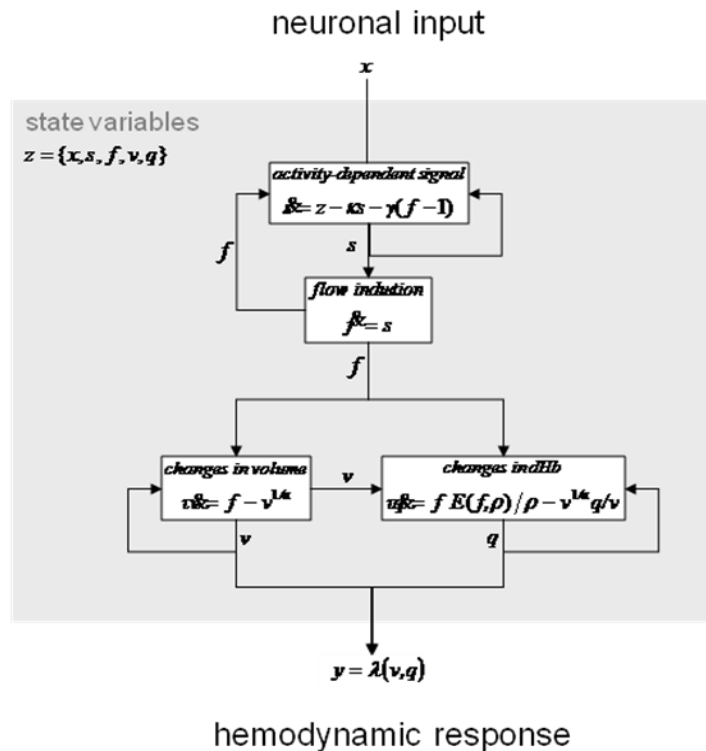


Figure 3.3 Summary of the hemodynamic model used by DCM Based on FMRI images time series

3.3.2. Stimulus propagation in DCM system

Given DCM, we explained how local brain responses were generated from the interplay of the three mechanisms described by the state equation, inter-regional connections, their contextual modulation and driving inputs. Figure 3.4 provides a simple schematic for the concept of DCM experiments and regions interaction when imposing external stimulus.

This interaction means that the difference between stimulus S_1 and stimulus S_2 is larger during task T_1 than during task T_2 . The stimulus main effect in area x_1 results from the driving inputs to x_1 being much stronger for stimulus S_1 than for stimulus S_2 . This differential effect is then conveyed onto area x_2 by the connection from x_1 to x_2 . Based on this idea; the strength of this connection is strongly enhanced during task T_1 , but only marginally influenced during task T_2 . This difference in modulation causes the interaction in area x_2 means that this model would have produced an interaction in area x_1 as well if we had chosen a stronger back-connection from x_2 to x_1 .

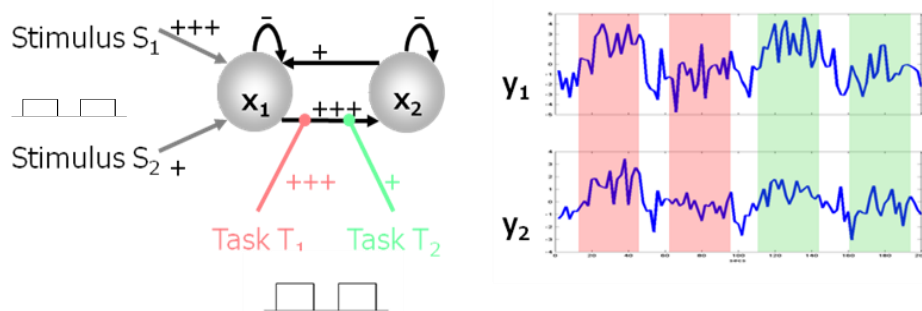


Figure 3.4 Simulated BOLD responses of two areas, y_1 and y_2

After simplifying the idea for stimulus/tasks of DCM, Parameters should be estimated with special criteria because model is constructed based on interactions dynamics, these parameters $\theta^{(n)} = \{A, B, C\}$ represents the system

dynamics as we described in previous section, we clarify how can we estimate these parameters in the next section.

3.3.3. Parameters Estimation

One of the best and robust algorithms used in this estimation for these dynamic systems is Expectation Maximization, EM, full description and mathematical clarification is introduced in Appendix B.

In the context of DCM, one potential solution could be to make use of the Laplace approximation, i.e. to approximate the model evidence by a Gaussian that is centered on its mode. The following expression for the natural logarithm (\ln) of the model evidence ($\eta_{\theta|y}$ denotes the MAP estimate, $C_{\theta|y}$ is the posterior covariance of the parameters, C_ε is the error covariance, θ_p is the prior mean of the parameters, and C_p is the prior covariance):

$$\begin{aligned} \ln p(y | m) &= \text{accuracy}(m) - \text{complexity}(m) \\ &= \left[-\frac{1}{2} \ln |C_\varepsilon| - \frac{1}{2} (y - h(u, \eta_{\theta|y}))^T C_\varepsilon^{-1} (y - h(u, \eta_{\theta|y})) \right] \\ &\quad - \left[\frac{1}{2} \ln |C_p| - \frac{1}{2} \ln |C_{\theta|y}| + \frac{1}{2} (\eta_{\theta|y} - \theta_p)^T C_p^{-1} (\eta_{\theta|y} - \theta_p) \right] \end{aligned} \quad (3.6)$$

This expression properly reflects the requirement, as discussed above, that the optimal model should represent the best compromise between model fit (accuracy) and model complexity, another estimation formula is the Bayesian Information Criterion (BIC) and Akaike Information Criterion (AIC), these approximations are given by:

$$\begin{aligned} BIC &= \text{accuracy}(m) - \frac{d_\theta}{2} \ln N \\ AIC &= \text{accuracy}(m) - d_\theta \end{aligned} \quad (3.7)$$

where d_θ is the number of parameters and N is the number of data points (scans). If one compares the complexity terms of BIC and AIC, it becomes obvious that BIC pays a heavier penalty than AIC as soon as one deals with 8 or more scans which is virtually always the case for FMRI Images time series data:

$$\begin{aligned} \frac{d_\theta}{2} \ln N &> d_\theta \\ \Rightarrow N &> e^2 \approx 7.39 \end{aligned} \quad (3.8)$$

Therefore, BIC will be biased towards simpler models whereas AIC will be biased towards more complex models. This can lead to disagreement between the two approximations about which model should be favored. In DCM for FMRI, we have therefore adopted the convention that, for any pairs of models m_i and m_j to be compared, a decision is only made if AIC and BIC concur (see below); the decision is then based on that approximation which gives the smaller Bayes factor (BF):

$$BF_{ij} = \frac{p(y | m_i)}{p(y | m_j)} \quad (3.9)$$

Just as conventions have developed for using p-values in frequentist statistics, there are conventions for the use of Bayes factors. For example, Raftery (1995) suggests interpretation of Bayes factors as providing weak ($BF < 3$), positive ($3 \leq BF < 20$), strong ($20 \leq BF < 150$) or very strong ($BF \geq 150$) evidence for preferring one model over another [100].

3.4 Results and Discussions

We used datasets of four brain regions from visual to specify the interaction and connectivity between them, these areas or regions are responsible for the main function of visual system. The primary visual cortex, V1 is anatomically equivalent to attention area or input area, Brodmann area. Visual area V5, also known as visual area MT or middle temporal, is a region of extrastriate visual cortex that is thought to play a major role in the perception of motion and mediator region, the integration of local motion signals into global percepts and the guidance of some eye movements. 4-Phenyl-4-(1-Piperidinyl)-Cyclohexanol, PPC, is an organic chemical which is often found as a metabolite of phencyclidine also integrates with others to complete the perception, The dorsolateral prefrontal cortex, DL-PFC or DLPFC, consists of the lateral portions of Brodmann areas and is connected to the orbitofrontal cortex. Its function is responsible for motor planning, organization, and regulation, as we illustrated in chapter one the schismatic of visual system the concepts of dynamic causal modeling, DCM, augmented by PPI. One, two or three inputs or perturbations can produce responses in the regions or nodes that comprise the model. In this model there are four nodes V1, V5, PFC and PPC Stimulus-bound perturbations designated U1 act as extrinsic inputs to the primary visual area V1. Stimulus-free or contextual inputs U 2 mediate their effects by modulating the coupling between V1 and V5 and between V5 and PFC. Y outputs of both neuronal activity and hemodynamic

DCM specify, estimate and review model to infer the interactions between V1, V5, PPC and PFC under external events based on DCM implemented on SPM8. There are the direct or extrinsic influence of inputs on brain states in any particular area and the intrinsic or latent connections that couple responses in one area to the state of others, also changes in this intrinsic coupling induced by inputs. Although, in some instances, the relative strengths of intrinsic connections studied alone, most analyses of DCM focuses on the changes in connectivity embodied in the bilinear parameters. The first set of parameters is generally of little interest in the context of DCM but is the primary focus in classical analyses of regionally specific effects [102].

DCM represents connectivity or interaction without inputs among the regions. Effective connectivity is the influence that one neuronal system exerts over another in terms of inducing a response A where it is intrinsic coupling, latent connectivity, in the absence of experimental perturbations. B is representing the change in coupling or interaction between regions according to the j inputs, B_j , induced connectivity, represent the entire coupling changed over A in the present of inputs j. finally C is the representation of extrinsic coupling or over the regions due to inputs j, these parameters have been estimated previously[101-102].

3.4.1. Data sets experimental verification

Based on dataset of Karl J. Friston [96], which he used it for estimating dynamic system parameters based on Bayesian estimation and derivation of Expectation Maximization, model was designed according General Linear Model,

GLM simplifications, and EM is used to estimate system parameters. This data set is prepared using Posterior Probability Map PPMs and Dynamic Causal system. Subjects were studied with fMRI under identical stimulus conditions (visual motion subtended by radially moving dots) while manipulating the attentional component of the task (detection of velocity changes). The data were acquired from normal subjects at 2 Tesla using a Magnetom VISION (Siemens, Erlangen, Germany) whole-body MRI system, equipped with a head volume coil. Contiguous multislice T2*-weighted fMRI images were obtained with a gradient echo-planar sequence (TE = 40 ms, TR = 3.22 seconds, matrix size = 64 x 64 x 32, voxel size 3 x 3 x 3 mm). Each subject had four consecutive 100-scan sessions comprising a series of ten scan blocks under five different conditions: D F A F N F A F N S. The first condition (D) was a dummy condition to allow for magnetic saturation effects. F (Fixation) corresponds to a low-level baseline where the subjects viewed a fixation point at the center of a screen, initialization state. In condition A (Attention) subjects viewed 250 dots moving in from the center at 4.7 degrees per second and were asked to detect changes in radial velocity, which did not actually occur. This attentional manipulation was validated post hoc using psychophysics and the motion aftereffect. In condition N (No attention), the subjects were asked simply to view the moving dots. In condition, S (Stationary) subjects viewed stationary dots. The order of A and N was swapped for the last two sessions. In all conditions, subjects fixated the center of the screen. In a pre scanning session the subjects were given five trials with five speed changes (reducing to 1%). During scanning there were no speed changes and no overt

response was required in any condition. In this chapter we analyze data from the first subject. For the purpose of the analyses in this chapter the above experimental conditions were formulated using the following factors or causes. "Photic" stimulation comprised the {A,B, S} conditions, "motion" comprised the {N,A} conditions and "Attention" comprised the A condition. These three variables are encoded into the design matrix. The relative contribution of each of these variables can be assessed using standard least squares or Bayesian estimation. Classical inferences about these contributions are made using T or F statistics, depending upon whether one is looking at a particular linear combination (e.g. a subtraction), or all of them together. Bayesian inferences are based on the posterior or conditional probability that the contribution exceeded some threshold, usually zero [96].

Using this dataset, we designed our DCM with a complementary views to interoperate a whole description of our visual system. The idea is to study the behavior of our visual system under all external effects and combination of them, we used the most generic effects for visual system.

The most effect we use for vision are three effects singular or combined, these effects are Attention, Motion and Photic which we use to interpreter the surroundings, we applied all of these three effects separately or combined, make all possible combination of these inputs, this will produce extra four inputs,

Beside applying three separate inputs , we combined all different combinations of these inputs, Attention with Motion, this can happens when we see new attention while we are already seeing motion or vice versa. The second is

Combination of Attention with Photic, the same for Attention and Photic, Photic and Motion and the fourth is all of these three effects

3.4.2. Interpretations from Parameters Estimations for all effects

As we mentioned before that we used EM to estimate dynamic system parameters as in equations 3.2, 3.3, the formula of EM in equation 3.6 is used. We found that the least number of estimates to reach steady state is Attention system, equal 8. Providing that all models are the same in design manipulations, Motion and Photic are equals 13, means we can infer that our brain takes time and calculations for Photic and Motion the same, while when we combine Attention with Motion the number was 9, means the Attention contributes higher weight. Another interesting thing is number of estimates of Photic and Motion, which each has 13, but combination effect has 16, means merging effects in sometimes increase the complexity and prolong the interpretation and time. The higher number is the combination of all three effects we visualize the least one the highest one in figure 3.5. The idea is based on priors, we can predict the future, so one of the promising application for DCM applied to fMRI time series is not only to infer the system dynamics, but also predicts the future behavior, it means we can use it to change or guide our bad behaviors. Also, open the channels and opportunities for psychologists to deal invasively with their cases without affecting their secretion of glands.

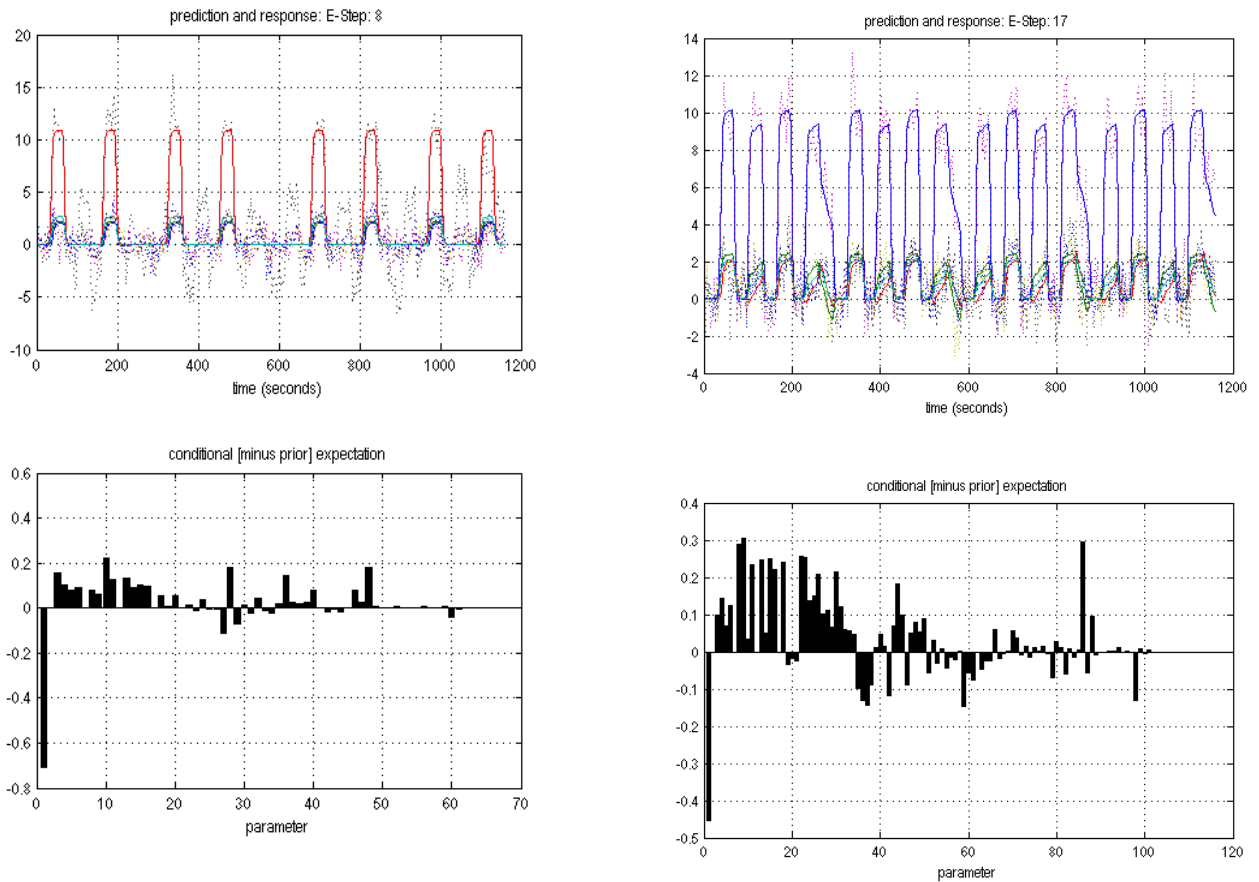


Figure 3.5 Estimation Using EM, upper figures are prediction or trail until steady state the lower for conditional priors for the expectation, left the minimum number of estimation for Attention and the right for the three combination of three effects Motion, Attention and Photic

3.4.3. DCM as MIMO system

The DCM as we designed contains Multiple Inputs Multiple Outputs, MIMO, 3 basics and 4 combines and the results are times series behaviors for four studied regions of visual system, figures 3.6 shows the inputs modulations and extracted time series for V1, V5, PFC and PPC. Later on, in the next chapter we

will use these extracted time series for extra investigations and reorganize them against effects to discover subgroups by Bi-Clustering.

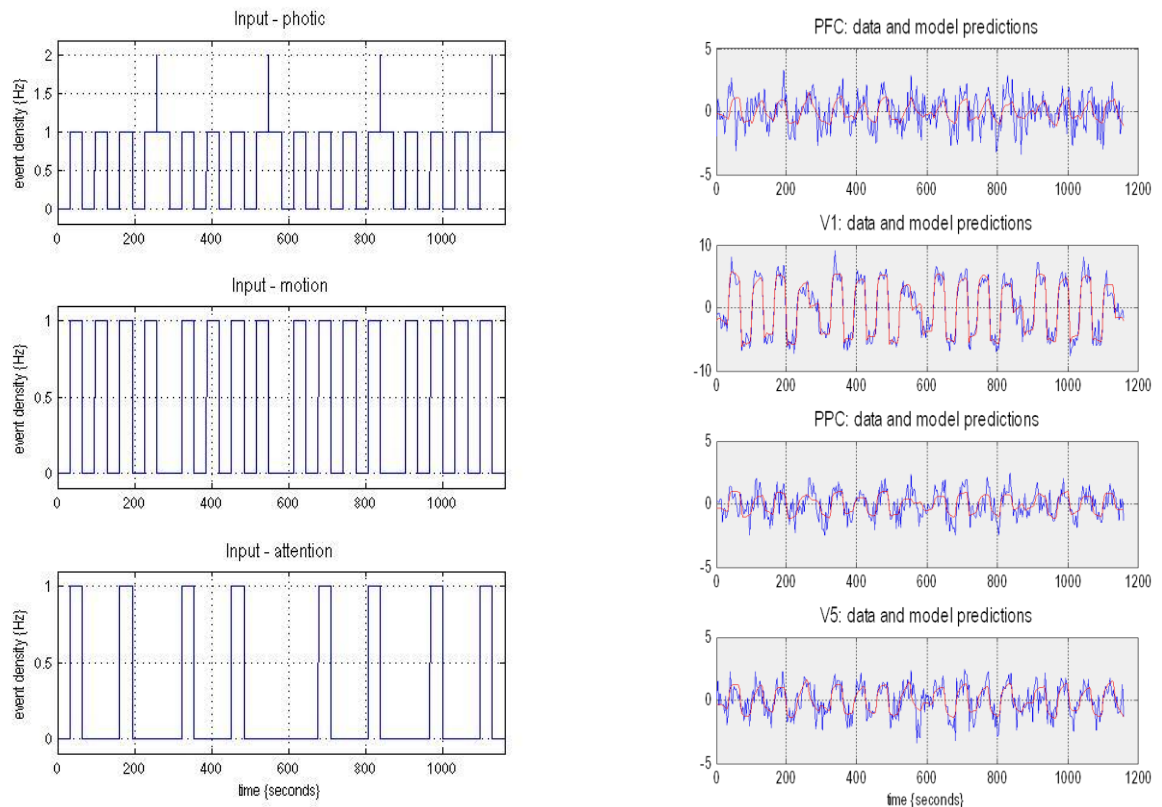


Figure 3.6 Left Three inputs U_i , visual (photic), motion and attention represented by event. Right is outputs of four visual system studied regions

3.4.4. Intrinsic Connectivity discrimination for all effects

A Matrix is representing Intrinsic or effective connectivity without effect of external effect, means internal behavior, from table 3.1 we infer that there is signal interaction between regions differ from one to another, and from effect to effect.

All interactions between brain regions internally is showed in table 3.1, these interactions are changes for four brain regions V1, V5, PFC and PPC, when applying Attention effect, the interaction from region V1 to PFC 0.224 is the highest value at this effect, this is effective or internal interaction.

It means that PFC will be ready to change and transfer the signal to the internal PPC. Another interaction from V1 to V5 and to PPC from V5 to PPC and from PFC to PPC, for motion effect, the highest interaction comes from PFC to PPC 0.349 and vice versa from V1 to V5 and PFC and then from V5 to PFC, PPC and V1.

Intrinsic connectivity Attention					Intrinsic connectivity Motion				
	'V1'	'V5'	'PFC'	'PPC'		'V1'	'V5'	'PFC'	'PPC'
'V1'	-1	0.094043	0.104624	0.078266		-1	0.149483	0.131953	0.156539
'V5'	0.129585	-1	0.077063	0.059071		0.137966	-1	0.220597	0.165575
'PFC'	0.223997	0.091959	-1	0.088217		0.208795	0.219091	-1	0.240075
'PPC'	0.124443	0.103688	0.158507	-1		0.068357	0.233252	0.34878	-1
Intrinsic connectivity Photic					Intrinsic connectivity Attention-Motion				
'V1'	-1	0.04007	0.02367	0.022904		-1	0.14107	0.084084	0.122477
'V5'	0.124484	-1	0.133423	0.122484		0.17276	-1	0.145209	0.116521
'PFC'	0.184406	0.187482	-1	0.179909		0.228669	0.175086	-1	0.165595
'PPC'	0.073743	0.158988	0.209028	-1		0.104701	0.199291	0.271885	-1
Intrinsic connectivity Attention-Photic					Intrinsic connectivity Motion-Photic				
'V1'	-1	-0.00457	-0.06713	-0.06972		-1	0.088825	0.039366	0.073513
'V5'	0.072917	-1	0.164704	0.131572		0.171497	-1	0.214715	0.205901
'PFC'	0.215541	0.165973	-1	0.179254		0.207265	0.222238	-1	0.236578
'PPC'	0.042467	0.183366	0.300221	-1		0.099452	0.230013	0.275337	-1
Intrinsic connectivity Attention-Motion-Photic									
'V1'	-1	0.122726	0.034823	0.048991					
'V5'	0.099729	-1	0.232876	0.250674					
'PFC'	0.14216	0.287555	-1	0.220433					
'PPC'	0.069141	0.304008	0.245486	-1					

Table 3.1 intrinsic connectivity matrices, effective connectivity interactions between four studied visual system regions at different effects.

Each region in the visual system affects and interacts with the others and may be the connection between them be effective according to the stimulus or the interaction. Figure 3.7 shows these intrinsic and their probabilities for Attention (left) and for Attention-Motion-Photic (right).

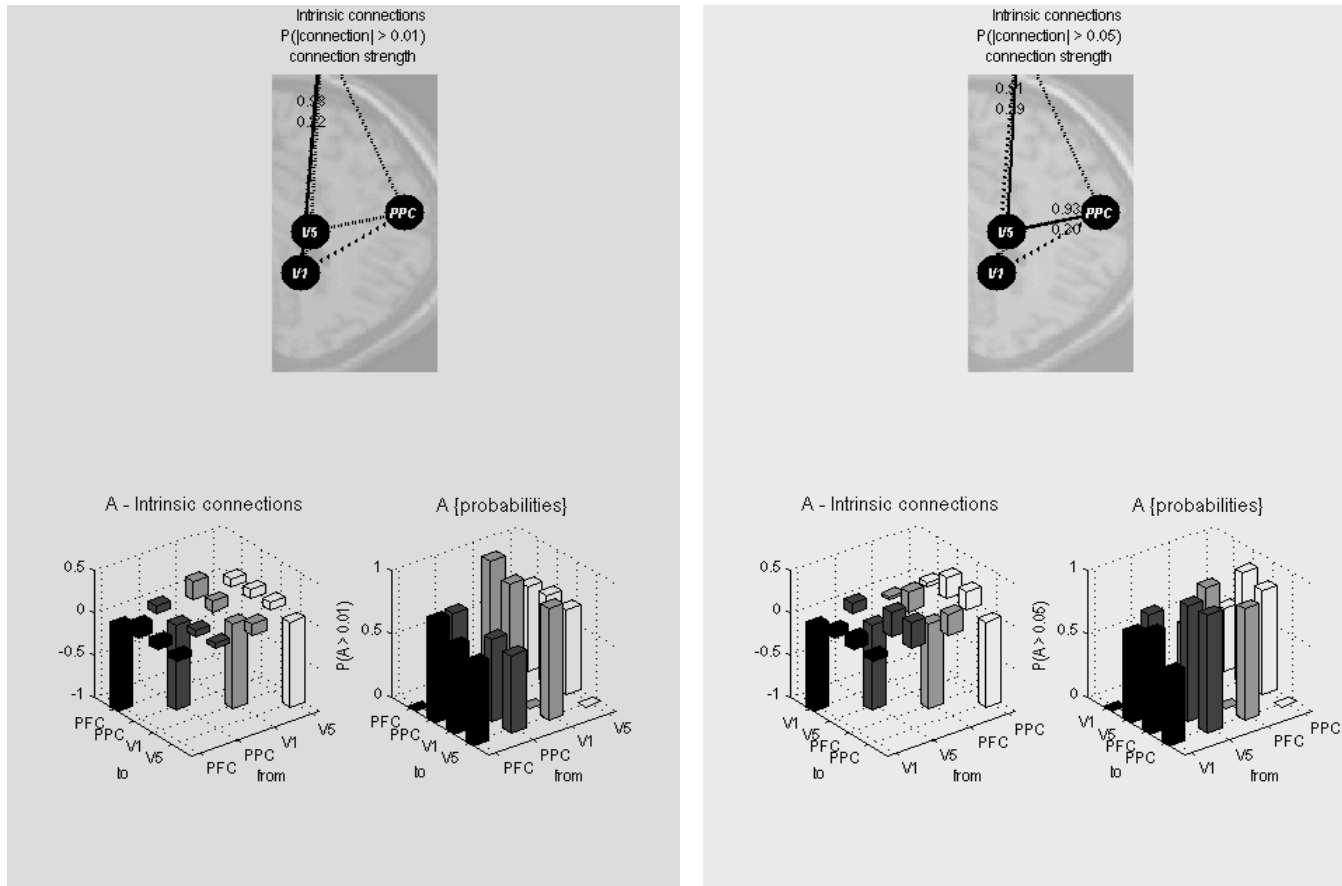


Figure 3.7 Intrinsic connectivity and their probabilities for Attention effect (left) and Attention-Motion-Photic effect (right)

The highest value for Photic is the same as Motion 0.21 from PFC to PPC, V1 to V5 and PFC, also from V5 to PFC and PPC, and then from PPC to PFC and PPC. From table 3.1 we can infer that all the highest interactions is the regions inside visual system PPC and PFC and their connections to V1 and V5, this

means this is a type of preparation for these regions to accept interaction when effect stimulate the outside region V1. This is like other system in our body, all of organ or region have their specific job to do regardless the signal comes or not.

3.4.5. Induced or changed Connectivity

Induced or change in Effective connectivity is represented in our model by Matrix B and is estimated with other system parameters by EM algorithm. In Previous section, we inferred that A is the preparation or internal communication between regions with no effect of external inputs while B is representing this effect. Figure 3.8 shows graphically two B matrices modulations and probabilities

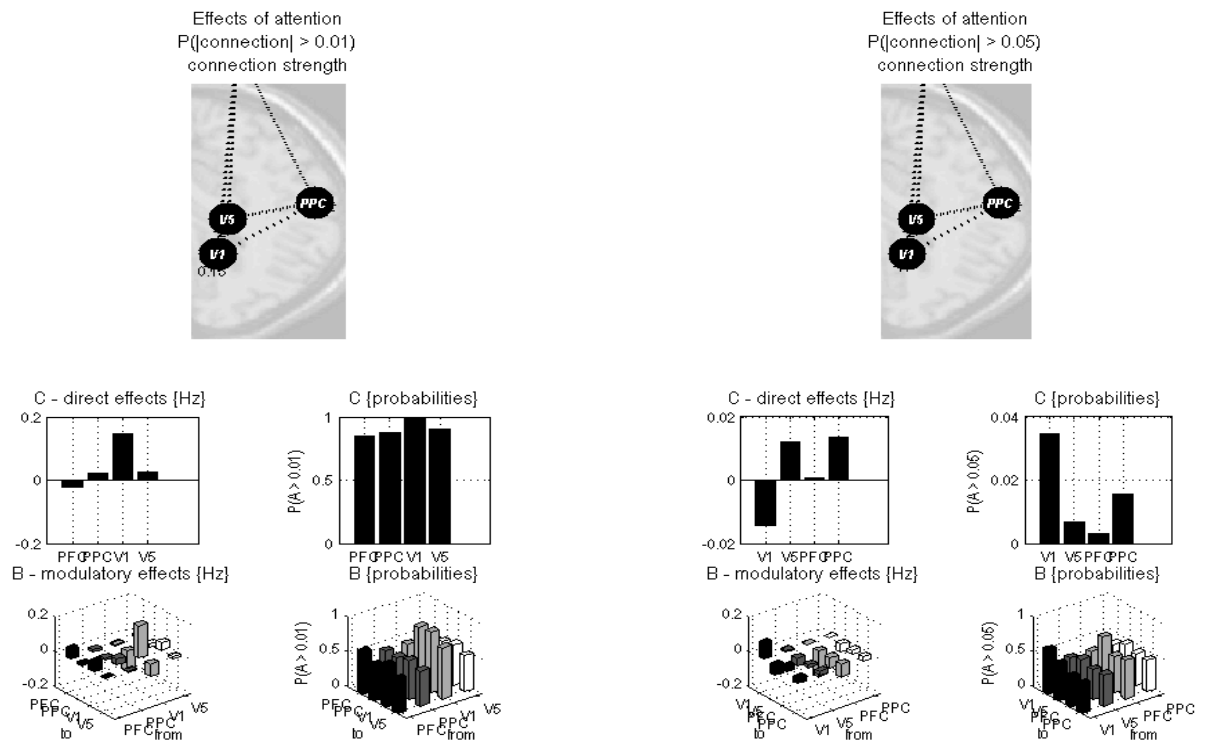


Figure 3.8 Effect of change of effective connectivity between regions after applying when Applying external effects or inputs, left is for attention model right is for attention when combined with Photic and Motion.

Table 3.2 shows that the main region which receive the external effect is V1 and some interactions occur on other regions B is representing the effect while we affect the system by external inputs and regions are interacting according to each effect in different ways. For the Attention only V1 interact internally with highest value 0.182 against the others.

Intrinsic connectivity <u>Attention</u>					Intrinsic connectivity <u>Motion</u>			
	'V1'	'V5'	'PFC'	'PPC'	'V1'	'V5'	'PFC'	'PPC'
'V1'	0.18217	0.04351	0.055475	0.034422	0.178699	0.012354	-0.0235	-0.00635
'V5'	-0.06983	-0.01197	0.001591	-0.00555	-0.16452	0.010923	0.092003	0.031596
'PFC'	-0.00643	0.010759	0.054822	0.012863	-0.10975	0.023803	0.128529	0.037971
'PPC'	-0.10976	-0.02013	0.008513	-0.01041	-0.17996	-0.00328	0.076317	0.014986
Intrinsic connectivity <u>Photic</u>					Intrinsic connectivity <u>Attention-Motion (attention)</u>			
'V1'	0.239027	0.047357	0.040859	0.035647	0.1633	0.0118	-0.0363	-0.0071
'V5'	-0.06333	-0.06536	-0.06769	-0.05503	-0.1616	0.0137	0.0847	0.0361
'PFC'	-0.0365	-0.00634	0.043473	0.005298	-0.1413	0.0139	0.1156	0.0314
'PPC'	-0.04916	-0.05659	-0.04253	-0.04413	-0.1661	0.0023	0.0799	0.0207
Intrinsic connectivity <u>Attention- Motion (Motion)</u>					Intrinsic connectivity <u>Attention-Photic (Attention)</u>			
'V1'	0.0670	-0.0024	-0.0398	-0.0123	0.1938	0.0250	-0.0156	-0.0157
'V5'	-0.0188	-0.0053	-0.0223	-0.0029	0	-0.0712	-0.0380	-0.0387
'PFC'	0.0546	0.0062	0.0260	-0.0024	-0.0977	0.0382	0.1313	0.0526
'PPC'	-0.0397	-0.0095	-0.0042	-0.0082	-0.1133	0.0244	0.0830	0.0355
Intrinsic connectivity <u>Attention-Photic (Photic)</u>					Intrinsic connectivity <u>Motion-Photic (Motion)</u>			
'V1'	0.2358	0.0457	0.0373	0.0199	0.3046	0.2124	0.2088	0.2279
'V5'	-0.0237	0.0015	0.0253	0.0146	-0.0585	0.1404	0.1347	0.1316
'PFC'	0.0181	0.0049	0.0483	0.0042	-0.0298	0.0769	0.1327	0.0770
'PPC'	-0.0360	-0.0022	0.0284	0.0075	-0.0318	0.1155	0.1289	0.1065
Intrinsic connectivity <u>Motion-Photic (Photic)</u>					Intrinsic connectivity <u>All (Attention)</u>			
'V1'	0.0386	-0.0907	-0.1269	-0.0979	0.2391	0.2560	0.2077	0.2142
'V5'	-0.1763	0.0134	0.0309	0.0305	-0.0351	0.2527	0.1005	0.1213
'PFC'	-0.1491	0.0493	0.1141	0.0576	-0.0167	0.1367	0.1114	0.0601
'PPC'	-0.1975	0.0107	0.0460	0.0237	-0.0237	0.1489	0.0652	0.0569
Intrinsic connectivity <u>All (Motion)</u>					Intrinsic connectivity <u>All (Photic)</u>			
'V1'	0.0479	-0.0881	-0.1180	-0.0903	0.0895	0.0075	0.0025	-0.0002
'V5'	-0.0991	0.0123	0.0696	0.0485	-0.0561	-0.0434	-0.1465	-0.0462
'PFC'	-0.1294	0.0474	0.1828	0.0775	0.0310	-0.0151	-0.0573	-0.0239
'PPC'	-0.1439	0.0157	0.0988	0.0521	-0.0297	-0.0222	-0.0750	-0.0251

Table 3.2 Induced or the change in effective connectivity over all studied regions at all applied events (Attention, Motion and Photic)

Like Attention effect, Motion affect V1 internally with also PFC, it is interacted internally, this due to motion require internal perception beside external stimulation it is prolonged than Attention, Photic is also make V1 interacts internally, when combine Attention with Motion, there is no effect of motion, the power is for attention. It means that Attention is affecting our vision more than Motion, but with Attention-Motion combination, both of them affect V1.

The highest value in all effects is when we combine Motion-Photic, the interaction value is 0.305 although no effect for Photic relative to Motion, the combination may empower the effect of one effect, Photic increase the power of affecting V1 of Motion.

3.4.6. Direct inputs Effects and first order kernel and regions localization

Studying the direct effect of external effect on each region not on the interaction is one of the strategies to test where the region or regions receive the stimulus, for all three effects separately, all stimulate V1. The same happens in attention for both combination with Photic or Motion, effect for motion when we combine Attention-Motion, the same for the rest of combination of effects.

Regions/ effects	Attention-Motion			Attention-Photic		Motion-Photic		Attention-Motion- Photic				
	Attention	Motion	Photic	Attention	Motion	Attention	Photic	Motion	Photic	Attention	Motion	Photic
V1	0.112	0.1122	0.132	0.1124	-0.005	0.107	0.001	0.050	0.057	0.059	0.058	-0.014
V5	0.0253	0.0254	0.021	0.0191	0.0073	0.008	0.020	-0.023	0.049	-0.018	0.037	0.012
PPC	-0.012	-0.012	-0.018	-0.0127	0.0023	-0.014	-0.001	-0.010	-0.002	-0.006	-0.007	0.001
PFC	0.0241	0.0241	0.016	0.01535	0.012	0.017	0.014	-0.001	0.028	0.003	0.015	0.013

Table3.3. Direct effects for all external inputs over four regions

As we mention before that all models are based on both Hemodynamic and Neural considerations, so it is important to use first order kernel to show the responses for all regions after applying different three effect, Attention, Motion and Photic as figure3.9.also the main difference against other modalities localization as on the left graph.

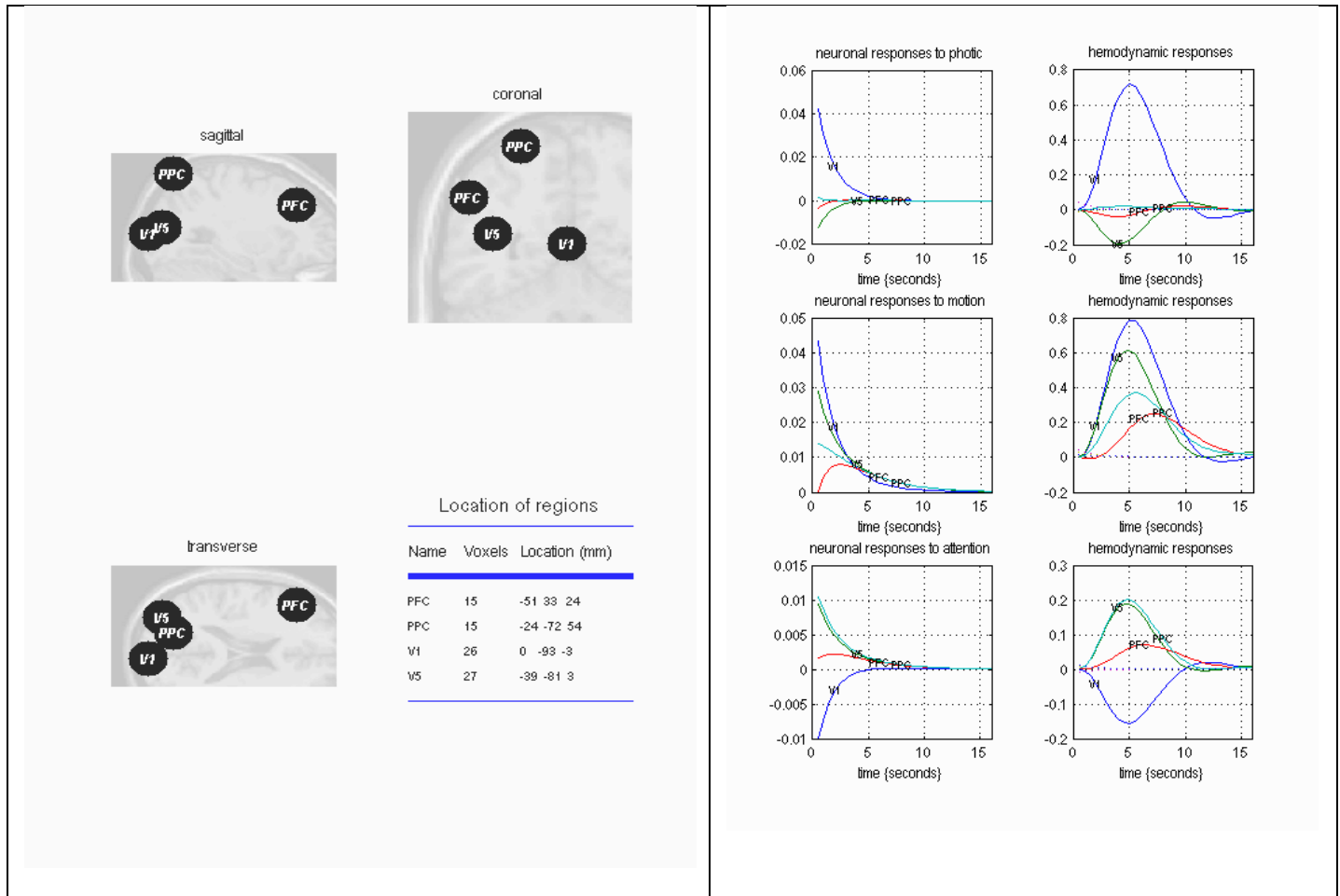


Figure 3.9 Left is the localization of anatomical structure for four regions. Right is the first order kernel for all four responses top-down line graphs V5,PPC,PFC and V1 after applying three effects

3.5 HRF and PPI Augmentation

As we described in previous chapter that PPI is used before, used to model the interactions,

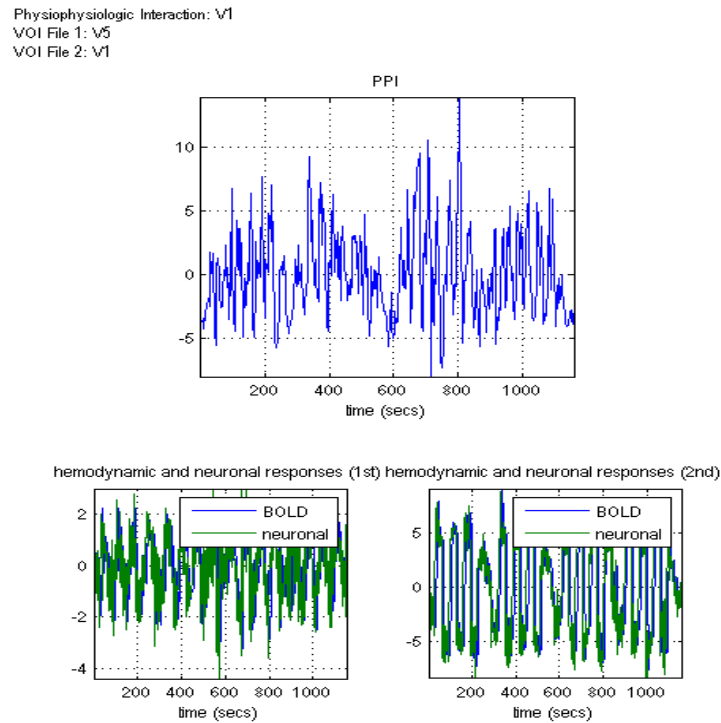


Figure.3.10 The upper part is the Psycho Physiologic interaction PPI for V1 against V1 and V5, The lower part is hemodynamic and neural response

it represents the neural signal convolved with some hemodynamic response function (HRF). However, interactions in the brain are expressed, not at the level of hemodynamic responses, but at a neural level. Therefore, veridical models of neuronal interactions require the neural signal or at least a well-constrained approximation to it. Given the blood oxygen level dependent BOLD signal in fMRI, the appropriate approximation can be obtained by deconvolution using an assumed hemodynamic response. The need for robust deconvolution is motivated for a complementary view beside neural complementary investigation.

Brain interactions occur at a neuronal level, yet the signal observed in fMRI is the hemodynamic response engendered by that neuronal activity. The reason for deconvolving is that the shape or lag of the HRF may be different

between brain regions, and if no deconvolution is applied, the PPI analysis can be biased towards areas with a similar shaped/delayed HRF. However, this is only important for event-related designs for block designs. the two methods are roughly equivalent. As shown in Figure 3.10 PPI of V1 and V5 as they are the main interests and focus of visual system and HRF.

3.6 Conclusion

From the beginning of this chapter, to the last previous section we introduced how we could represent the human brain as a dynamic system, based on the studies and limitations and drawback of methods used for functional connectivity and effective connectivity, we start this chapter to overcome all this limitation, DCM is since 2003 as a dynamic system model.

We introduced all outlines and basics for our problems and the construction and processes for DCM, we contributed with a complementary DCM, the idea that is first we defined all system effects. In this study we used Attention, Motion and Photic as basic effects and then combine all possible combination of these effects, extra four effects were introduced, after we defined these effect we applied these effect to our system making all possible discrimination for all results from DCM parameters which were estimated by EM,

Effective connectivity matrix A was clarified in all different effects for all different regions and comments on these results were stated. We saw that the main effect or interactions were related to the regions behind the front or receiving ones, V1 or V5 but PPC and PFC where signal is translated and transferred to the higher order. It means it is the preparation, these characteristics

differ from person to another. Our brain or higher order center control these interactions and guide them. The induced or change on effective connectivity was described and modulated by B matrices for all events, B is responsible for the characteristics of studied brain region after considering the effect of these external effects, this means also that the behaviors occurs when we interact with the external environment. The direct effects for the external effects, C matrices are also important indicators to differentiate which one from these regions contacts and transfer the stimulus from outside to internal structure.

We simply infer that these three matrices represent what we face against outside events; we cannot recognize any thing if the receptor region is not working and transfer the signal through the internal required system. In sometimes you pass over something but you did not recognize it, means region was not stimulated or the region was off for that event, C matrix not working, if we recognized, we have two ways to represent against the events, the believes and internal history in our mind means A matrix, effective connectivity. Second is to reply directly according to the event, B matrix, modular connectivity or the change. We should control our behavior according to these ways; the optimum way is to compromise the both to behave in a good manner.

HRF is very important because as we mentioned, it is a part of our model and all times series investigations have been concentrating on neural part parameters estimations, so we used PPI convolving both neural and HRF to complement and see the responses, also we introduced all neural and HRF responses using first order kernel

3.7 Summary

We introduced one of the best algorithms for detecting brain dynamics, complementary DCM augmented by PPI to infer the brain dynamics between Brain regions and selecting the four regions related to the visual system V1, V5, PPC and PFC using experimentally designed inputs and brain responses. Based on DCM concept, applied to SPM8, one of the best free software, we made investigations of extracted time series for these studied brain regions. From these time series we will start the next chapter and overcome some drawback and enhance the and contribute our investigations, the first is to use Granger Causality, GC to infer easily the direction of signal path and signal source, second is to make define all subgroups for different responses based on BI-Clustering technique.

Chapter 4

Extracted time series analysis using Granger

Causality and Bi-Clustering analysis

Implementation for DCM as mentioned in the previous chapter with a complementary perspective related to literature review of previous algorithms and DCM itself gave us a good interpretation and perception for modeling brain dynamic system in any target region or spatial system in the brain. As we specified later, that all estimations of connectivity parameters are at the end values. These values are in sometimes negative and can't be investigated easily to infer the direction or path of signal and where is the source and destination. This drawback was solved previously by building specific DCM forward or backward or both to overcome but costs more time. One of the fast and applied methods we used directly to extracted time series of studied brain regions is Granger Causality, GC.

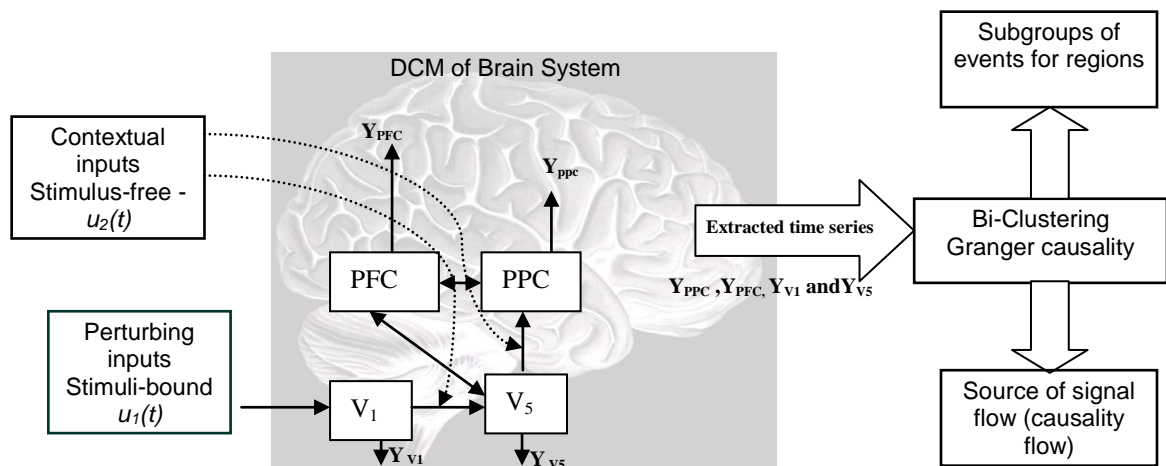


Figure 4.1 a schematic illustrating the concepts of DCM augmented Granger Causality and Bi-Clustering Technique

GC is a potentially promising approach to address some of these issues which is the Granger causality concept [103]. It was borrowed from econometrics and based on the notion of the predictability of one signal by another, subjected to the time constraint that the effect cannot precede the cause. It is specially suited to study partially ordered linear dependences in multivariate contexts without assuming any prior connectivity structure. GC is not enough to infer effective causal relations or full dynamic representation, as it is based only on predictive power. Recent developments in graphical models have worked towards the identification of effective causal links [104].

4.1. Introduction

GC defined for linear stationary multi channel signals but, as with most biological signals, there is no unique model for FMRI data and no strong theoretical or experimental basis for the assumptions of stationary of processes. It is widely recognized that incorrect use of these assumptions can lead to incorrect inferences. We are not applying GC directly for FMRI images time series, but we applied to the extracted time series of studied regions for visual system. We used it to infer easily and accurately with graphical representation the signal source, destination, and causality flow, also we verified our main DCM system.

In this analysis, we combined the Granger causality concept given by Vector Autoregressive, VAR, models to extend the methodology available for the study of brain connectivity. We used Granger Causality of VAR approach and

made inferences about granger causality and signal source and destination over extracted time series of studied brain regions.

In the following section, we will give a review of GC theory and the mathematical derivation; we will apply data using GCCA toolbox, one of the proved and official toolbox used in multivariate granger causality analysis. After clarifying and inferring the causality graph and signal path, we will apply Bi-clustering technique to allow finding subgroups of studied regions that show the same response under a subset of conditions or events, not all conditions. In addition, regions may participate in more than one function, resulting in one regulation pattern in one context and a different pattern in another.

4.2 Granger Causality for Extracted time series

Granger Causality, GC, [105] is a concept that originated in the area of econometrics, focusing on understanding the relationships between two time series. Granger defined the causality in terms of predictability; it is a fact of GC that the effect cannot come before the cause. Subsequently, first time applied GC to the description of interregional connectivity in FMRI data and to detection of the direction of information flow between brain regions was done by Goebel; he applied GC before to analyze time series of BOLD signals in FMRI data [106]. There are two main obstacles to the application of Granger causality mapping in FMRI [103]. The first obstacle is that the BOLD response is not a direct measure of neural activity and the hemodynamic blurring. Despite these apparent problems when applied to FMRI image time series. We apply here, as we mentioned before,

GC for time series extracted from DCM. Formally, consider we a k -dimensional Granger causality

This temporal ordering implies that the past and present values of a series X that influences another series Y should help to predict future values of this latter series Y . Moreover, this improvement in the prediction of future values should persist after any other relevant information for the prediction. This leads to the following definition of Granger-causality: For two time series X and Y let Z be the (vector) time series that comprises all variables that might affect the dependence between X and Y . We say that X Granger-causes Y if the current value of Y can be predicted from the past values of all three series X , Y , and Z than from the past values of the two processes Y and Z alone. Here, better predicted, means a smaller mean square prediction error. We note that the definition depends on the set of variables Z included in the analysis [107].

The vector autoregressive, VAR, model is a straightforward extension of the unvaried autoregressive model [55] and describes how the values of the variables at time t depend linearly on the values at previous time points. The model can be thought as a linear prediction model that predicts the current value of a variable based on its own past value on the previous point in time and the past values of the other variables.

We model these vector time series jointly by one common, VAR process assuming that there are no dependences between subjects. Thus, if the time series of K subjects in n variables are given and $X_{i,k}(t)$ represents the score of the k th person in the i th variable at time t , we consider the joint regression model

$$X_{i,k}(t) = \sum_{j=1}^n \beta_{ij} X_{j,k}(t-1) + \varepsilon_{i,k}(t) \quad (4.1)$$

for $i = 1, \dots, n$ and $k = 1, \dots, K$, which yields n^2 regression coefficient β_{ij} , $i, j = 1, \dots, n$. For the errors $\varepsilon_{i,k}(t)$, we assume that they have mean zero and are uncorrelated between different points in time or different subjects, that is, $E(\varepsilon_{i,k}(t)) = 0$ for all $i = 1, \dots, n$, $k = 1, \dots, K$ and $E(\varepsilon_{i,k}(t)\varepsilon_{j,l}(s)) = 0$, whenever $t \neq s$ or $k \neq l$. Intuitively, the regression coefficients measure the direct influences of the explanatory lagged variables on the dependent variables. Thus, in the above VAR(1) model, variable X_j Granger-causes X_i if the coefficient β_{ij} differs from zero. For the general case of a VAR model of order p , we refer to Eichler [104-108]. Furthermore, the strength of the direct same-time relationships among the variables is quantified by the entries in the inverse of the variance-covariance matrix--the so-called concentration matrix--of the residuals $\varepsilon_1, k(t), \dots, \varepsilon_n, k(t)$.

The VAR analysis is carried out under the assumption of normality of the data. The method, however, is known to be reasonably robust against departures from the distributional assumptions. In such cases, the fitted model describes the linear relationships found in the data. Furthermore, the assumption of stationary can be relaxed by defining VAR models with a deterministic or a stochastic trend. Fitting of a deterministic trend basically results in removing the fitted trend whereas a stochastic trend (random walk behavior) does not require special treatment when fitting by least squares or conditional maximum likelihood. These estimation methods do not necessarily require stationary, which means that time series have time invariant expected values, variances and covariance, but only stationary dynamics in the sense that the internal dependence of the process does

not change between different time points. We note that removing of trends frequently is achieved by differencing the series. We do not recommend this practice since in the case of a deterministic trend this will create a serial dependence not previously in the data that cannot be modeled by a VAR process [55-103]. Likewise in the case of a stochastic trend, fitting of a VAR model upon differencing is inadequate if the series are co-integrated [55].

The VAR model allows an easy way of identifying Granger causality. An important result of the VAR model, is that the series y_{jt} non-causes y_{it} , if and only if, the coefficient $a_{jti}=0$ for any i . In other words, the past values of y_{jt} aid the prediction of future values of y_{it} . Hence, GC simply defined by looking for the VAR representation, and the direction of causality can be interpreted as the direction of information flow. Furthermore, GC relationship is not necessarily reciprocal, for example, y_{jt} may Granger cause the signal y_{it} , and without any implication that y_{it} Granger causes y_{jt} .

In other words, in this case, we allow a time-variant structure for the intercept, auto regression coefficients and covariance matrix. Time-varying autoregressive models have previously been estimated using adaptive filters or windowed models. However, these approaches are suitable only in the context of time-series with many sample points.

Granger causality analysis (GCA) is a method for investigating whether one time series can correctly forecast another. This method is based on multiple regression analysis. At the individual level, many studies performed F statistics on the residuals [103].

4.2.1. GC Mathematical derivation

The importance of identifying causal structure within data, especially during exploratory analysis phases, indicates a need for easy-to-apply, transparent, and extensible software methods. Such methods are provided by the GCCA toolbox described here. The toolbox includes several different types of function. The core functions implement G-causality analysis given multivariate time series data. Other functions test whether the provided data satisfies necessary assumptions, assess the statistical significance and validity of inferred interactions, generate network-level descriptions of patterns of causal interactions, and graphically display analysis results. Functions are also included to apply various preprocessing techniques and to demonstrate the toolbox capabilities. The toolbox is intentionally small **comparing to other several** brain signal analysis toolboxes [108-109],

In terms of linear regression modelling, of Wiener's and Akaike's intuition that X2 'causes' X1 if knowing X2 helps predict the future of X1 (Granger, 1969; Seth, 2007). According to G-causality, X2 causes X1 if the inclusion of past observations of X2 reduces the prediction error of X1 in a linear regression model of X1 and X2, as compared to a model which includes only previous observations of X1. To illustrate G-causality, suppose that the temporal dynamics of two time series X1(t) and X2(t) (both of length T) can be described by a bivariate autoregressive model:

$$\begin{aligned}
 X_1(t) &= \sum_{j=1}^P A_{11,j} X_1(t-j) + \sum_{j=1}^P A_{12,j} X_2(t-j) + \varepsilon_1(t) \\
 X_2(t) &= \sum_{j=1}^P A_{21,j} X_1(t-j) + \sum_{j=1}^P A_{22,j} X_2(t-j) + \varepsilon_2(t)
 \end{aligned} \tag{4.2}$$

where p is the maximum number of lagged observations included in the model (the model order $< T$), A contains the coefficients of the model, and $_1, _2$ are the residuals (prediction errors) for each time series. If the variance of $_1$ (or $_2$) is reduced by the inclusion of the X_2 (or X_1) terms in the first (or second) equation, then it is said that X_2 (or X_1) G-causes X_1 (or X_2). Assuming that X_1 and X_2 are covariance stationary (i.e., unchanging mean and variance), the magnitude of this interaction can be measured by the log ratio of the prediction error variances for the restricted (R) and unrestricted (U) models:

$$\mathcal{F}_{2 \rightarrow 1} = \ln \frac{\text{var}(\xi_{1R(12)})}{\text{var}(\xi_{U1})} \quad (4.3)$$

where $\xi_{1R(12)}$ is derived from the model omitting the $A_{12,j}$ (for all j) coefficients in the first equation and ξ_{U1} is derived from the full model. Importantly, G-causality is easy to generalize to the multivariate (conditional) case in which the G-causality of X_2 on X_1 is tested in the context of multiple additional variables $X_3 \dots X_n$ (Geweke, 1982). In this case, X_2 G-causes X_1 if knowing X_2 reduces the variance in X_1 's prediction error when all other variables $X_3 \dots X_n$ are also included in the regression model. Model order The estimation of MVAR models requires as a parameter the number of time-lags (p) to include, i.e., the model order. Too few lags can lead to a poor representation of the data, whereas too many can lead to problems of model estimation. A principled means to specify the model order means to minimize a criterion that balances the variance accounted for by the model, against the number of coefficients to be estimated. Two criteria are implemented in the toolbox: the Akaike information criterion (AIC, Akaike, 1974) and the Bayesian information criterion (BIC, Schwartz, 1978).

For n variables, the BIC is more often used for application to neural systems because it compensates for the large number of data points commonly found in neural data sets or extracted time series.

4.2.2. GC results and conclusion

Finally GC has drawback in inferring Brain dynamic but strongly integrated to infer easily the causal flow and analysis of time series of extracted regions of interest of a node in a G-causality network is defined as the difference between its out-degree (number of outgoing connections) and its in-degree (number of incoming connections). Causal flow and density can identify nodes that have distinctive causal effects on network dynamics as shown in figure6; A node with a highly positive flow is a causal ‘source’, a node with a highly negative flow is a causal ‘sink’. These after applying extracted region of interest series based on DCM on GCCA toolbox. Also we can easily and accurately recognize the direction of signal flow and its source without building forward or backward model in DCM and also it is another way to verify our designed model beside inside verification.

Based on GCCA toolbox we apply time series for extracted data from DCM to infer easily the direction and signal flow or path and graphically represent the network of signal path, figure 4.2 shows the causal flow and causal unit flow, also figure 4.3 shows Demonstrations of causal connectivity toolbox. The top row shows the raw data (left), the un-weighted significant Granger causality interactions (middle) and the weighted interactions (right). The bottom row shows the causal flow profile (left, see below), and two graphical

representations of causal connectivity: un-weighted (middle) and weighted (right). We inferred with graphical representation a causality and signal path and direction which shows that signal generally is initiated from V1 and stimulating V5 and PPC, also PFC itself transfer the information to PPC, all coordinate together to transfer the outside for the internal system to be recognized via PPC.

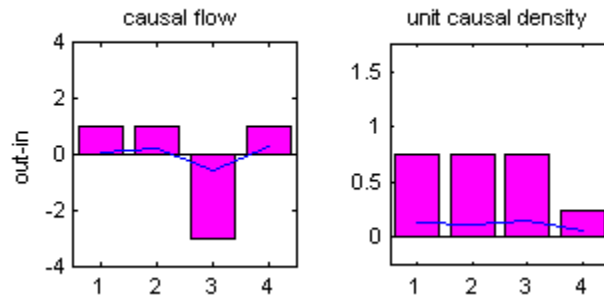


Figure 4, 2 the bar charts show un weighted causal density/flow, and the lines show density/flow weighted by magnitude of causal interaction.

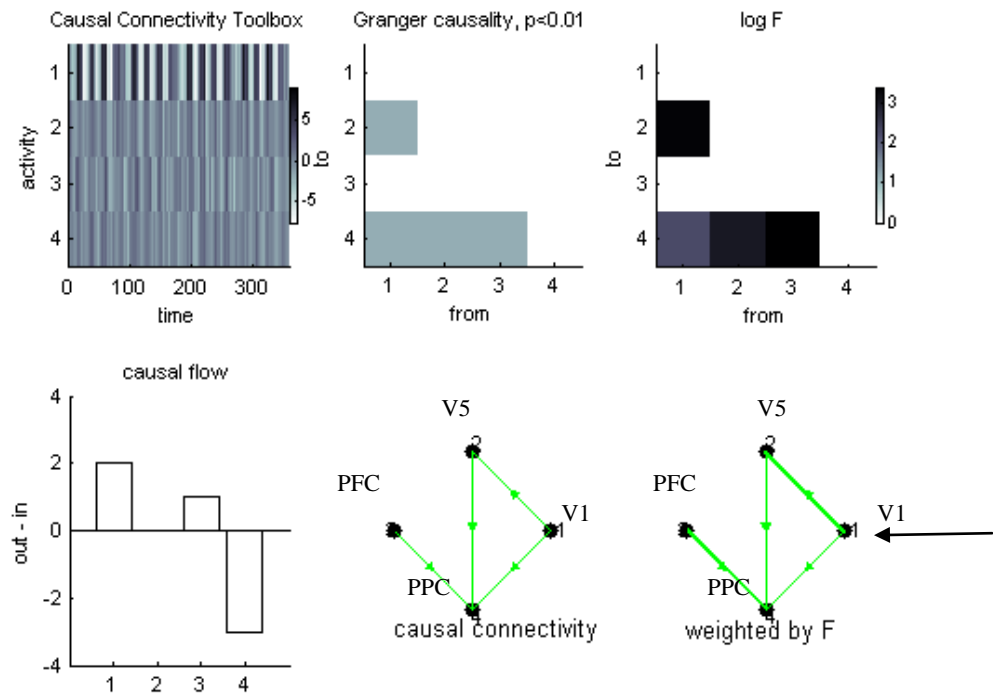


Figure 4.3 Demonstrations of causal connectivity toolbox

4.3 Biclustering for Extracted time series

If we are considering that these behaviors for all brain regions are representing their characters as gene's function, we prepare data in the two-dimensional, rows for regions and columns for values of outputs of these regions at specific effects, attention, motion and Photic and combination of these effects. One of the useful algorithms used in genes analysis is clustering and Biclustering.

Traditional clustering approaches such as k-means and hierarchical clustering also used to infer for functional connectivity and put each gene in exactly one cluster based on the assumption that all genes behave similarly in possible for subset of genes to be co expressed under certain experimental conditions, and at the same time; to behave almost independently under other conditions. To overcome clustering in one dimension, a new two mode clustering approach called biclustering introduced to group the genes or genes and conditions, events, in both dimensions simultaneously. This allows finding subgroups of genes or regions that show the same response under a subset of conditions or events, not all conditions. In addition, genes or regions, may participate in more than one function, resulting in one regulation pattern in one context and a different pattern in another. We expect this gene or region to be included in more than one cluster; and this is useful infer where the similar activity for all region over all effects which cannot be achieved by traditional clustering techniques.

Biclustering outperforms traditional clustering because of its two main characteristics: simultaneous grouping of genes or regions and conditions events,

and overlapping. Simultaneous grouping means that bi clusters that the groups found by biclustering algorithms contain genes or regions with similar behavior under a certain number of conditions or events, the bi cluster will group regions and the conditions events under which the genes regions are related. Overlapping means that regions and events can group together in more than one bicluster, so bi clusters somehow can intersect or overlap among them [110].

4.3.1 Introduction

Biclustering is a non-supervised classification method that, given a data matrix $A = a_{ij}$, groups rows with similar behavior under a subset of columns. We consider regions expression data matrices, where rows are regions and columns are experimental events. What we should consider as similar behavior depends on the kind of biclusters that the method searches for, but typically, it means that all the regions in the bicluster have expression levels within the same range or that the expression varies in the same fashion along the events.

An example of gene expression matrix visualized in figure 4.4 as a heatmap, a representation where transcription levels is represented by a color scale, red conveys high expression and green conveys low expression, two profiles, Therefore, a bicluster $B = (R,E)$ is defined by the subset of region R and the subset of Even E that it groups together. For region R_i and event E_j . We define the overlap sub matrix as $O(B_1, B_2) = A(R_1 \cap R_2, E_1 \cap E_2)$. Note that $O(B_1, B_2)$ can have zero rows or columns, but not both [112-120].

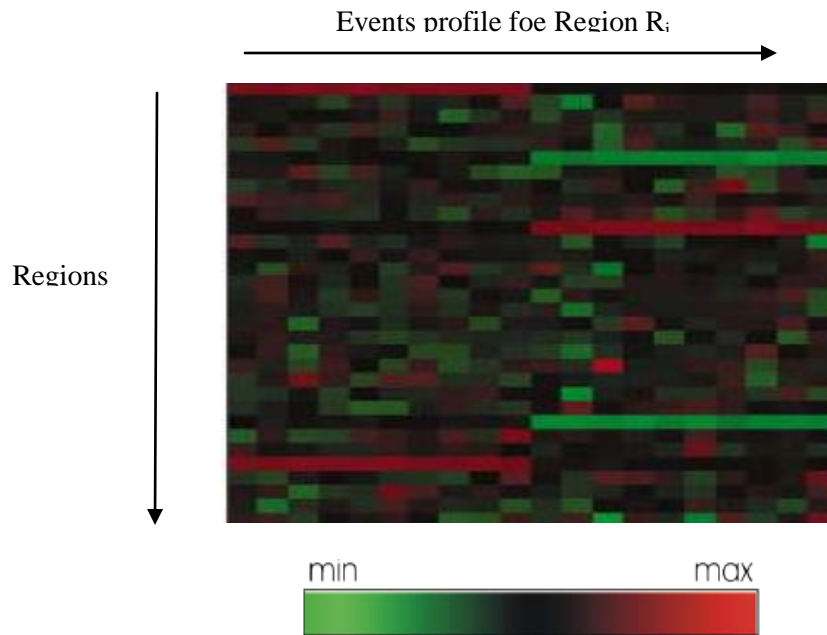


Figure 4.4 Regions expression matrix visualized as a heatmap,

4.3.2 Data Preparation

Before applying to these Bicluster algorithms, one important issue is to rearrange data to be adapted for these programs as gens and conditions, as we specified that if we are considering that we have specific characters against surrounding even twins or people whose in the same environment. Therefore, we rearranged our extracted data of time series for the studied regions assuming that regions like gens and events or behaviors as conditions, our brains have ,as our gens, our characters and codes for what all we doing. The idea is to define system construction and its studied elements or regions, apply different effects that can represent all behaviors for that regions and system, make matrix for these regions in rows and events or behaviors in columns. After we described data, we applied it to the most important and used biclusters, in the second section we will describe the most used biclusters and their results.

4.3.3 Bicluster Types and Results

We selected many Biclusters algorithms applied in BICAT and BIGGEST TS toolboxes; there are basic three main classes of bicluster :Constant Value Bicluster: all the expression levels in the bicluster have exactly the same value. This ideal bicluster of events and is usually relaxed to a merit function with mean and an interval. Coherent Value Bicluster: the expression levels vary along rows and/or columns with some type of coherence, despite their overall level. This relationship may be additive or multiplicative, so rows and/or columns in the biclusters differ one to another in an additive or multiplicative factor [121].

4.3.3.1 Cheng and Church, CC, Bicluster

CC algorithm is the first real biclustering implementation after the primary idea appeared. CC defines a bicluster as a subset of rows and a subset of columns with a high similarity. The proposed similarity score is mean squared residue (H) and it is used to measure the coherence of the rows and columns in the single bicluster. Given the regions expression data matrix $A = (X;Y)$, a bicluster is defined as a uniform sub matrix $(I;J)$ having a low mean squared residue score as following: [122].

The CC Mean Squared Residue:

$$H(I,J) = \frac{1}{|I| |J|} \sum_{i \in I, j \in J} (a_{ij} - a_{iJ} - a_{Ij} + a_{IJ}) \quad (4.4)$$

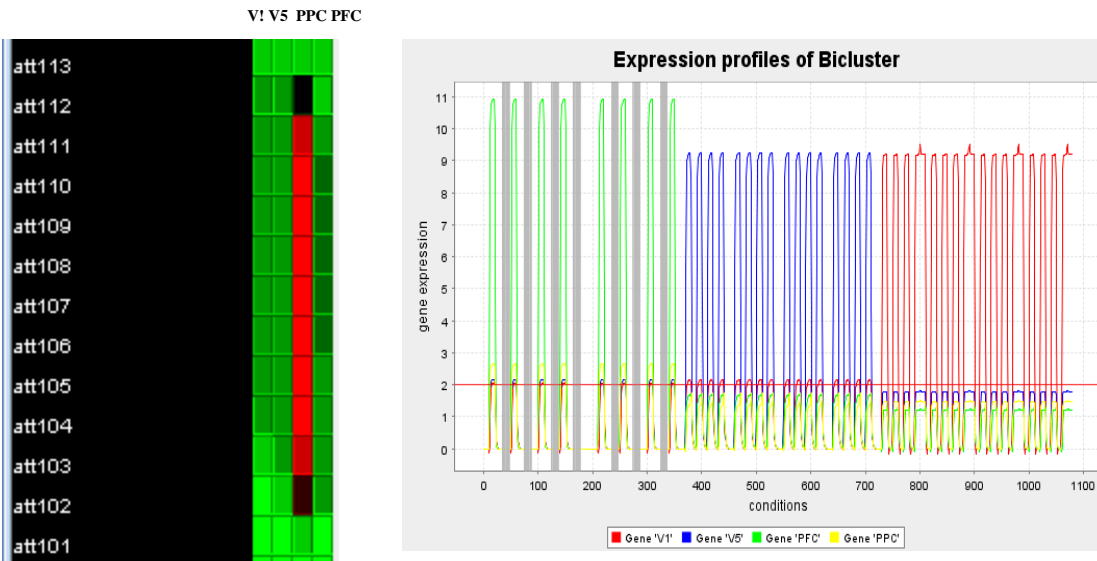


Figure 4.5 first bicluster for CC and expression profile of this bicluster,

Where: a_{ij} is region expression level at row i and column j , $a_{i\cdot}$ is the mean of row i , $a_{\cdot j}$ is the mean of column j , a_{IJ} is the overall mean. CC algorithm will identify the sub matrix as a bicluster if the score is below a level α , which is the input parameter to control the quality of the output biclusters. Generally, CC algorithm performs the its task based on deleting rows and columns with a score larger than α then adding rows or columns until α level is reached, we Iterate these steps until a maximum number of biclusters is reached or no bicluster is found. Figure 4.5 shows for the first bicluster that the high expression profile starts from Att102 to Att112 for region PPC all the rest surrounding this high expression varies from V1 and V5 to PFC for the lowest expression profile. The flow for the data manipulated on **BICAT** toolbox over all events gives us all the information and similarities of events for all events and groups.

4.3.3.2 Contiguous Column Coherent, CCC Biclusters with exact patterns

The linear time complexity of CCC-Biclustering relies on the use of a discredited matrix and efficient string processing techniques based on suffix trees. CCC proposes a method for ranking biclusters based on their statistical significance and a methodology for filtering highly overlapping and, therefore, redundant biclusters. We apply our data via **Biggest TS** toolbox and real data showing the effectiveness of the approach and its relevance in the discovery of regulatory modules. A CCC-Bicluster is Row-Maximal if no more rows can be added to its set of rows I while maintaining the coherence property. It is Right Maximal if its expression pattern S cannot be extended to the right by adding one more symbol at its end the column contiguous to its last column of cannot be added to J without removing genes from I . It is Left Maximal if its expression pattern S cannot be extended to the left by adding one more symbol at its beginning the column contiguous to its first column of cannot be added to J without removing genes from I . It is Maximal if it is Row-Maximal, Left Maximal and Right-Maximal. For CCC-Bicluster we assume defining that A_{IJ} is a subset of row $I = \{i_1, \dots, i_k\}$ and subset of contiguous columns $J = \{r, r+1, \dots, s-1, s\}$, such that $A_{ij} = A_{ij}$ for all rows $i, i \in I$ and columns $j \in J$. Each CCC-Bicluster defines a string S that is common to every row in I for the columns in J the bicluster pattern [123-124].

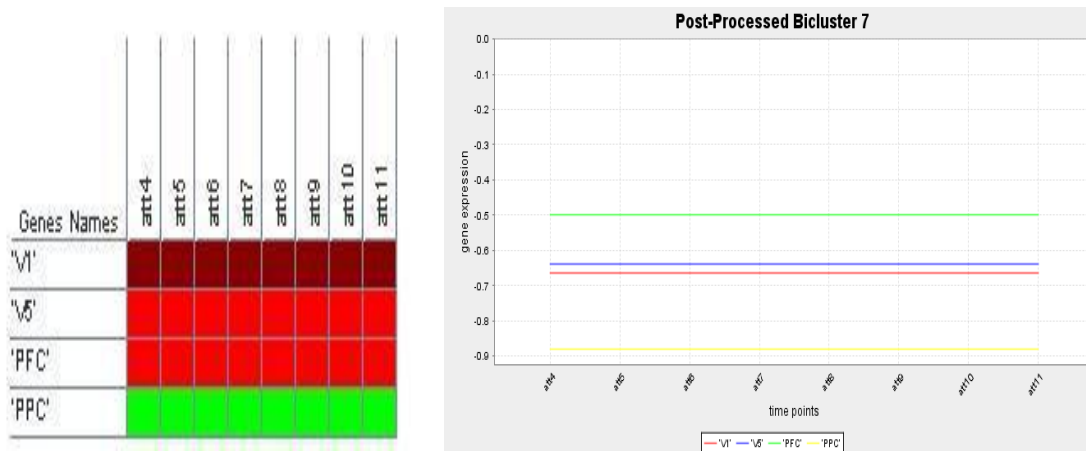


Figure 4.6 Matrix of bicluster for CCC and expression profile of this bicluster7,

Applying our data for the biclustering technique, CCC after discretized matrices and apply bicluster, we review for all possible bicluster after, which are around 3827 Bicluster. For No.7 as shown figure 4.6 the bicluster shows the highest expression in V1, and then V5 and PFC and then the lower expression at PPC. This is for attention events from Att4 to att11. This means number of regions of population and bicluster is four at p value 0.01

We select some clusters to see the expressions for different levels of bicluster; we post processed data after discretized matrices. For bicluster 1283, the highest expression happened to all of V1, V5 and PFC. It is limited for Mot142 events for V1 and V5. While is distributed for all events through Mot138 to Mot142 for PFC, the rest of all subset are for PPC and V1 is lower than it, and V5 is the lowest expression for this Bicluster at p value 0.01 for 4 regions participate in this bicluster and this population as shown in figure 4.7.

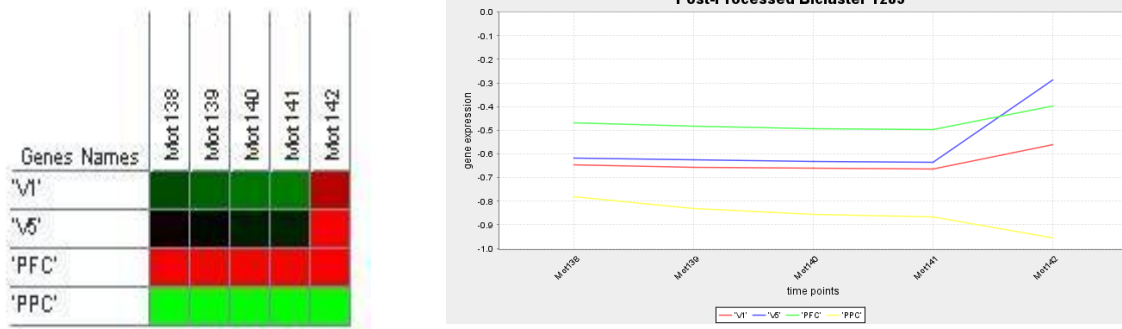


Figure 4.7 Matrix of bicluster for CCC and expression profile of this bicluster1283,

Figure 4.8 shows the outputs of biclusters directly for the data prepared and collecting 12-expression profile for the first twelve biclusters and matrices of biclusters from one which catch the Photic events against V1 and lowered from V5 to PPC .

Bicluster 3 has the highest expression level for V5, also all regions contribute in the highest level for all events. PFC contributes for all values of events, bicluster 8 has the same expression but for different range from Phot314 to 322 instead of Phot334 to 342, bicluster 4 has the highest cell for PFC at Phot334 and only two regions not 4 like above contribute for the highest expression level from Phot342 to Phot360.

e-CCC-Biclustering is finding biclusters with approximate expression patterns based maximum of e errors in discrete data; required parameters: the maximum number of errors allowed per pattern; when activated, the restricted errors variation considers as valid errors only the substitutions of symbols which are on a given neighborhood in the alphabet of discretization. When in the presence of missing values, the algorithm may follow one of two approaches: ignore them, as in the case of the CCC-Biclustering algorithm,

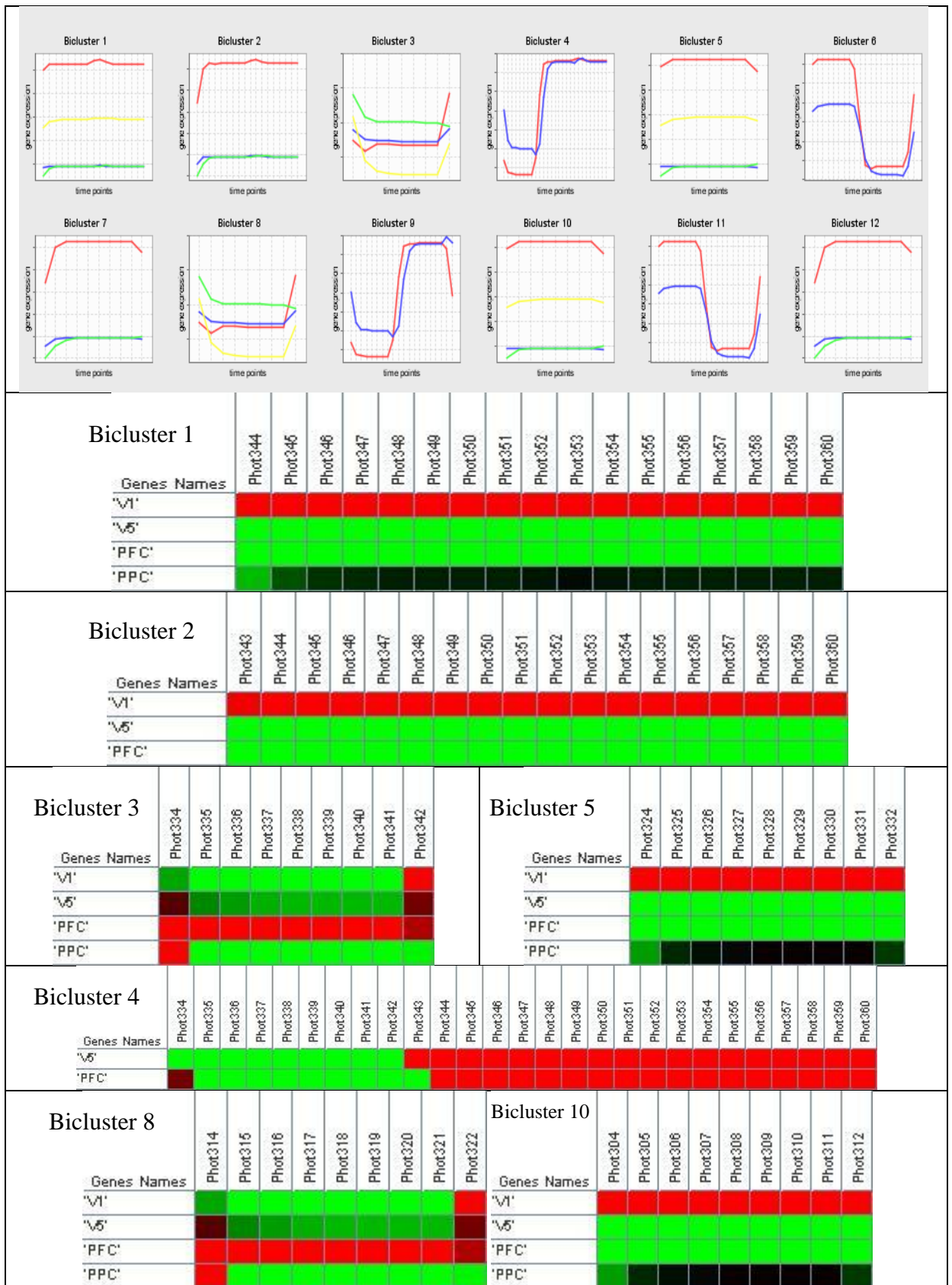


Figure 4.8 graphic representations for matrices of seven bicluster and expression

or consider them as errors. The default behavior is to ignore the missing elements. The difference is all data of bicluster is concentrating Photic events while e-CCC is covering the beginning event in our data, which is attention and contribute all regions and Attention event.

4.3.3.3 Biclusters Inclusion Maximal (Bimax)

Bimax is a simple binary model and new fast divide-and-conquer algorithm used to cluster the gene, region, and expression data. Bimax discretized the region expression data matrix and convert it into a binary matrix by identifying a threshold, so transcription levels, regions expression values, above this threshold become ones and transcription levels below become zeros or vice versa. Then, it searches for all possible bi-clusters that contain only ones. It is first rearrange the rows and columns to concentrate ones in the upper right of the matrix then divide the matrix into two sub matrices, whenever in one of the sub matrices only ones are found, this sub matrix is returned [125].

As shown in figure 4.9 all matrix profile and expression profile for four regions. The first bicluster, ID0 contains all regions and attention effect, the highest value of bicluster expression in 8 points in PFC row. It is repeated regularly every 4 points, the rest of row are lower expression, the same for PPC in lower expression profile, and the lowest expression is V1, and V5, this is from Att17 to Att61 and then Att107 to Att111 and then varies up to Att350.

4.3.3.4 Order Preserving Submatrix (OPSM)

The order preserving submatrix, OPSM, algorithm is a probabilistic model introduced to discover a subset of regions identically ordered among a subset of

events. It focuses on the coherence of the relative order of the events rather than the coherence of actual expression levels. The expression values of the regions within a bicluster induce an identical linear ordering across the selected events.

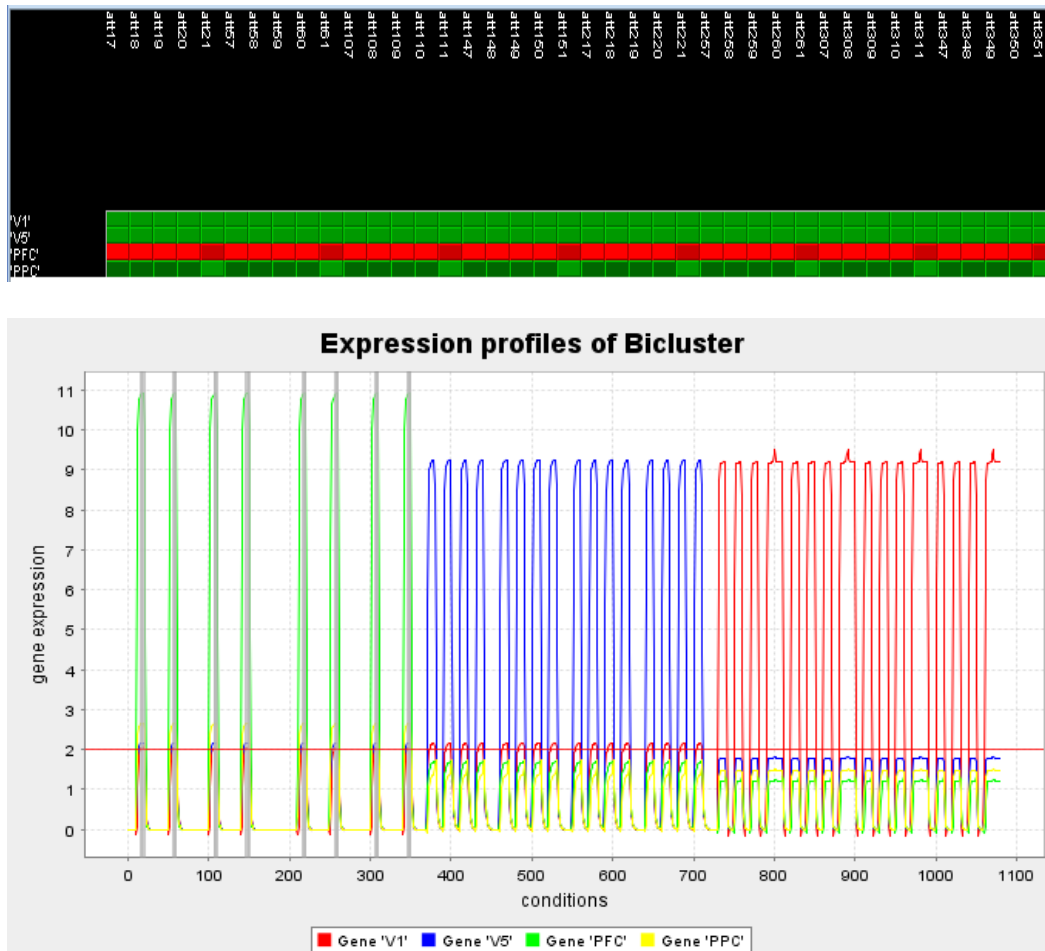


Figure 4.9 Bicluster of Bimax matrix view and expression profile for 4 regions

It is defined that a subset of rows whose values induce a linear order across a subset of the columns [126]. As shown in figure 4.10 Bicluster three in the OPSM Bicluster contributes two events at the end of matrix, and contributes all regions in the other event Motion. In this area, four regions and two events contribute the same expression in v_1 on point att21 and many pints of Photic for the lower expression V_1 , V_5 , PFC and PPC contribute at events Attention and

Photic in different locations. The drawback for this bicluster is that it takes more time for large volumetric data. However, it has a power to combine all different events from the beginning to the last and give us the possibilities to see the performance of these regions at different far locations.

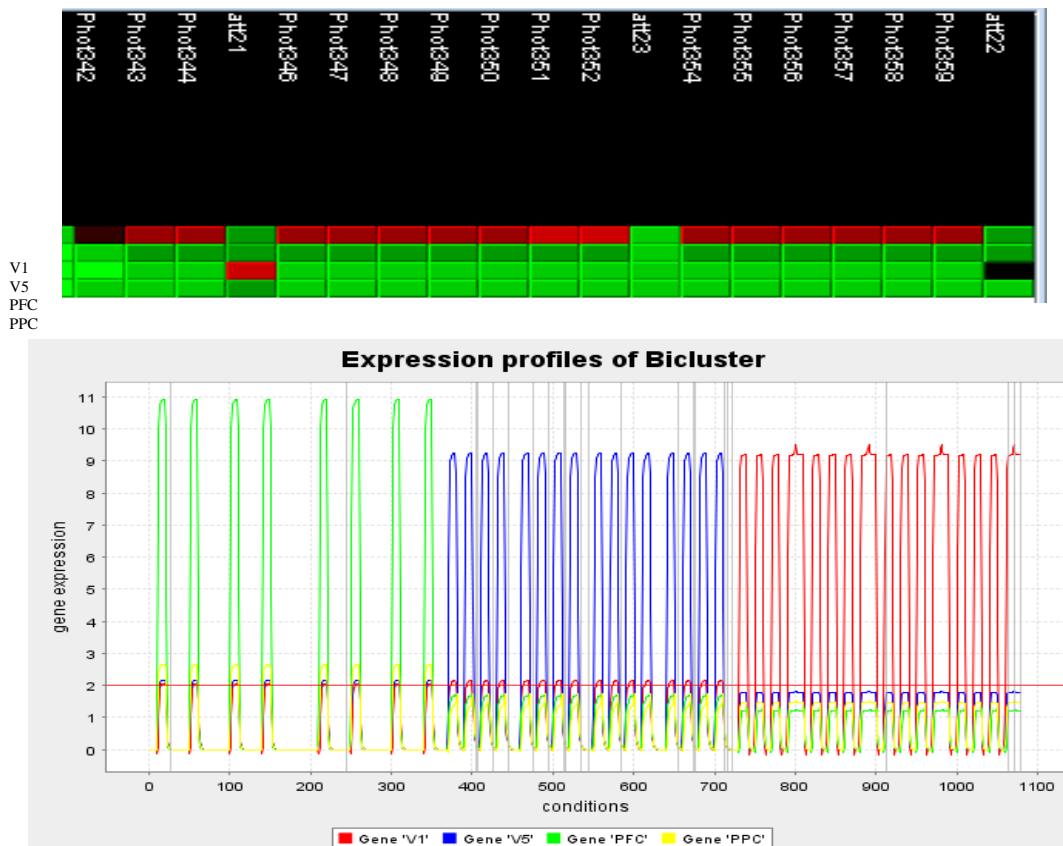


Figure 4.10 Bicluster of OPSM, matrix view and expression profile for 4 regions and two events

4.4 Summary

The main idea comes from our vision to introduce complementary work for what we inferred about our brain from dynamic representation and causality investigations also biclustering time series as we consider it as our genes have codes. In the first section, we introduced at the beginning of this chapter that we have some limitations of DCM or complexity and need to build new forward or

backward model or both to infer the direction or the source or distention of signal, it is the first time that DCM augmented by GC.

GC has been used before for analyzing and inferring the causality of FMRI data. It had a limitation for representing the dynamics of system as DCM, we used it in our thesis not for FMRI data but for time series extracted from DCM for studied regions of visual system, the basic idea was introduced and full description of signal path and causality flow and direction was inferred. All of these investigations were built under the GCCA toolbox, one of the official toolboxes for Granger causality, it is augmented by SPM8.

In the second section we introduced Biclustering which we can't not only subset from conditions as genes biclustering but also subsets from both gens, regions and conditions, events, we applied extracted time series for two official toolboxes, one for CCC and eCCC Biclustering which is Biggest TS and the other for CC, OPSM and Bimax which is BiCat. We inferred subsets for all regions and events. It is assumed that these regions have codes and store information from past, it will be used at events in the future, so reading this subsets and defining them will open the challenges to represent these time series as genes and apply all bioinformatics algorithms to make brain map for all connections and subsets at all possible different events.

Chapter 5

Conclusion and Future work

In this chapter, we will introduce a summary of all work, and comment all what we introduced in all chapters of the thesis. In the second section, we will add the limitation for this area of research; finally, in the last section we will give the ways and recommendations to open the challenges of making complete map and defining all tasks and break all codes in all regions of all subsystem for overall brain system.

5.1 Summary

In chapter one, we introduced and defined the main idea of our work in this thesis, define the problem, and then put the plan of thesis chapters. In chapter two, we gave the core of the background and literature review of our thesis, we started from human brain dynamic system history giving the layout of the brain as a dynamic and a complex system and specifying the preliminary efforts for inferring and investigating human brain complexities, we went through the improvement of technologies and focusing on FMRI.

We gave a general background for FMRI as human brain investigator and the concept of activation process and the role of attention; also, we differentiate why we use it instead of other modalities. After that, we introduced all brain connectivity's types and discriminated the differences between these connectivity and literature review of each one; we answered the question for defining what is inside our brains? The first which region will interact means anatomical, and then

is there any connection and the functionality between this target region and other one? Meant functional connectivity, the last one is at any time this region interacts and affects the surrounding ones? that means considering external inputs or internal changes in regions, this meant effective connectivity or dynamic system representation,

In chapter three, we took from these ideas mentioned above the lines to start in our system. We used DCM in this chapter while we overcome the limitations of the previous methods and give a complementary view for dynamic mapping and causality. This idea was to build a complete DCM, enhancing with PPI, gave a complementary view of different outputs after applying several combinations of effects, and then used extracted time series of this designed model to infer the causality and path of signal using Granger Causality.

We introduced one of the best algorithms for detecting brain dynamics, complementary DCM augmented by PPI to infer the brain dynamics between Brain regions and selecting the four regions related to the visual system V1, V5, PPC and PFC using experimentally designed inputs and brain responses. Based on DCM concept, applied to SPM8 one of the best free software, we made investigations of extracted time series for these studied brain regions. From these time series we will start the next chapter and overcome some drawback and enhance the and contribute our investigations, the first is to use Granger Causality, GC to infer easily the direction of signal path and signal source, second is to make define all subgroups for different responses based on Biclustering techniques.

In chapter 4, we clarified the Granger Causality and its algorithm. We also applied Biclustering to identify and group target regions that exhibit similar response patterns over several events and group the conditions from output profiles across set of regions based on Biclustering technique.

The main idea comes from our vision to introduce complementary work for what we inferred about our brain from dynamic representation and causality investigations also biclustering time series as we consider it as our genes have codes. In the first section, we introduced at the beginning of this chapter that we have some limitations of DCM or complexity and need to build new forward or backward model or both to infer the direction or the source or distention of signal, it is the first time that DCM augmented by GC.

GC has been used before for analyzing and inferring the causality of FMRI data. It had a limitation for representing the dynamics of system as DCM, we used it in our thesis not for FMRI data but for time series extracted from DCM for studied regions of visual system, the basic idea was introduced and full description of signal path and causality flow and direction was inferred. All of these investigations were built under the GCCA toolbox, one of the official toolboxes for Granger causality, it is augmented by SPM8.

In the second section we introduced Biclustering which we can not only subset from conditions as genes biclustering but also subsets from both gens, regions and conditions, events, we applied extracted time series for two official toolboxes, one for CCC and eCCC Biclustering which is Biggest TS and the other for CC, OPSM and Bimax which is BiCat. We inferred subsets for all regions and

events. If we assumed that these regions have codes and store information from past, it will be used at events in the future, so reading this subsets and defining them will open the challenges to represent these time series as genes and apply all bioinformatics algorithms to make brain map for all connections and subsets at all possible different events.

5.1 Limitation

As we mentioned that the brain connectivity A, effective connectivity was stimulated and managed from the higher order centers, all functions of subsystems are managed by higher centers in our brain. Discovering all signals paths for all connections at all different possible events in our brain is the promising idea in the future, some question should be answered, is there any change in subsystem when we study specific system? When subsystem undertakes stored and memorized information? How can it store and retrieve this information during events recognition? The problem of regions of what we are dealing is known, there are still other regions not defined and jobs not localized.

5.1 Challenges and recommendations

The robust challenges is make brain map for all tasks and events for all Usystems and subsystems and try to standardized their normal behaviors leaving harmonics which may represent the characters of one and differentiate him than the others. One of the best way to infer all of these is to use all above methodologies online in the machine and make all feedback to enhance and make volumetric scan for all brain subsystems even those are not in the scope to discover all the surrounding and all functions for all events and conditions.

References

- [1] A. Ammar, R. T. Martin and R. Shane Delamont, "The Brain A Beginner's guide," *Oneworld Publications, 185 Banbury Road, Oxford OX2 7AR, England.* ISBN 978-1-85168-594-3, 2006. [online] available: www.oneworld-publications.com
- [2] A.R. Moller,. "Hearing: Its Physiology and Pathophysiology,". SanDiego: *Academic Press* ,2000.
- [3] J.L. Northern and M.P. Downs, "Hearing in Children, 5th edition," *Philadelphia: Lippincott Williams and Wilkins*, 2002.
- [4] B. Pakkenberg, D. Pelvig, L. Marner, M.J. Bundgaard, H.j.G. Gundersen, H.J.G., J.R. Nyengaard, and L. Regeur, "Aging and the, human neo-cortex" *Exp. Gerontology*, 38:95-99, 2003.
- [5] H.R. Schiffman, "Sensation and Perception. An Integrated Approach," *New York: John Wiley and Sons*, 2001.
- [6] E. Başçar, "Memory and Brain Dynamics Oscillations Integrating Attention, Perception, Learning, and Memory," *Brain Dynamics Research Center Dokuz Eylül University, Izmir*, 2006.
- [7] R.J.Barry, S.J. Johnstone, and A.R.Clarke, "Review of electrophysiology in attention deficit/hyperactivity disorder II. Event-related potentials," *Clinical Neurophysiology*, 114: 184-198, 2003.
- [8] M. M. Bradley and P. J. Lang, "Measuring emotion: The self-assessment manikin (SAM) and the semantic differential," *Journal of Experimental Psychiatry & Behavior Therapy*, 25(1):49{59, 1994.
- [9] R. Zimmer, R. Lang, and G. Oberdorster, "Post-ischemic reactive hyperemia of the isolated perfused brain of the dog," *Pflugers Arch*, vol. 328, no. 4, pp. 332-343, 1971.
- [10] J. K. Gourley and D. D. Heistad, "Characteristics of reactive hyperemia in the cerebral circulation," *Am J Physiol*, vol. 246, no. 1 Pt 2, pp. 52-58, Jan 1984.
- [11] D. MIGUEL, "Brain Functional Assessment With fMRI Joint Bayesian Activity Detection and Hemodynamic Response Estimation in Brain function," *INSTITUTO SUPERIOR TECNICO, Universidade Technica de Lisboa*, 2007.
- [12] K. J. Friston, "Analyzing brain images: Principles and overview," in *Human Brain Function*, Press USA, pp. 25-41. 1997.

- [13] S. L. Z. Nicholas Lange, “Non-linear fourier time series analysis for human brain mapping byfunctional magnetic resonance imaging.” *Applied Statistics*, vol. 46, no. 1, pp. 1–29, 1997.
- [14] K. J. Friston, P. Fletcher, O. Josephs, A. Holmes, M. D. Rugg, and R. Turner, “Event-related FMRI: characterizing differential responses,” *Neuroimage*, vol. 7, no. 1, pp. 30–40, Jan 1998. [Online]. Available: <http://www.fmri.org/>
- [15] S. Ogawa, T. M. Lee, A. R. Kay, and D. W. Tank, “Brain magnetic resonance imaging with contrast dependent on blood oxygenation,” *Proc Natl Acad Sci U S A*, vol. 87, no. 24, pp. 9868–9872, Dec 1990.
- [16] S. Ogawa, D. W. Tank, R. Menon, J. M. Ellermann, S. G. Kim, H. Merkle, and K. Ugurbil, “Intrinsic signal changes accompanying sensory stimulation: functional brain mapping with magnetic resonance imaging,” *Proc Natl Acad Sci U S A*, vol. 89, no. 13, pp. 5951–5955, Jul 1992.
- [17]. A. Mahroos and Y. M. Kadah, “ Modeling the Interaction of Brain Regions Based on Functional Magnetic Resonance Imaging Time series,” *Radio science conference 2008*.
- [18] S. FINGER, “Minds Behind the brain - A History of the Pioneers and Their Discoveries,” *Oxford, Oxford University Press*. 2000,.
- [19] A. GJEDDE, “Brain energy metabolism and the physiological basis of the haemodynamic response in Functional MRI: an introduction to methods,” *Oxford, Oxford University Press*. 37-66, 2001.
- [20] A. GJEDDE, “The Relation Between Brain Function and Cerebral Blood Flow and Metabolism in Cerebrovascular Disease,” *New York, Lippincott-Raven*.23-40, 1997.
- [21] P. A. BANDETTINI, “The temporal resolution of Functional MRI in Functional Magnetic resonance Imaging,” *Berlin, Springer*, 1999.
- [22] A. M. OWEN, R. EPSTEIN, AND I. S. JOHNSRUDE, “FMRI: applications to cognitive neuroscience in Functional MRI: an introduction to methods,” *Oxford, Oxford University Press*. 311 - 328, 2001.
- [23] V. K Jirsa, A. McIntosh, “Handbook of Brain Connectivity,” *Springer-Verlag Berlin Heidelberg*, ISBN 978-3-540-71462-0.2007.
- [24] S. Amari,” Dynamics of pattern formation in lateral-inhibition type neural,” *fields. Biol. Cybern.* 27, 77–87, 1977.
- [25] R.L. Beurle “Properties of a mass of cells capable of regenerating pulses,” *Philos Trans. Soc. London Ser. A*240, 55–94,1956.

- [26] M. Breakspear, J. Terry, K.J. Friston, "Modulation of excitatory synaptic coupling facilitates synchronization and complex dynamics in a nonlinear model of neuronal dynamics Network," *Computation in Neural Systems* 14, 703–732, 2003.
- [27] B. Cessac, M. Samuelides "From Neuron to Neural Network Dynamics. To appear in Dynamical Neural Network. Models and Applications to Neural Computation," *Springer Berlin Heidelberg New York*, 2006.
- [28] S. Fusi, P.J. Drew, L.F. Abbott, "Cascade models of synaptically stored memories," *Neuron*. 45, 599–611. 2005.
- [29] S. Ogawa, et al., "Oxygenation-sensitive contrast in magnetic resonance image of rodent brain at high magnetic fields," *Magn Reson Med*, 14: p. 68-78. 1990.
- [30] S. Ogawa, et al. "Functional brain mapping by blood oxygenation level-dependent contrast magnetic resonance imaging. A comparison of signal characteristics with a biophysical model," *Biophys J*, 64(3): p. 803-12. 1993.
- [31] J.W. Belliveau, et al. "Functional cerebral imaging by susceptibility-contrast NMR," *Magn Reson Med*, 14(3): p. 538-46. 1990.
- [32] J.W. Belliveau, et al. "Functional mapping of the human visual cortex by magnetic resonance imaging," *Science*, 254(5032): p. 716-9. 1991.
- [33] P.T. Fox, and M.E. Raichle, "Stimulus rate determines regional brain blood flow in striate cortex," *Ann Neurol*, 17(3): p. 303-5. 1985.
- [34] R. Turner, et al., "Echo-planar time course MRI of cat brain oxygenation changes," *Magn Reson Med*, 22(1): p. 159-66. 1991.
- [35] D.W. Tank, S. Ogawa, and K. Ugurbil, "Mapping the brain with MRI," *Curr Biol*, 2(10): p. 525-8. 1992.
- [36] P.A. Bandettini, et al., "Time course EPI of human brain function during task activation," *Magn Reson Med*, 25(2): p. 390-7. 1992.
- [37] P.A. Bandettini, et al., "Processing strategies for time-course data sets in functional MRI of the human brain," *Magn Reson Med*, 30(2): p. 161-73. 1993.
- [38] W. Schneider, D.C. Noll, and J.D. Cohen, "Functional topographic mapping of the cortical ribbon in human vision with conventional MRI scanners," *Nature*, 365(6442): p. 150-3. 1993.
- [39] k.K. Kwong, et al., "Dynamic magnetic resonance imaging of human brain activity during primary sensory stimulation," *Proc Natl Acad Sci U S A*, 89(12): p. 5675-9. 1992.

- [40] S.G. Kim, et al., "Functional imaging of human motor cortex at high magnetic field," *J Neurophysiol*, 69(1): p. 297-302. 1993.
- [41] S.G. Kim, et al., "Functional magnetic resonance imaging of motor cortex: hemispheric asymmetry and handedness," *Science*, 261(5121): p. 615-7. 1993.
- [42] A.M. Blamire, et al., "Dynamic mapping of the human visual cortex by high-speed magnetic resonance imaging," *Proc Natl Acad Sci U S A*, 89(22): p. 11069-73. 1992.
- [43] R.M. Hinke, et al., "Functional magnetic resonance imaging of Broca's area during internal speech," *Neuroreport*, 4(6): p. 675-8. 1993.
- [44] S.W. Atlas, et al., "Functional magnetic resonance imaging of regional brain activity in patients with intracerebral gliomas: findings and implications for clinical management," *Neurosurgery*, 38(2): p. 329-38. 1996.
- [45] A. Puce, et al., "Functional magnetic resonance imaging of sensory and motor cortex: comparison with electrophysiological localization," *J Neurosurg*, 83(2): p. 262-70. 1995.
- [46] R.C. Burgess, R.C., "Functional localization by neurophysiologic and neuroimaging techniques," *J Clin Neurophysiol*, 12(5): p. 405.1995.
- [47] F. Analysis Group, "Analysis Group, FMRIB, Oxford, UK. p. FSL is a comprehensive library of image analysis and statistical tools for FMRI, MRI and DTI brain imaging data," *Oxford, UK, FSL - FMRIB Software Library*. 2006.
- [48] S.M. Smith, et al., "Advances in functional and structural MR image analysis and implementation as FSL," *Neuroimage*, 23 Suppl 1: p. S208-19. 2004.
- [49] I.o.N. "SPM - Statistical Parametric Mapping," *University College London*. 2005.
- [50] M.C.O. Wisconsin, "AFNI - software for analysis and visualization of functional magnetic resonance neuroimages," *Medical College of Wisconsin*. 2007.
- [51] R.W. Cox, "AFNI: software for analysis and visualization of functional magnetic resonance neuroimages," *Comput Biomed Res*, 29(3): p. 162-73. 1996.
- [52] M. J. SCHLOSSER, N. AOYAGI, R. K. FULBRIGHT, J. C. GORE, and G. MCCARTHY, "auditory cortex along the sides of the brain shows increased signal," *Hum. Brain Mapp*. 6, 1 - 13. 1998,
- [53] T.D. Wager, J. Jonides, E.E. Smith, and T.E. Nichols, "Towards a taxonomy of attention-shifting: Individual differences in fMRI during multiple shift types," *Cogn Affect Behav Neurosci*, 5(2), 127-143. 2005.

- [54] S. Yantis, J. Schwarzbach, J.T. Serences, R.L. Carlson, M.A. Steinmetz, J.J. Pekar, et al. "Transient neural activity in human parietal cortex during spatial attention shifts," *Nat Neurosci*, 5(10), 995-1002. 2002.
- [55] R. Goebel, A. Roebroeck, D.S. Kim, E. Formisano, "Investigating directed cortical interactions in time-resolved fMRI data using vector autoregressive modeling and Granger causality mapping," *Magnetic Resonance Imaging* 21, 1251–1261. 2003.
- [56] B. Horwitz, J.M. Rumsey and B.C. Donohue, "Functional connectivity of the angular gyrus in normal reading and dyslexia," *Proceedings of the National Academy of Sciences USA* 95, 8939–8944. 1998.
- [57] C.K. Jirsa, "Connectivity and dynamics of neural information processing," *Neuroinformatics*. 2, 183–204. 2004
- [58] S.J. Kiebel, O. David and K.J. Friston, "Dynamic causal modelling of evoked responses in EEG/MEG with lead-field parameterization," *NeuroImage* 30, 1273–1284. 2006.
- [59] R. Kottler, "Online retrieval, processing, and visualization of primate connectivity data from the CoCoMac database," *Neuroinformatics* 2, 127–144. 2004.
- [60] D.S. Tuch, D.H. Salat, J.J. Wisco, A.K. Zaleta, N.D. Hevelone, H.D. Rosas, "Choice reaction time performance correlates with diffusion anisotropy in white matter pathways supporting visuospatial attention," *Proceedings of the National Academy of Sciences of the United States of America* 102: 12212–12217. 2005.
- [61] S. Dehaene, et al. "Conscious, preconscious, and subliminal processing: a testable taxonomy," *TRENDS in Cognitive Sciences*, 10, 204-211. 2006.
- [62] H. Johansen-Berg, T.E. Behrens, E. Sillery, O. Ciccarelli, A.J. Thompson, S.M. Smith and P.M. Matthews "Functional-anatomical validation and individual variation of diffusion tractography-based segmentation of the human thalamus," *Cereb Cortex*. Jan;15(1):31–9. 2005.
- [63] M.A. Tagamets, B. Horwitz, "Integrating electrophysiological and anatomical experimental data to create a large-scale model that simulates a delayed match-to-sample human brain imaging study," *Cereb. Cortex* 8, 310–320. 1998.
- [64] C.C. Hilgetag, G.A. Burns, M.A. O'Neill, J.W. Scannell, M.P. Young, M.P. "Anatomical connectivity defines the organization of clusters of cortical areas in the macaque monkey and the cat," *Philos Trans R Soc Lond B Biol Sci* 355, 91–110. 2000.

- [65] RE. Passingham, KE. Stephan, R. Kötter, "The anatomical basis of functional localization in the cortex," *Nature Rev Neurosci* 3, 606–616.2002.
- [66] O. Sporns, G.Tononi, GM. Edelman, " Theoretical neuroanatomy: Relating anatomical and functional connectivity in graphs and cortical connection matrices.Cereb," *Cortex* 10, 127–141.2000.
- [67] JC. Fiala , "Three-dimensional structure of synapses in the brain and on the web," *Presentation at the World Congress on Computational Intelligence, Honolulu*.2002.
- [68] O. David, L. Harrison, J. Kilner, W. Penny, and K.J. Friston, "Studying effective connectivity with a neural mass model of evoked MEG/EEG responses," *BioMag –in press*. 2004.
- [69] K. Friston, P. Jezzard, R. Turner "Analysis of functional MRI time series," *Hum Brain Mapp*.1:153–171. 1994.
- [70] KJ. Worsley, JI. Chen, J. Lerch, AC. Evans, "Comparing functional connectivity via thresholding correlations and singular value decomposition," *Philos Trans R Soc Lond B Biol Sci*. 360(1457):913–920. 2005.
- [71] L.I. Kaiming, G. Lei, N. Jingxin, L. Gang and L. Tianming "Review of methods for functional brain connectivity detection using FMRI," *Med Imaging Graph*. March; 33(2): 131–139. 2009.
- [72] J. Cao and K.J. Worsley, "The geometry of correlation fields, with an application to functional connectivity of the brain," *Ann Appl Probab*. 9:1021–1057. 1999.
- [73] K. Friston, P. Jezzard, R. Turner, "Analysis of functional MRI time series," *Hum Brain Mapp*. 1:153–171. 1994.
- [74] S.P. Lee SP, TQ. Duong, G.Yang, C. Iadecola, SG. Kim, "Relative changes of cerebral arterial and venous blood volumes during increased cerebral blood flow," *implications for BOLD fMRI. Magn Reson Med*. 45(5):791–800. 2001.
- [75] F.M. Miezin, L. Maccotta, J.M. Ollinger, SE. Petersen and RL. Buckner, "Characterizing the hemodynamic response: effects of presentation rate, sampling procedure, and the possibility of ordering brain activity based on relative timing," *NeuroImage*. 11(6 Pt1):735–759. 2000.
- [76] Z.S. Saad, K.M. Ropella, RW. Cox and EA. DeYoe, "Analysis and use of FMRI response delays," *Hum Brain Mapp*. 13(2):74–93. 2001.

- [77] K.J. Friston, AP. Holmes, KJ. Worsley, J.B. Poline, CD. Frith, RSJ. Frackowiak, "Statistical parametric maps in functional imaging: a general linear approach," *Hum Brain Mapp.* 2:189–210. 1995.
- [78] G.A. Cecchi, AR. Rao, MV. Centeno, M. Baliki Av. Apkarian and DR. Chialvo. "Identifying directed links in large scale functional networks: application to brain fMRI," *BMC Cell Biol.* 8(1):S5. 2007.
- [79] L. Ma, B. Wang, X. Chen and J. Xiong, "Detecting functional connectivity in the resting brain: a comparison between ICA and CCA," *Magn Reson Imaging.* 25(1):47–56. 2007.
- [80] A. Hyvärinen and E. Oja "Independent component analysis: algorithms and applications," *Neural Netw.* 13(4–5):411–430. 2000.
- [81] M.J. McKeown, S. Makeig, GG. Brown, T.P. Jung, SS. Kindermann and AJ. Bell, "Analysis of fMRI data by blind separation into independent spatial components," *Hum Brain Mapp.* 6:160–188. 1998.
- [82] C.F. Beckmann and SM. Smith, "Probabilistic independent component analysis for functional magnetic resonance imaging," *IEEE Trans Med Imaging.* 23:137–152. 2004.
- [83] K. Chuang, M. Chiu, C. Lin, and J.Chen, "Model-free functional mri analysis using kohonen clustering neural network and fuzzy c-means," *IEEE Trans Med Imaging.* 18(8):1117–1128. 1999.
- [84] X. Golay, S. Kollias, G. Stoll, D. Meier, A. Valavanis and P. Boesiger, "A new correlation-based fuzzy logic clustering algorithm for fMRI," *Magn Reson Med.* 40:249–260. 1998.
- [85] D. Cordes, V.Haughton, J.Carew, K. Arfanakis, and K. Maravilla, "Hierarchical clustering to measure connectivity in fMRI resting-state data," *J Magn Reson Med.* 20(4):305–317. 2002.
- [86] K.J. Friston, J. Ashburner, S. Kiebel, T. Nichols and W. Penny, "STATISTICAL PARAMETRIC MAPPING: THE ANALYSIS OF FUNCTIONAL BRAIN IMAGES," *Neuroscience, University College London, London, UK.* Hardbound, 656 pages, publication date: NOV-2006.
- [87] K.S. Enno and K.J. Friston, "Analyzing effective connectivity with FMRI," *Wiley Interdiscip Rev Cogn Sci.* June; 1(3): 446–459. 2010.

- [88] A. Aertsen and H. Preißl, “Dynamics of activity and connectivity in physiological neuronal networks. In: HG S, editor. *Nonlinear Dynamics and Neuronal Networks*,” *VCH Publishers; New York*: pp. 281–302. 1999.
- [89] K.E. Stephan, “On the role of general system theory for functional neuroimaging,” *J Anat. Dec*;205(no. 6):443–70. 2004.
- [90] V.K. Jirsa, “Connectivity and dynamics of neural information processing,” *Neuroinformatics. Sum*;2(no. 2):183–204. 2004.
- [91] K.J. Friston, N. Trujillo-Barreto, J. Daunizeau, “DEM: a variational treatment of dynamic systems,” *Neuroimage. Jul 1*;41(no. 3):849–85. 2008.
- [92] O. David, S.J. Kiebel, L.M. Harrison, J. Mattout, J.M. Kilner and K.J. Friston, “Dynamic causal modeling of evoked responses in EEG and MEG,” *Neuroimage. May 1*;30(no. 4):1255–72. 2006.
- [93] K.J. Friston, A. Mechelli, R. Turner, And C.J. Price , “Nonlinear responses in FMRI: the Balloon model, Volterra kernels and other hemodynamic,” *NeuroImage 12*: 466–477. 2000.
- [94] K.E. Stephan, N. Weiskopf, P.M. Drysdale, P.A. Robinson and K.J. Friston “Comparing hemodynamic models with DCM,” *Neuroimage. Nov 15*;38(no. 3):387–401.2007.
- [95] K.J. Friston, L. Harrison and Penny, “Dynamic causal modeling,” *Neuroimage 19*:1273-1302. 2003.
- [96] K.J. Friston, “Bayesian estimation of dynamical systems: an application to FMRI,” *Neuroimage. Jun*;16(no. 2):513–30. 2002.
- [97] F. Acs and M.W. Greenlee. “Connectivity modulation of early visual processing areas during covert and overt tracking tasks,” *Neuroimage. Jun*;41(no. 2):380–8. 2008.
- [98] P.R. Baxter and L.M. Victoria, T.N Allen and C.G. John “Assessing functional connectivity in the human brain by FMRI,” *Magnetic Resonance Imaging 25*:1347–1357. 2007.
- [99] K. Jieun and H. Barry “Investigating the neural basis for fMRI-based functional connectivity in a blocked design: application to interregional correlations and psycho-physiological interactions,” *Magnetic Resonance Imaging. 26*:583–593. 2008.
- [100] K.E. Stephan, W.D. Penny, J. Daunizeau, R.J. Moran and K.J. Friston, “Bayesian model selection for group studies,” *Neuroimage. Jul 15*;46(no. 4):1004–17. 2009.

- [101] A. Mahroos and Y. M. Kadah “Modeling the Interaction of Brain Regions Based on Functional Magnetic Resonance Imaging Time series,” *Radio science conference* 2008.
- [102] A. Mahroos and Y. M. Kadah, “Inferring visual system connectivity using dynamic causal modeling of functional magnetic resonance imaging data,” *SPIE Medical Imaging conference*, 2010.
- [103] A. Roebroeck, E. Formisano, et al. "Mapping directed influence over the brain using Granger causality and fMRI." *Neuroimage* 25(1): 230-42. 2005.
- [104] M. Eichler, "A graphical approach for evaluating effective connectivity in neural systems". *Philos Trans R Soc Lond B Biol Sci.* 29;360(1457):953-67. 2005.
- [105] C.W. J. Granger, "Investigating causal relations by econometric models and cross-spectral methods,". *Econometrica* 37: 424-438.1969.
- [106] R. Goebel, A. Roebroeck, et al. "Investigating directed cortical interactions in time-resolved FMRI data using vector autoregressive modeling and Granger causality mapping," *Magn Reson Imaging* 21(10): 1251-61. 2003.
- [107] K. Anil. Seth “A MATLAB toolbox for Granger causal connectivity analysis,” *Journal of Neuroscience Methods.*186: 262–273. 2010.
- [108] J.Cui J. L. Xu, SL. Bressler, M. Ding and H. Liang.. “BSMART: a Matlab/C toolboxfor analysis of multichannel neural time series,”. *Neural Netw.* 21:194–104. 2008.
- [109] A. Delorme, S. Makeig , “EEGLAB: an open source toolbox for analysis of single-trial EEG dynamics including independent component analysis,” *J Neurosci Methods.* 134:9–21. 2004.
- [110] F. M. Al-Akwaa. “Construction the Gene Regulatory Network Using Bayesian Network and Biclustering,” *Faculty of Engineering, Cairo University.* Ph.D. Thesis.2010.
- [112] J. S. Aguilar-Ruiz. “Shifting and scaling patterns from gene expression data. *Bioinformatics*,” 21:3840–3845, 2005.
- [113] A. Ben-Dor, B. Chor, R. Karp, and Z. Yakhini, “Discovering local structure in gene expression data: the order-preserving submatrix problem,” *Journal of Computational Biology*, 10:373–384, 2003.
- [114] T. Buering, J. Gerken, and H. Reiterer, “User interaction with scatterplots on small screens - a comparative evaluation of geometricsemantic zoom and fisheye

- distortion,” *IEEE Transactions on Visualization and Computer Graphics*, 12(5):829–836, 2006.
- [115] S. Busygin, G. Jacobsen, and E. Kramer, “Double conjugated clustering applied to leukemia microarray data,” *In Second SIAM ICDM, Workshop on clustering high dimensional data*. 2002.
- [116] A. Califano, G. Stolovitzky, and Y. Tu, “Analysis of gene expression microarrays for phenotype classification,” *Proc. Int. Conf. Intell. Syst. Mol. Biol.*, 8:75–85, 2000.
- [117] P. Carmona-Saez, R. D. Pascual-Marqui, F. Tirado, J. M. Carazo, and A. Pascual-Montano, “Biclustering of gene expression data by non-smooth non-negative matrix factorization,” *BMC Bioinformatics*, 7(78), 2006.
- [118] Y. Cheng and G. M. Church, “Biclustering of expression data,” *Proc. Int’l Conf Intell Syst Mol Biol.*, 8:93–103, 2000.
- [119] Y. Kluger, R. Basri, J. T. Chang, and M. Gerstein, “Spectral biclustering of microarray data: Coclustering genes and conditions,” *Genome Research*, 13:703–716, 2003.
- [120] L. Lazzeroni and A. Owen, “Plaid models for gene expression data,” *Technical Report, Stanford University*, 2002.
- [121] S. Madeira and A. Oliveira, “Biclustering algorithms for biological data analysis: a survey,” *IEEE/ACM Transactions of Computational Biology and Bioinformatics*, 1(1):24–45, 2004.
- [122] Y. Cheng and G. Church, “Biclustering of expression data,” *Proceedings of 8th International Conference on Intelligent Systems for Molecular Biology*, pp. 93–103, 2000.
- [123] C. Sara, Madeira, L. Arlindo, “e-CCC-Biclustering: Related work on biclustering algorithms for time series gene expression data,” *Proceedings of the 5th AsiaPacific Bioinformatics Conference*. 2007.
- [124] P. Joana, Gonçalves, C. Sara, Madeira and L. Arlindo Oliveira, “BiGGES: integrated environment for biclustering analysis of time series gene expression data,” *BMC Research Notes* 2009,
- [125] A. Prelic, S. Bleuler, P. Zimmermann, A. Wille, P. Buhlmann, W. Gruissem, L. Hennig, L. Thiele, and E. Zitzler, “A systematic comparison and evaluation of biclustering methods for gene expression data,” *Bioinformatics*, p. bt1060, 2006.

- [126] A. Ben-Dor, B. Chor, R. Karp, and Z. Yakhini, “Discovering local structure in gene expression data: the order-preserving submatrix problem,” *Journal of Computational Biology*, vol. 10, no. 3-4, pp. 373–384, 2003.
- [127] A. Mahroos and Y. M. Kadah “Brain Causality Investigation Based on FMRI Images Time Series Using Dynamic Causal Modelling Augmented by Granger Causality,” *Radio science conference* 2011.

Appendices

Appendix A. Survey of Major fMRI Software Packages

The focus of this appendix is FMRI software. Although there is both commercial software and freely downloadable software available for the analysis of FMRI data, many groups also develop their own procedures using programming languages such as MATLAB. Software is constantly being updated and upgraded; readers are advised that the content of this appendix is current to the time of writing, and they should check the relevant links for the newest versions.

Homepages for the various software packages give detailed explanation on downloading and use, SPM and AFNI both have active user lists (email for a for discussion); SPM also has several “wikis” that users new and old can consult and contribute to. The electronic resources for these packages in particular are extensive and are an important source of knowledge and information for the communities of users.

1. Analysis of Functional NeuroImages: AFNI

This package, AFNI, (homepage <http://afni.nimh.nih.gov>) was developed by Robert Cox starting in 1994, originally, today it is one of the most widely used packages for the analysis of FMRI data, providing a full range of tools for statistical modeling and inference, and the visual display of results. AFNI is a collection of programs written in C, and runs in Unix environments (including Linux and Mac OS X).

2. Statistical Parametric Mapping: SPM

The package SPM (homepage <http://www.fil.ion.ucl.ac.uk/spm>) is a suite of MATLAB programs for the analysis of brain imaging data in general, including imaging modalities beyond FMRI. It was originally developed in 1991 by Karl Friston to analyze images collected using positron emission tomography (PET). SPM can be run in both Unix (including Linux) and Windows environments. Among the capabilities of SPM are realignment of image sequences; automated spatial normalization; segmentation of images; spatial smoothing; data analysis via a general linear model approach (maximum likelihood and Bayes estimation); display of statistical maps; display of posterior probability maps; analysis of functional connectivity.

SPM is perhaps the leading software package for the analysis of FMRI data in terms of popularity and as such, it played a prominent role in shaping how practitioners think about the statistical aspects of their data. The general linear model approach and in particular the random effect model, the canonical HRF model, the ways in which SPM presents the output of an analysis, have all become standards in the literature. This is useful, on the one hand, since it

provides a uniform frame of reference for researchers from different laboratories; however, this uniformity can pose problems for neuroimagers who use other software packages, or indeed who develop their own programs. SPM is base for our work that we construct a complementary DCM on its platform augmented by PPI and applied GC and Biclustering for extracted time series of studied regions.

3. Other Packages

Although SPM and AFNI are widely used, there are other prominent packages also available. Some of these are described here. The list is by no means exhaustive, however. Functional Imaging Analysis Software, Computational Olio (FIASCO; homepage <http://www.stat.cmu.edu/~fiasco/>) was developed at Carnegie Mellon University's Statistics Department, primarily by Bill Eddy. FIASCO is a collection of shell scripts and executables written in C and Python. It performs preprocessing (detrending, motion correction, and so forth), fits linear models to the data, thresholds and displays images. Users can also write their own procedures to customize their analyses. Automated Image Registration (AIR; homepage <http://bishopw.loni.ucla.edu/AIR5/index.html>) was developed by Roger Woods to perform automated registration of two- and three-dimensional images, both within and across subjects. FMRIB Software Library, FSL; homepage <http://www.fmrib.ox.ac.uk/fsl>) is written mainly by the members of the Analysis Group, FMRIB, at Oxford University. FSL is a library of tools for image analysis and statistical processing of FMRI data, among other modalities. It runs in Apple, PC (Linux and Windows), and Unix environments. Among the capabilities of FSL for functional imaging are: general linear model analysis;

Bayesian analysis; model-free analysis via Independent Component Analysis; spatial mixture modeling; thresholding using the permutation test, Gaussian random field, and false discovery rate approaches; interactive display of three- and four-dimensional images; registration and segmentation of images.

FSL has an email list for users; archives and information on joining this list can be found at <http://www.jiscmail.ac.uk/lists/fsl.html>. VoxBo (homepage <http://www.voxbo.org>) is a suite of C/C++ programs that runs in a Linux environment, including OS X for Mac and Cygwin for Windows. VoxBo performs standard preprocessing (motion correction, normalization, smoothing); data analysis via the general linear model for block and event-related designs; and graphical presentation at the voxel level (voxel time series, for example). The analysis focus is on the univariate general linear model; other types of analysis are not supported in VoxBo. A characteristic of VoxBo is its scheduling mechanisms, which allow for easy batch processing of fMRI data sets. Like SPM, VoxBo has a wiki, found at <http://voxbo.org/wiki/index>. for information on the lists and how to join them, see <http://www.voxbo.org/lists.html>. FMRI stat (homepage <http://www.math.mcgill.ca/keith/fmristat>) was developed by Keith Worsley of McGill University. It is a MATLAB-based collection of tools and can be run in Windows and Linux environments. FMRI stat features a variety of linear model analyses, analysis of the hemodynamic response function, thresholding via random field theory or false discovery rate control, and an advanced suite of visualization modules.

4. Comparison of Imaging Software Packages

Gold et al. (1998) report a descriptive comparison of many of the packages (both freeware and commercial) available in the late 1990s for the analysis of FMRI data. The comparison considers operating system; availability of source code; completeness of documentation (including ease of learning and the inclusion of a graphical user interface – GUI); necessary preprocessing steps; inclusion of image realignment routines; capability to input images of different dimension; types of statistical analysis; image display features; inclusion of spatial transformations; and corrections for multiple testing. As might be expected, Gold et al. (1998) find that each package has advantages and drawbacks. The choice of software depends, to a large extent, on the requirements of the particular laboratory or group. Hence it is not possible to conclusively recommend one package over the others. AFNI and SPM, for example, have extensive GUIs, which make them easy to use. On the other hand, SPM relies heavily on MATLAB, a potential barrier for users who would therefore be required to obtain the latter in order to run the former. FIASCO doesn't have a GUI at all; rather, routines are invoked on command line operations, in a hierarchical structure (scripts call scripts); while some may see this as a drawback, it does in fact allow users a great deal of flexibility in customizing analysis. The following table summarizes some of the features of the packages described in this appendix. In practice, many people find it helpful to use different packages for different parts of their analyses in order to build on the strengths of

each. The software developers themselves generally take an ecumenical “mix and match” approach; useful analyses from one package are also often quickly adopted by others.

Feature	AFNI	SPM	FIASCO	FSL	VoxBo	fMRIstat
Computing environment	Unix	Linux Windows	Unix	Linux Windows	Linux	Linux Windows
Source code language	C	MATLAB	C/Python	Unknown	C/C++	MATLAB
GUI	Yes	Yes	No	Yes	Yes	No
Email list	Yes	Yes	No	Yes	Yes	No
Other user resources	No	Wiki	No	No	Wiki	No
Statistical analysis	LM+	LM+	LM+	LM+	LM	LM+
Multiple testing	CT/FDR	RF/FDR	FDR	CT/FDR	CT+	RF/FDR

Table A1. Summary of FMRI software analysis packages.

Appendix A.2: Parameter and hyperparameter estimation with EM

In this appendix we provide a heuristic motivation for the E- and M-Steps of the estimation scheme summarized in Equation 3.6. These steps can be regarded on as Fisher Scoring ascent on an objective function F that embodies the log posterior.

The E-Step

The conditional expectations and covariances of the parameters are estimated in the E-Step that performs a gradient ascent on the log posterior comprising the likelihood and prior potentials

$$\begin{aligned}
 l &= \ln p(\theta|y, \lambda; u) \\
 &= \ln p(y|\theta, \lambda; u) + \ln p(\theta) + \dots \\
 \ln p(y|\theta, \lambda; u) &= -\frac{1}{2}(y - h(u, \theta))^T C_\varepsilon^{-1}(y - h(u, \theta)) \\
 \ln p(\theta; u) &= -\frac{1}{2}(\eta_\theta - \theta)^T C_\theta^{-1}(\eta_\theta - \theta)
 \end{aligned}
 \tag{A2.1}$$

On taking gradients with respect to the parameters, the following Fisher scoring scheme ensues.

$$\begin{aligned}
 \eta_{\theta|y} &\leftarrow \eta_{\theta|y} - \left\langle \frac{\partial^2 l}{\partial \theta^2} \right\rangle^{-1} \frac{\partial l}{\partial \theta}(\eta_{\theta|y}) \\
 \frac{\partial l}{\partial \theta} &= \mathbf{J}^T \mathbf{C}_\varepsilon^{-1} \mathbf{r} + \mathbf{C}_\theta^{-1} (\eta_\theta - \eta_{\theta|y}) \\
 - \left\langle \frac{\partial^2 l}{\partial \theta^2} \right\rangle &= \mathbf{J}^T \mathbf{C}_\varepsilon^{-1} \mathbf{J} + \mathbf{C}_\theta^{-1} = \mathbf{C}_{\theta|y}^{-1}
 \end{aligned}
 \tag{A2.2}$$

where $\mathbf{J} = \partial h(\eta_{\theta|y}) / \partial \theta$, $\mathbf{r} = \mathbf{y} - h(\mathbf{u}, \eta_{\theta|y})$ and $\mathbf{C}_\varepsilon = \sum \lambda_i \mathbf{Q}_i$ is the hyperparameterized error covariance.

The M-Step

The hyperparameters are estimated in the M-Step in exactly the same way as the parameters but accounting for the fact that the log likelihood depends on the unknown parameters by integrating them out using the approximate conditional distribution $q(\theta)$. Note there are no priors on the hyperparameters. This integration motivates a lower bound on the log likelihood called the [negative] free energy in statistical physics (Neal & Hinton 1998). By Jensen's inequality

$$\begin{aligned}
 \ln p(y|\lambda; u) &= \ln \int q(\theta) \frac{p(\theta, y|\lambda; u)}{q(\theta)} d\theta \geq \\
 F &= \int q(\theta) \ln \frac{p(\theta, y|\lambda; u)}{q(\theta)} d\theta
 \end{aligned}
 \tag{A2.3}$$

On taking gradients with respect to the hyperparameters, the following Fisher scoring scheme can be derived.

$$\begin{aligned}
\lambda &\leftarrow \lambda - \left\langle \frac{\partial^2 F}{\partial \lambda^2} \right\rangle^{-1} \frac{\partial F}{\partial \lambda}(\lambda) \\
\frac{\partial F}{\partial \lambda_i} &= \frac{1}{2} \text{tr}\{PQ_i\} - \frac{1}{2} r^T P^T Q_i P r \\
-\left\langle \frac{\partial^2 F}{\partial \lambda^2} \right\rangle_{ij} &= \frac{1}{2} \text{tr}\{PQ_i P Q_j\}
\end{aligned} \tag{A2.4}$$

$P = C_\varepsilon^{-1} - C_\varepsilon^{-1} J C_{\theta|y}^{-1} J^T C_\varepsilon^{-1}$. The parameter ascent on the log posterior l in the E-Step is closely related to an ascent on the negative free energy F used for the hyperparameters in the M-Step, with exact equivalence when $q(\theta)$ is deterministic. This can be seen if we write

$$\begin{aligned}
F &= \int q(\theta) \ln p(y|\theta, \lambda; u) d\theta - \int q(\theta) \ln \frac{q(\theta)}{p(\theta)} d\theta \\
&= \left\langle \ln p(y|\theta, \lambda; u) \right\rangle_q - KL(q(\theta), p(\theta))
\end{aligned} \tag{A2.5}$$

F comprises the expected log likelihood under $q(\theta)$ and a prior term embodying the Kullback-Leibler (KL) divergence between the conditional and prior densities.

$F = l$ when $q(\theta)$ shrinks to a point density over $\eta_{\theta|y}$. For completeness, it is noted that, in a linear setting, F is also the ReML (Restricted Maximum Likelihood) objective function used in classical variance component estimation (Harville 1977).

This EM algorithm is simple, robust and has found multiple applications in our data analysis; ranging from ReML estimates of serial correlations in fMRI to hyperparameter estimation in hierarchical observation models using empirical

Bayes, see Friston et al (2002) for details. In our implementation we iterate the E and M-Steps until convergence before re-computing $J = \partial h(\eta_{\theta|y}) / \partial \theta$.

Appendix A3. HRF Estimation

As noted above, the estimation scheme is a posterior density analysis under Gaussian assumptions. This is described in detail in Friston (2002). In short, the estimation scheme provides the approximating Gaussian posterior density of the parameters $q(\theta)$ in terms of its expectation $\eta_{\theta|y}$ and covariance $C_{\theta|y}$. The expectation is also known as the posterior mode or maximum a posteriori (MAP) estimator. The marginal posterior probabilities are then used for inference that any particular parameter or contrast of parameters $c^T \eta_{\theta|y}$ (e.g. average) exceeds a specified threshold γ .

$$p = \phi_N \left(\frac{c^T \eta_{\theta|y} - \gamma}{\sqrt{c^T C_{\theta|y} c}} \right) \quad \text{A3.1}$$

ϕ_N is the cumulative normal distribution. In this paper, we are primarily concerned with the coupling parameters θ^c and, among these, the bilinear terms. The units of these parameters are Hz or per second or a dimensional if normalized and the thresholds are specified as such. In dynamical modelling strength corresponds to a fast response with a small time constant as in the following Table.

Parameter	Description	Prior mean η_θ	Prior variance C_θ
κ	rate of signal decay	0.65 per sec	0.015
γ	rate of flow-dependent elimination	0.41 per sec	0.002
τ	hemodynamic transit time	0.98 sec	0.0568
α	Grubb's exponent	0.32	0.0015
ρ	resting oxygen extraction fraction	0.34	0.0024

Table A2. Priors of HRF after estimation